Electronic Supplementary Information

Chiral π-Extended Diindenoperylenes Featuring Dithia[7]helicenes

Georg Berger,[a] Jan Borstelmann, [a] Frank Rominger,[a] and Milan Kivala*[a]

[a] *Organisch-Chemisches Institut, Universität Heidelberg, Im Neuenheimer Feld 270, 69120 Heidelberg, Germany. E-mail: milan.kivala@oci.uni-heidelberg.de*

Contents

1. General Experimental Methods

1.1. General Reaction Conditions

All solvents and reagents were purchased at reagent grade from commercial suppliers (Merck/Sigma-Aldrich, TCI, Thermo Fisher Scientific, Acros Organics, Honeywell, BLD Pharmatech) and used without further purification. When indicated, reactions were performed in sealed Biotage microwave reaction vials (10−20 mL, or 2.0−5.0 mL, in combination with aluminum crimp caps and septa). Thin layer chromatography (TLC) was performed on ALUGRAM aluminum plates from Macherey-Nagel, coated with 0.20 mm SiO_2, and observed upon irradiation with UV light (λ = 365 and 254 nm). Flash column chromatography was carried out with SiO_2 from Macherey-Nagel (technical grade 60 M, pore size 60 Å, 40−63 µm particle size) on a Biotage Isolera One chromatography system.

1.2. Instruments Used

Nuclear Magnetic Resonance spectra were recorded, unless indicated otherwise, at room temperature (295 K) on a Bruker Avance III 300, 400, 500, 600 or 700 or on a Bruker at the Institute of Organic Chemistry (Heidelberg University). Proton broad band decoupling was applied for ^{13}C measurements. Deuterated solvents were used as purchased from Merck/Sigma-Aldrich and Deutero. Chemical shifts (reported in parts per million ppm) were referenced[1] to δ_H = 7.26 ppm ($CDCl_3$) and 5.32 ppm (CD_2Cl_2) for ^1H and δ_C = 77.16 ppm ($CDCl_3$) and 53.84 ppm (CD_2Cl_2) for ^{13}C and interpreted with MestReNova Version 14.0.1-23559. Apparent signal multiplicity is reported as s (singlet), d (doublet), dd (doublet of doublets), t (triplet), h (hextet) or m (multiplet).

Absorption and Emission Spectra. UV/Vis-NIR spectra were recorded on an Agilent Cary 5000 UV/Vis-NIR spectrometer and measured in CH_2Cl_2 or THF in the wavelength region of 230 to 3000 nm under N_2 atmosphere at room temperature (rt). Fluorescence analysis was carried out employing a JASCO FP-8500 Fluorescence Spectrometer with a JASCO ILF-835 (100 mm) integrating sphere. The data obtained was interpreted with Spectra Manager from JASCO.

Chiral High-Performance Liquid Chromatography. High-performance liquid chromatography (HPLC) was performed on a setup from Shimadzu consisting of a LC20-AP preparative pump, a DGU-405 degassing unit, a CTO-40C column oven, an SPD-M40 diode array detector, an FCV-20AH_2 valve unit, an FRC-10A fraction collector and an CBM-20A

communication bus module. On the analytical scale, a Daicel CHIRALPAK IA-3 (250 × 4.6 mm) column equipped with a column protection system and a Daicel precolumn (10 mm × 4.0 mm) was used. On the semi-preparative scale, a Daicel CHIRALPAK IA-5 (250 × 20 mm) column equipped with a column protection system and a Daicel 5 µm (20 mm × 10 mm) precolumn was employed. The column temperature was set at 25 °C for *n*-heptane/dichloromethane mixtures and the flow rate was constant at 15–20 mL min^{-1}.

Electronic Circular Dichroism. Electronic Circular Dichroism (ECD) spectra of the enantiopure samples were recorded on a JASCO J-1700 spectrometer and measured at concentrations of approximately 10^{-5} M in CH_2Cl_2 in the wavelength region 230 to 800 nm under ambient conditions at rt.

X-ray Crystallography. Single crystals were obtained by slow gas phase diffusion under the given conditions. The Bruker APEX-II Quazar diffractometer (radiation MoKα, λ = 0.71073 Å) with a CCD area detector and the STOE Stadivari instrument (radiation CuKα, λ=1.54178 Å) with a Pilatus CCD area detector (0.5° ω-scans) were used for data collection by the X-Ray crystallography department of the Institute of Organic Chemistry of Heidelberg University. Structures were solved with the ShelXT[2] structure solution program and refined against F2 with a full-matrix least-squares algorithm with ShelXL.[3] Hydrogen atoms were treated with riding models. Graphic visualization and measurement of torsion angles were done with Mercury 2020.1.[4]

Cyclic Voltammetry. A BASi Cell Stand instrument and a BASi Epsilon EClipse potentiostat, with a glassy carbon disk working electrode (3.0 mm diameter), an Ag/AgCl (3 M NaCl) quasi-reference electrode, and a platinum wire auxiliary electrode were used to record cyclic voltammograms. Before each measurement, a 0.1 M electrolyte solution of *n*-Bu_4NPF_6 in anhydrous CH_2Cl_2 or THF was degassed with nitrogen for 20 min. The respective compounds were measured either at a scan rate of 50 mV s^{-1} or 149 mV s^{-1}, followed by the addition of ferrocene as the internal standard and re-measurement. For differential pulse voltammetry the same setup with a step potential of 20 mV, pulse width of 50 ms, pulse period of 200 ms and pulse amplitude of 50 mV was used. For square-wave voltammetry the same setup with a step potential of 10 mV, square-wave amplitude of 25 mV and square-wave frequency of 15 Hz was used. Both measurements were also performed after addition of ferrocene as the internal standard.

Infrared Spectroscopy. A JASCO FT/IR-6000 FT-IR or JASCO 4X spectrometer was operated in ATR mode to record infrared spectra. The respective transmission spectra are baseline corrected, depicted in cm^{-1} and labeled according to the following abbreviations: s (strong), m (medium), w (weak), and br (broad).

Melting Point. The melting point was determined on a Büchi M-560 melting point apparatus in open capillaries. Decomp. refers to decomposition.

Mass Analysis. Mass spectra were received from the facility of Institute of Organic Chemistry, Heidelberg University, and recorded on a JEOL AccuTOF GCx (electron ionization (EI)) or a Bruker timsTOFfleX (matrix assisted laser desorption ionization (MALDI)) instrument. If not indicated otherwise, MALDI-MS was acquired in positive ionization mode.

Computational Details. Quantum chemical calculations were performed using the Gaussian 16 program package.[5] Ground state geometry optimizations were performed by employing the B3LYP[6–9] functional, the 6-311G(d,p)[10,11] basis set and Grimmes D3 dispersion correction[12] with BJ-damping.[13] Thereby, ultra-tight convergence criteria of the respective computational method were used. Frequency calculations at the same level of theory were employed to verify the geometries as local minima possessing no imaginary frequencies. Excited state calculations were carried out within the time-dependent TD-DFT approximation, using the CAM-B3LYP[14] functional with the same basis-set and dispersion correction as above alongside the polarizable continuum model (PCM)[15,16] for solvation using dichloromethane parameters. For every compound, the energetically lowest 100 excited states were calculated. A linewidth of 0.10 eV was assumed for the predicted UV/Vis spectra and a line-width of 0.10 eV was assumed for the predicted CD spectra using the Gaussview 6 software.[17] For better comparability the simulated spectra of the neutral compounds were redshifted by 0.39 eV. Nucleus independent chemical shifts (NICS) were calculated using the Gauge-Independent Atomic Orbital (GIAO)[18–22] approach, as implemented in Gaussian 16 at the (GIAO[18–24]-CAM-B3LYP[14]/D3BJ[13]/def2-TZVP[25,26]/SMD(CH_2Cl_2)[27]) level of theory. Analysis and visualization of the results were done with the py.Aroma 4 software.[28] Ring-current analysis was accomplished by using the Continuous Set of Gauge Transformations (CSGT)[18,23,24] method at the CSGT-B3LYP(D3BJ)/6-311G(d,p) level of theory and visualized using the ACID program package of the Herges group.[29,30] Some geometry optimizations and frequency analyses, including those for the determination of configurational barriers, were performed in ORCA 5.0 and 6.0.[27,31–33] Configurational barriers were computed using the r^2SCAN-3c method.[34]

2. Synthesis Protocols

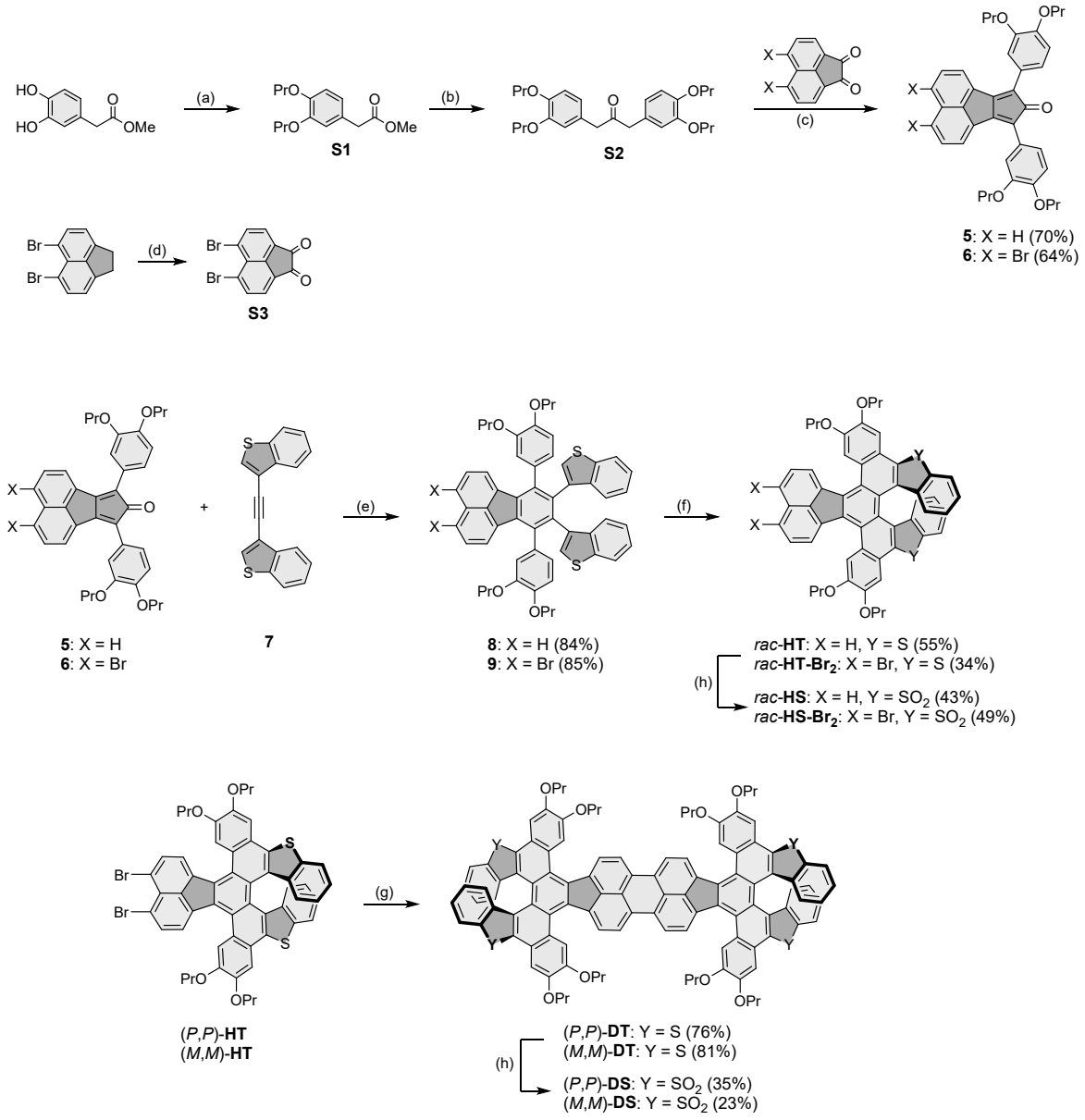

Figure S1. Overview of the syntheses described in this section. (a) *n*-PrBr, K_2CO_3, DMF, 60 °C, 18 h, 82% (b) i) NaOH, H_2O, reflux, 16 h. ii) HCl, H_2O. iii) *N,N'*-dicyclohexylcarbodiimide, DMAP, rt, 16 h, 34%. (c) KOH, EtOH, PhMe, 80 °C, 30 min. (d) CrO_3, Ac_2O, 110–160 °C, 125 min, 66%. (e) 200–220 °C, 14–18 h. (f) DDQ, TfOH, CH_2Cl_2, 0 °C, 30 min. (g) [Ni(COD)$_2$], COD, DMAP, THF, 60 °C, 2 h. (h) *m*-chloroperoxybenzoic acid, CH_2Cl_2, 0 °C, 5–24 h. COD = 1,5-cyclooctadiene; DDQ = 2,3-dichloro-5,6-dicyano-1,4-benzoquinone; DMAP = 4-dimethylaminopyridine; DMF = *N*,*N*-dimethylformamide; Pr = *n*-propyl; THF = tetrahydrofuran; TfOH = trifluoromethanesulfonic acid.

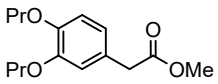

S1

Methyl 2-(3,4-dipropoxyphenyl)acetate (S1). The synthesis was performed based on a modified procedure by *Miao* and coworkers.[35] In a heated Schlenk flask K_2CO_3 (148 g, 1.07 mol) and methyl 2-(3,4-dihydroxyphenyl)acetate (24.5 g, 134 mmol) were suspended in DMF (300 mL). 1-Bromopropane (40.0 mL, 439 mmol) was added under N_2 atmosphere and the mixture was stirred for 18 h at 60 °C. After cooling to rt, water (500 mL) was added. The mixture was extracted with diethyl ether (4 × 150 mL), washed with water (3 × 100 mL) and dried over $MgSO_4$. The solvent was removed under reduced pressure to afford the product **S1** (29.5 g, 111 mmol, 82%) as an orange-brown oil.

R_f = 0.20 (SiO_2, PE/EtOAc 9:1).

^{1}H NMR (300 MHz, $CDCl_3$): δ 6.84 – 6.78 (m, 3H), 3.96 (t, *J* = 6.6 Hz, 2H), 3.94 (t, *J* = 6.6 Hz, 2H), 3.69 (s, 3H), 3.54 (s, 2H), 1.87 – 1.79 (m, 4H), 1.06 – 1.00 (m, 6H) ppm.

^{13}C NMR (75 MHz, $CDCl_3$): δ 172.5, 149.3, 148.5, 126.8, 121.7, 115.2, 114.2, 71.0, 70.9, 52.1, 40.9, 22.8, 10.6 ppm. Two signals coincident or not observed.

IR (FT-ATR): $\tilde{\nu}$ = 2963 (w), 2938 (w), 2877 (w), 1736 (s), 1590 (w), 1511 (s), 1470 (w), 1430 (s), 1390 (w), 1303 (w), 1259 (s), 1228 (s), 1139 (s), 1064 (m), 1045 (m), 1014 (s), 995 (s), 979 (s), 924 (w), 910 (w), 889 (w), 844 (w), 803 (w), 765 (w), 751 (w), 709 (w), 606 (w) cm^{-1}.

HRMS (EI+): calcd. for $C_{15}H_{22}O_4$: 266.1513 [M^+]; found: 266.1529.

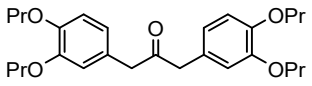

S2

1,3-Bis(3,4-dipropoxyphenyl)propan-2-one (S2). The synthesis was performed based on a modified procedure by *Miao* and coworkers.[35] Methyl 2-(3,4-dipropoxyphenyl)acetate (29.5 g, 111 mmol) was suspended in aq. NaOH (2M, 300 mL) and the mixture was heated to reflux for 16 h. After cooling to rt, conc. aq. HCl was added until the pH was 2–3. The mixture was extracted with CH_2Cl_2 (3 × 200 mL) and the combined organic phases were dried over Na_2SO_4. Then, the solvent was removed and the crude 2-(3,4-dipropoxyphenyl)acetic acid was used without further purification.

In a heated Schlenk flask *N,N'*-dicyclohexylcarbodiimide (26.8 g, 130 mmol) and 4-dimethylaminopyridine (3.45 g, 28.2 mmol) were dissolved in anhydrous CH_2Cl_2 (100 mL) under N_2 atmosphere. A solution of 2-(3,4-dipropoxyphenyl)acetic acid (28.5 g, 113 mmol) in CH_2Cl_2 (15 mL) was added and the mixture was stirred at rt for 16 h. The suspension was filtered and the filtrate was concentrated under reduced pressure. The crude product was purified by flash column chromatography (SiO_2, PE:EtOAc 6:1) to afford the product **S2** (8.47 g, 19.1 mmol, 34%) as a colorless solid.

R_f = 0.55 (SiO_2, PE/EtOAc 4:1).

^{1}H NMR (400 MHz, $CDCl_3$): δ 6.82 (d, *J* = 7.9 Hz, 2H), 6.67 – 6.64 (m, 4H), 3.96 – 3.89 (m, 8H), 3.61 (s, 4H), 1.85 – 1.79 (m, 8H), 1.06 – 1.01 (m, 12H) ppm.

^{13}C NMR (101 MHz, $CDCl_3$): δ 206.6, 149.3, 148.3, 126.8, 121.9, 115.2, 114.2, 70.9, 70.8, 48.5, 22.7, 22.6, 10.5 ppm. One signal coincident or not observed.

IR (FT-ATR): $\tilde{\nu}$ = 2965 (w), 2938 (w), 2908 (w), 2876 (w), 1702 (w), 1586 (w), 1512 (s), 1471 (m), 1426 (m), 1395 (w), 1255 (s), 1230 (s), 1203 (s), 1155 (m), 1138 (s), 1083 (w), 1045 (s), 1015 (s), 999 (m), 974 (w), 910 (w), 804 (s), 766 (w) cm^{-1}.

HRMS (EI+): calcd. for $C_{27}H_{38}O_5$: 442.2714 [M$^+$]; found: 442.2715.

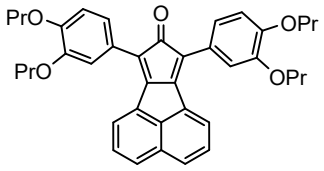

5

7,9-Bis(3,4-dipropoxyphenyl)-8*H*-cyclopenta[*a*]acenaphthylen-8-one (5). The synthesis was performed based on a modified procedure by *Miao* and coworkers.[35] To a suspension of **S2** (2.00 g, 4.52 mmol, 1.05 equiv.) and acenaphthoquinone (784 mg, 4.30 mmol, 1.00 equiv.) in ethanol (27 mL) and toluene (2.7 mL) heated in an oil bath at 80 °C was added a solution of KOH (121 mg, 2.15 mmol, 0.50 equiv.) in ethanol (6 mL). Stirring and heating was continued for 30 min. After cooling in an ice bath for 30 min, the dark green suspension was filtered and the solid product washed with cold ethanol (30 ml) and dried under reduced pressure to afford the product **5** as dark green solid (888 mg, 1.51 mmol, 70%).

M.p.: 145–165 °C.

R_f = 0.33 (SiO_2, PE/CH_2Cl_2 9:1).

^{1}H NMR (400 MHz, $CDCl_3$): δ 8.05 (d, *J* = 7.2 Hz, 2H), 7.83 (d, *J* = 7.8 Hz, 2H), 7.56 (t, *J* = 7.7 Hz, 2H), 7.40 (m, 4H), 7.02 (d, *J* = 8.3 Hz, 2H), 4.06 (t, *J* = 6.6 Hz, 8H), 1.94 – 1.85 (m, 8H), 1.08 (q, *J* = 7.4 Hz, 12H) ppm.

^{13}C NMR (101 MHz, $CDCl_3$): δ 203.0, 152.8, 149.7, 149.2, 144.8, 132.4, 132.1, 128.5, 127.4, 124.5, 122.4, 121.6, 120.7, 114.9, 113.9, 71.1, 70.9, 22.84, 22.79, 10.7, 10.6 ppm.

IR (FT-ATR): $\tilde{\nu}$ = 2963 (w), 2934 (w), 2875 (w), 1700 (s), 1599 (w), 1574 (w), 1510 (s), 1468 (m), 1325 (w), 1250 (s), 1215 (s), 1200 (s), 1137 (s), 1121 (m), 1101 (m), 1064 (w), 977 (s), 858 (w), 811 (m), 771 (s) cm^{-1}.

UV/Vis (CH_2Cl_2, rt): λ_{max} (ε) 626 (2330), 401 (13900), 275 (40500) nm (M^{-1} cm^{-1}).

HRMS (MALDI, dctb): calcd. for $C_{39}H_{40}O_5$: 588.2876 [M^+]; found: 588.2878.

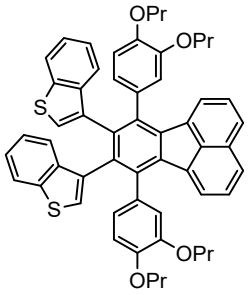

8

3,3'-[7,10-Bis(3,4-dipropoxyphenyl)fluoranthene-8,9-diyl]bis(1-benzothiophene) (8). In a microwave flask were placed **5** (193 mg, 328 µmol, 1.00 equiv.) and **7** (100 mg, 344 µmol, 1.05 equiv.), flushed with N_2, and sealed. The mixture was stirred at 200 °C for 18 h, then the crude product was dissolved in CH_2Cl_2 and purified via column chromatography (SiO_2, PE/CH_2Cl_2 7:3 → 5:5) to afford the product **8** (233 mg, 273 µmol, 84%) as orange solid.

M.p.: 114.3–118.5 °C.

R_f = 0.65 (SiO_2, PE/CH_2Cl_2 1:1).

^{1}H NMR (700 MHz, $C_2D_2Cl_4$, 295 K) δ = 7.80 (d, *J* = 8.1 Hz), 7.68 (d, *J* = 7.9 Hz), 7.65 (d, *J* = 7.9 Hz), 7.60 – 7.51 (m), 7.50 – 7.37 (m), 7.33 – 7.15 (m), 7.06 – 6.56 (m), 3.96 – 3.62 (m), 3.56 – 3.39 (m), 3.21 – 3.13 (m), 3.10 – 3.04 (m), 3.04 – 2.94 (m), 1.82 – 1.65 (m), 1.53 – 1.38 (m), 1.06 – 0.95 (m), 0.92 – 0.76 ppm. Large number of signals indicates the presence of multiple diastereomers. Consequently, the NMR spectrum is reported as an empirical enumeration of the observed signals.

^{13}C NMR (175 MHz, $CDCl_3$, 354 K): δ 149.06, 149.03, 148.99, 148.87, 148.68, 148.64, 148.46, 140.53, 140.45, 139.91, 139.88, 139.31, 139.25, 138.62, 138.57, 138.51, 138.33, 138.32, 138.15, 138.10, 137.45, 137.36, 136.36, 136.34, 136.32, 135.84, 135.72, 135.64, 135.55, 135.40, 135.32, 135.10, 135.08, 134.92, 133.02, 133.00, 132.49, 132.32, 132.29, 132.27, 132.11, 129.70, 127.67, 127.64, 127.60, 126.57, 125.69, 125.55, 125.50, 125.40, 124.49, 124.41, 124.19, 124.08, 123.78, 123.62, 123.55, 123.47, 123.32, 123.28, 123.26, 123.18, 123.09, 122.99, 122.69, 122.66, 122.63, 122.57, 122.37, 122.30, 121.91, 121.84, 121.74, 121.68, 121.49, 121.31, 117.91, 117.87, 117.74, 117.67, 117.04, 116.77, 116.32, 116.24, 115.37, 115.34, 115.27, 115.17, 115.13, 115.09, 71.70, 71.65, 71.58, 71.47, 71.45, 71.32, 71.21,

71.12, 71.04, 71.00, 22.64, 22.61, 22.59, 22.54, 22.34, 22.26, 22.24, 22.21, 10.27, 10.26, 10.24, 10.09, 10.06, 10.04 ppm. Observed signals: 114. Some signals coincident or not observed due to low signal/noise ratio. Expected number of signals for symmetrical conformer: 29. Expected for unsymmetrical conformer: 56. At least three diastereomeric conformers are present.

IR (FT-ATR): $\tilde{\nu}$ = 2956 (m), 2929 (m), 2873 (m), 2367 (w), 2350 (w), 2323 (w), 2310 (w), 1603 (w), 1578 (w), 1511 (s), 1460 (m), 1426 (s), 1390 (m), 1244 (s), 1224 (m), 1197 (m), 1176 (m), 1133 (s), 1061 (m), 1042 (m), 1012 (m), 975 (m), 825 (m), 806 (m), 775 (m), 762 (s), 747 (m), 732 (m) cm^{-1}.

HRMS (MALDI, dctb): calcd. for $C_{56}H_{50}O_4S_2$: 850.3151 [M^+]; found: 850.3140.

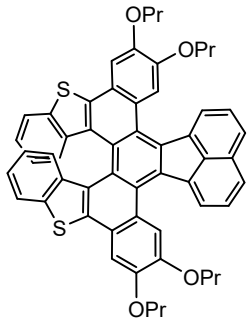

HT

2,3,12,13-Tetrapropoxyacenaphtho[1',2':13,14][1]benzothieno[3',2':7,8]piceno [5,6-*b*][1]benzothiophene (HT). In a heated Schlenk flask **8** (20.0 mg, 23.5 µmol, 1.00 equiv.) and DDQ (12.0 mg, 51.7 µmol, 2.20 equiv.) were dissolved in anhydrous CH_2Cl_2 (20 mL) under N_2 atmosphere. Trifluoromethanesulfonic acid (0.2 ml) was added dropwise while stirring at 0 °C. The mixture was stirred for 30 min, then sat. aq. $NaHCO_3$ (20 mL) was added and the mixture was extracted with CH_2Cl_2 (3 × 50 mL). The combined organic phases were washed with aq. sat. NaCl solution and dried over anhydrous $MgSO_4$ and the solvent was evaporated under reduced pressure. The crude product was purified via column chromatography (SiO_2, PE/CH_2Cl_2 6:4) to afford the product **HT** (11.0 mg, 13.0 µmol, 55%) as red solid. Enantiopure (*P*)-**HT** and (*M*)-**HT** were obtained by chiral HPLC chromatography (Chiralpak IA5, *n*-Heptane/CH_2Cl_2 5:1).

M.p.: 285.2 °C (*rac*-**HT**), 305.7 °C ((*M*)-**HT**).

R_f = 0.75 (SiO_2, PE/CH_2Cl_2 1:1).

^{1}H NMR (600 MHz, $CDCl_3$): δ 8.97 (s, 2H), 8.78 (d, *J* = 7.2 Hz, 2H), 7.80 (d, *J* = 8.0 Hz, 2H), 7.64 (d, *J* = 7.8 Hz, 2H), 7.59 (s, 2H), 7.49 (t, *J* = 7.6 Hz, 2H), 7.15 (d, *J* = 8.4 Hz, 2H), 6.97 (ddd, *J* = 8.0, 7.0, 1.1 Hz, 2H), 6.66 (ddd, *J* = 8.3, 7.0, 1.1 Hz, 2H), 4.34 (t, *J* = 6.6 Hz, 4H), 4.18 (t, *J* = 6.6 Hz, 4H), 2.12 – 2.06 (m, 4H), 2.00 – 1.92 (m, 4H), 1.23 (t, *J* = 7.4 Hz, 6H), 1.08 (t, *J* = 7.4 Hz, 6H) ppm.

^{13}C NMR (151 MHz, $CDCl_3$): δ 150.4, 147.8, 138.3, 138.2, 137.6, 133.5, 132.4, 130.2, 129.8, 127.8, 127.1, 124.6, 124.3, 123.6, 123.3, 123.0, 122.0, 112.9, 106.5, 70.9, 70.8, 22.9, 22.8, 10.8, 10.7 ppm. Four signals coincident or not observed.

IR (FT-ATR): $\tilde{\nu}$ = 2959 (m), 2925 (m), 2872 (m), 1609 (m), 1507 (s), 1446 (s), 1425 (m), 1376 (m), 1255 (s), 1227 (s), 1203 (m), 1193 (m), 1169 (m), 1107 (m), 1064 (m), 1043 (m), 1022 (m), 1007 (w), 971 (m), 885 (m), 820 (m), 806 (m), 774 (s), 748 (s), 730 (s), 629 (w), 607 (m), 537 (m), 441 (w) cm^{-1}.

UV/Vis (CH_2Cl_2, rt): λ_{max} (ε) 493 (8110), 464 (7110), 400 (36300), 379 (34600), 356 (41000), 334 (40600), 305 (39893), 257 (63100) nm (M^{-1} cm^{-1}).

HRMS (MALDI, dctb): calcd. for $C_{56}H_{46}O_4S_2$: 846.2838 [M^+]; found: 846.2845.

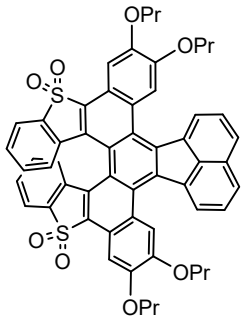

HS

2,3,12,13-Tetrapropoxyacenaphtho[1',2':13,14][1]benzothieno[3',2':7,8]piceno [5,6-*b*][1]benzothiophene-*S,S,S',S'*-tetroxide (HS). In a microwave flask **HT** (15.0 mg, 17.7 µmol, 1.00 equiv.) and *m*CPBA (70%, 31.4 mg, 127 µmol, 7.20 equiv.) were dissolved in anhydrous CH_2Cl_2 (8 mL) under N_2 atmosphere while cooling in an ice bath. The mixture was stirred for 1 d, then aq. K_2CO_3 (0.7 M, 50 mL) was added and the mixture was extracted with CH_2Cl_2. The combined organic phases were dried over anhydrous $MgSO_4$ and the solvent was evaporated under reduced pressure. The crude product was purified via column chromatography (SiO_2, PE/EA 80:20 → 65:35) to afford the product (7.0 mg, 7.68 µmol, 43%) as red solid.

M.p.: 315 – 320 °C.

R_f = 0.55 (SiO_2, PE/EtOAc 7:3).

^{1}H NMR (600 MHz, $CDCl_3$): δ 8.89 (s, 2H), 8.75 (d, *J* = 7.3 Hz, 2H), 7.92 (d, *J* = 8.0 Hz, 2H), 7.92 (s, 2H), 7.64 – 7.62 (m, 4H), 7.54 (t, *J* = 7.6 Hz, 2H), 7.24 (td, *J* = 7.7, 1.3 Hz, 2H, partially overlapping with solvent residual signal), 7.19 (td, *J* = 7.4, 1.0 Hz, 2H), 4.40 – 4.34 (m, 4H), 4.21 – 4.13 (m, 4H), 2.08 – 2.04 (m, 4H), 1.99 – 1.93 (m, 4H), 1.20 (t, *J* = 7.4 Hz, 6H), 1.08 (t, *J* = 7.4 Hz, 6H) ppm.

^{13}C NMR (151 MHz, $CDCl_3$): δ 152.0, 149.6, 136.9, 136.5, 135.9, 134.0, 133.3, 131.8, 130.4, 129.6, 129.5, 128.0, 127.4, 126.0, 125.8, 123.2, 122.0, 121.7, 121.5, 111.8, 103.8, 70.8, 22.7, 22.6, 10.8, 10.7 ppm. Three signals coincident or not observed.

IR (FT-ATR): $\tilde{\nu}$ = 2959 (w), 2929 (w), 2875 (w), 1606 (w), 1508 (s), 1462 (m), 1453 (s), 1423 (m), 1412 (m), 1388 (m), 1372 (w), 1298 (s), 1260 (s), 1223 (m), 1198 (m), 1155 (s), 1126 (s), 1107 (s), 1058 (m), 1038 (m), 1022 (m), 1006 (w), 967 (m), 909

(w), 879 (m), 822 (m), 777 (m), 755 (s), 718 (m), 584 (m), 569 (m), 548 (m), 532 (m) cm^{-1}.

UV/Vis (CH_2Cl_2, rt): λ_{max} (ε) 513 (14200), 369 (42800), 334 (44000), 271 (55600), 245 (80000) nm (M^{-1} cm^{-1}).

HRMS (MALDI, dctb): calcd. for: $C_{56}H_{46}O_8S_2$ [M^+] 910.2629; found: 910.2623.

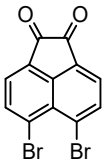

S3

5,6-Dibromoacenaphthylene-1,2-dione (S3). The synthesis was performed based on a literature procedure by *Kivala* and coworkers.[36] In a Schlenk flask 5,6-dibromoacenaphthene (4.00 g, 12.8 mmol) was suspended in acetic anhydride (350 mL) under N_2 atmosphere and heated to 110 °C. Chromium trioxide (12.8 g, 128 mmol) was added in small portions over 35 min. A reflux condenser was added and the oil bath temperature was increased to 160 °C. The reaction was stirred for 90 minutes. After removal of the oil bath and cooling to rt, the reaction mixture was poured onto ice (500 g) while cooling in an ice bath. Hydrochloric acid (conc., 75 mL) was added in small portions to give a dark green solution with a brown precipitate. The precipitate was collected by filtration, washed with water (150 mL), dried under reduced pressure, recrystallized from acetic anhydride (800 mL), washed with water (50 mL), and dried under reduced pressure to yield the product as a brown solid (2.89 g, 8.50 mmol, 66%).

^{1}H NMR (300 MHz, $CDCl_3$): δ 8.27 (d, *J* = 7.7 Hz, 2H), 7.93 (d, *J* = 7.6 Hz, 2H) ppm.

HRMS(EI+): calcd. for $C_{12}H_4Br_2O_2$ 337.8573 [M^+], found: 337.8585.

The spectroscopic data are in agreement with literature.[36]

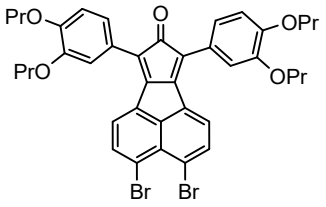

6

3,4-Dibromo-7,9-bis(3,4-dipropoxyphenyl)-8H-cyclopenta[a]acenaphthylen-8-one (6). To a suspension of **S2** (640 mg, 1.45 mmol, 1.00 equiv.) and 5,6-dibromo-acenaphthoquinone (**S3**) (500 mg, 1.47 mmol, 1.02 equiv.) in ethanol (10 mL) and toluene (1.0 mL) heated in an oil bath at 80 °C was added a solution of KOH (41.0 mg, 731 µmol, 0.51 equiv.) in ethanol (3.5 mL) dropwise over 10 min. Stirring and heating was continued for 10 min. After cooling in an ice bath for 30 min, the dark green suspension was filtered, the solid product washed with cold ethanol (30 ml) and dried under reduced pressure to afford the product as brown solid (690 mg, 926 µmol, 64%).

M.p.: 149.7 °C.

R_f = 0.44 (SiO_2, PE/CH_2Cl_2 1:2).

^{1}H NMR (400 MHz, $CDCl_3$): δ 7.93 (d, *J* = 7.8 Hz, 2H), 7.84 (d, *J* = 7.8 Hz, 2H), 7.36 – 7.28 (m, 4H), 7.00 (d, *J* = 8.2 Hz, 2H), 4.04 (m, 8H), 1.96 – 1.82 (m, 8H), 1.08 (m, 12H) ppm.

^{13}C NMR (101 MHz, $CDCl_3$): δ 202.2, 150.7, 150.0, 149.3, 146.6, 136.8, 132.7, 129.2, 123.9, 122.4, 122.3, 121.2, 120.4, 114.8, 113.8, 71.1, 70.9, 22.8, 22.7, 10.7, 10.6 ppm.

IR (FT-ATR): $\tilde{\nu}$ = 2961 (w), 2936 (w), 2877 (w), 1709 (m), 1595 (m), 1575 (w), 1515 (s), 1463 (m), 1389 (m), 1357 (w), 1322 (m), 1275 (m), 1258 (s), 1250 (s), 1220 (s), 1181 (w), 1138 (s), 1113 (m), 1094 (m), 1068 (m), 1047 (m), 1016 (w), 978 (s), 866 (m), 852 (m), 824 (s), 799 (s), 774 (m), 768 (m), 725 (w), 614 (m), 586 (w), 541 (m), 452 (w) cm^{-1}.

HRMS (MALDI, dctb): calcd. for: $C_{39}H_{38}Br_2O_5$ [M^+] 744.1081; found: 744.1073.

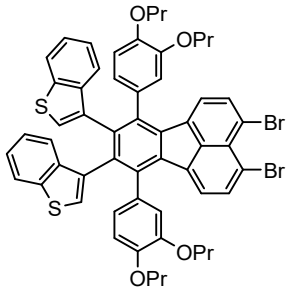

9

3,3'-[7,10-Bis(3,4-dipropoxyphenyl)fluoranthene-8,9-diyl]bis(1-benzothiophene) (9). In a microwave flask **6** (204 mg, 273 µmol, 1.00 equiv.) and **7** (94.0 mg, 324 µmol, 1.18 equiv.) were placed, flushed with N_2, and sealed. The mixture was stirred at 220 °C for 14 h, then the crude product was dissolved in CH_2Cl_2 and purified via column chromatography (SiO_2, PE/CH_2Cl_2 7:3 → 5:5) to afford the product **9** (233 mg, 231 µmol, 85%) as yellowish solid.

M.p.: 127.6 – 131.8 °C.

R_f = 0.35 (SiO_2, PE/CH_2Cl_2 1:1).

^{1}H NMR (300 MHz, $CDCl_3$): δ 7.74 – 7.65 (m), 7.60 – 7.49 (m), 7.48 – 7.37 (m), 7.32 – 7.12 (m), 7.00 – 6.56 (m), 4.00 – 3.64 (m), 3.60 – 3.40 (m), 3.24 – 2.94 (m), 1.92 – 1.66 (m), 1.62 – 1.40 (m), 1.08 – 0.92 (m), 0.90 – 0.76 (m) ppm. Large number of signals indicates the presence of multiple diastereomers. Consequently, the NMR spectrum is reported as an empirical enumeration of the observed signals.

^{13}C NMR (75 MHz, $CDCl_3$): δ 148.61, 148.57, 148.5, 148.4, 148.25, 148.22, 148.20, 140.6, 140.5, 139.8, 139.34, 139.30, 138.9, 138.82, 138.80, 138.73, 138.70, 138.6, 138.5, 138.4, 137.24, 137.22, 137.17, 136.9, 136.83, 136.75, 136.4, 136.35, 136.33, 136.0, 135.2, 134.8, 134.7, 131.4, 131.15, 131.12, 131.0, 130.9, 126.8, 125.9, 125.72, 125.67, 125.6, 124.8, 124.7, 124.5, 124.4, 123.9, 123.7, 123.62, 123.58, 123.52, 123.45, 123.2, 123.1, 123.0, 122.9, 122.8, 122.4, 122.3, 122.22, 122.17, 122.0, 121.93, 121.85, 121.81, 121.77, 121.6, 121.5, 120.08, 120.06, 115.6, 115.5, 115.0, 114.6, 114.3, 114.2, 113.30, 113.28, 113.2, 70.9, 70.8, 70.7, 70.5, 70.4, 70.35, 70.28, 22.73, 22.69, 22.60, 22.57, 22.4, 22.31, 22.29, 10.6, 10.5, 10.4, 10.3 ppm. Observed signals: 98. Some signals coincident or not observed due to low signal/noise ratio.

Expected number of signals for symmetrical conformer: 29. Expected for unsymmetrical conformer: 56. At least two diastereomeric conformers are present.

IR (FT-ATR): $\tilde{\nu}$ = 2979 (m), 2970 (m), 2929 (m), 2871 (m), 1510 (m), 1427 (m), 1407 (m), 1242 (s), 1208 (m), 1189 (m), 1154 (m), 1134 (m), 1062 (m), 1008 (m), 966 (m), 834 (m), 806 (m), 761 (m), 748 (m), 731 (m), 652 (m) cm^{-1}.

HRMS (MALDI, dctb): calcd. for: $C_{56}H_{48}Br_2O_4S_2$ [M^+] 1006.1355; found: 1006.1347.

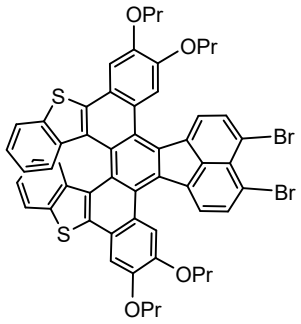

(*P*)-**HT-Br$_2$**

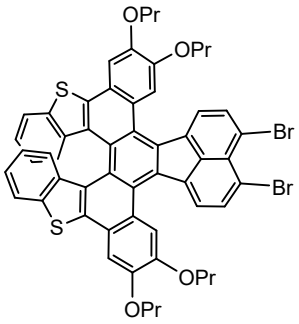

(*M*)-**HT-Br$_2$**

***P/M*-7,8-Dibromo-2,3,12,13-tetrapropoxyacenaphtho[1',2':13,14][1]benzothieno [3',2':7,8]piceno[5,6-*b*][1]benzothiophene (HT-Br$_2$).** In a heated Schlenk flask **11** (233 mg, 231 µmol, 1.00 equiv.) and DDQ (113 mg, 497 µmol, 2.15 equiv.) were dissolved in anhydrous CH_2Cl_2 (100 mL) under N_2 atmosphere. Trifluoromethanesulfonic acid (1.0 ml) was added dropwise while stirring at 0 °C. The mixture was stirred for 30 min, then sat. aq. $NaHCO_3$ (20 mL) was added and the mixture was extracted with DCM (3 × 50 mL). The combined organic phases were washed with aq. sat. NaCl solution and dried over anhydrous $MgSO_4$ and the solvent was evaporated under reduced pressure. The crude product was purified via column chromatography (SiO_2, PE/CH_2Cl_2 1:1) to afford the *rac*-**HT-Br$_2$** (80.0 mg, 79.6 µmol, 34%) as dark red-black solid. Enantiopure compounds (*P*)-**HT-Br$_2$** and (*M*)-**HT-Br$_2$** were obtained by chiral HPLC (Chiralpak IA5, *n*-heptane/CH_2Cl_2 5:4 or *n*-heptane/^{i}PrOH 98:2).

M.p.: 354 °C ((*P*)-**HT-Br$_2$**).

R_f = 0.35 (SiO_2, PE/CH_2Cl_2 3:2).

^{1}H NMR (600 MHz, $CDCl_3$): δ 8.71 (s, 2H), 8.48 (d, *J* = 7.8 Hz, 2H), 7.78 (d, *J* = 7.8 Hz, 2H), 7.63 (dt, *J* = 7.9, 0.8 Hz, 2H), 7.57 (s, 2H), 7.11 (d, *J* = 8.3 Hz, 2H), 6.97 (ddd, *J* = 8.0, 7.0, 1.1 Hz, 2H), 6.66 (ddd, *J* = 8.4, 7.0, 1.2 Hz, 2H), 4.33 (t, *J* = 6.5 Hz, 4H), 4.11 (t, *J* = 6.6 Hz, 4H), 2.12 – 2.06 (m, 4H), 1.98 – 1.02 (m, 4H), 1.23 (t, *J* = 7.4 Hz, 6H), 1.10 (t, *J* = 7.4 Hz, 6H) ppm.

^{13}C NMR (151 MHz, $CDCl_3$): δ 150.6, 147.9, 139.0, 138.0, 137.6, 136.5, 135.4, 135.0, 132.3, 129.8, 127.0, 124.8, 124.7, 123.2, 123.2, 123.0, 122.1, 120.6, 112.5, 106.6, 70.9, 70.8, 22.84, 22.79, 10.85, 10.75 ppm. Three signals coincident or not observed.

IR (FT-ATR): $\tilde{\nu}$ = 2959 (w), 2931 (w), 2871 (w), 1610 (w), 1508 (s), 1456 (s), 1445 (s), 1408 (s), 1390 (m), 1373 (m), 1283 (w), 1257 (s), 1241 (s), 1227 (s), 1195 (m), 1177 (s), 1161 (m), 1140 (m), 1128 (s), 1103 (s), 1064 (m), 1043 (w), 1023 (w), 1011 (w), 989 (m), 971 (s), 887 (w), 875 (m), 859 (w), 825 (s), 803 (w), 759 (m), 748 (s), 728 (s), 661 (w), 632 (w), 574 (w), 436 (w) cm^{-1}.

UV/Vis (CH_2Cl_2, rt): λ_{max} (ε) 513 (6860), 411 (26500), 390 (21200), 338 (29000), 269 (40700) nm (M^{-1} cm^{-1}).

HRMS (MALDI, dctb): calcd. for: $C_{56}H_{44}Br_2O_4S_2$ [M^+] 1002.1042; found: 1002.1030.

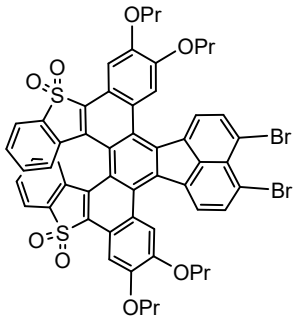

rac-**HS-Br$_2$**

***rac*-7,8-Dibromo-2,3,12,13-tetrapropoxyacenaphtho[1',2':13,14][1]benzothieno [3',2':7,8]piceno[5,6-*b*][1]benzothiophene-*S,S,S',S'*-tetroxide (HS-Br$_2$).** In a round-bottom flask **HT-Br$_2$** (30.0 mg, 29.9 µmol, 1.00 equiv.) and *m*CPBA (70%, 53.0 mg, 215 µmol, 7.20 equiv.) were dissolved in anhydrous CH_2Cl_2 (8 mL) under N_2 atmosphere while stirring in an ice bath at 0 °C. The mixture was stirred for 5 h, then was added to aq. K_2CO_3 (0.7 M, 20 mL) and extracted with CH_2Cl_2. The combined organic phases were dried over anhydrous $MgSO_4$ and the solvent was evaporated under reduced pressure. The crude product was purified via column chromatography (SiO_2, PE/EtOAc 3/1) to afford the product *rac*-**HS-Br$_2$** (15.6 mg, 14.6 µmol, 49%) as red solid.

The enantiopure compounds were synthesized analogously starting from the enantiopure starting material **HT-Br$_2$** (11.0 mg, 11.0 µmol) (9.30 mg, 8.70 µmol, 79% (*P*); 8.40 mg, 7.86 µmol, 72% (*M*)).

M.p.: 380 °C (decomp.) (*P*-**HS-Br$_2$**).

R_f = 0.53 (SiO_2, PE/EtOAc 7:3).

^{1}H NMR (600 MHz, CD_2Cl_2): δ 8.69 (s, 2H), 8.53 (d, *J* = 8.5 Hz, 2H), 7.91 (d, *J* = 7.9 Hz, 2H), 7.87 (s, 2H), 7.62 – 7.59 (m, 4H), 7.22 (m, 4H), 4.35 – 4.29 (m, 4H), 4.15 – 4.13 (m, 4H), 2.06 – 2.00 (m, 4H), 1.97 – 1.91 (m, 4H), 1.19 (t, *J* = 7.4 Hz, 6H), 1.10 (t, *J* = 7.4 Hz, 6H) ppm.

^{13}C NMR (151 MHz, CD_2Cl_2): δ 152.3, 150.1, 137.7, 136.8, 135.6, 135.0, 134.7, 133.9, 133.3, 129.7, 128.0, 127.3, 126.3, 125.9, 123.3, 122.9, 122.7, 121.8, 121.5, 111.6, 104.0, 71.03, 70.96, 22.9, 22.8, 10.7, 10.6 ppm. Two signals coincident or not observed.

IR (FT-ATR): $\tilde{\nu}$ = 2966 (w), 2936 (w), 2877 (w), 1610 (w), 1556 (w), 1510 (s), 1457 (s), 1408 (s), 1389 (s), 1370 (m), 1298 (s), 1261 (s), 1245 (s), 1222 (w), 1200 (m), 1181 (m), 1156 (s), 1127 (s), 1105 (s), 1060 (m), 1043 (w), 1025 (m), 1006 (m), 965 (s), 828 (s), 758 (s), 740 (w), 720 (w), 665 (w), 584 (w), 567 (s), 553 (m), 545 (m), 526 (w), 518 (w), 465 (w) cm^{-1}.

UV/Vis (CH_2Cl_2, rt): λ_{max} (ε) 526 (16800), 403 (41400), 366 (51600), 271 (75700), 250 (75000) nm (M^{-1} cm^{-1}).

HRMS (MALDI, dctb): calcd. for: $C_{56}H_{44}Br_2O_8S_2$ [M^+] 1066.0839; found: 1066.0829.

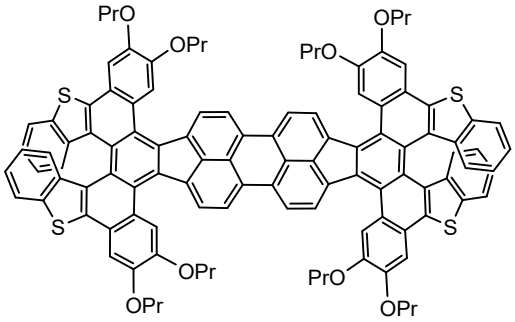

(*M*,*M*)-**DT**

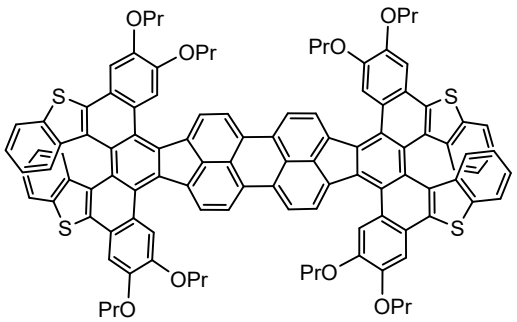

(*P*,*P*)-**DT**

Bis(2,3,12,13-tetrapropoxyacenaphtho[1',2':13,14][1]benzothieno[3',2':7,8] piceno[5,6-*b*][1]benzothiophene-7,8-ylene) (DT). The reaction was conducted twice, once for each enantiomer of the starting material. In a glove box, [Ni(COD)$_2$] (6.02 mg, 21.9 µmol, 2.20 equiv.) was placed in a heated microwave flask, which was sealed with a rubber septum crimp cap and exported from the glove box. In a heated Schlenk flask was dissolved (*P*)/(*M*)-**HT-Br$_2$** (10.0 mg, 9.95 µmol, 1.00 equiv.) and 4-(dimethylamino)pyridine (*P*: 5.50 mg, 45.0 µmol, 4.52 equiv.; *M*: 6.80 mg, 55.7 µmol, 5.59 equiv.) in anhyd. THF (5.0 mL, degassed by three freeze-pump-thaw cycles). To the microwave flask was added cyclooctadiene (0.02 mL, 159 µmol, 16.0 equiv.) and the prepared solution of the starting material and 4-(dimethylamino)pyridine. The flask was placed in a heated block (60 °C) and stirred for 2 h, then, the heating was switched off and the reactions stirred for further 20 h. The contents of the flask were transferred to a round-bottom flask and the solvent was removed under reduced pressure. The product was purified by flash column chromatography (SiO$_2$, PE/CH$_2$Cl$_2$ 4:6 → 3:7) and obtained as dark green solid ((*P*,*P*): 6.40 mg, 3.79 µmol, 76%; (*M*,*M*): 6.80 mg, 4.02 µmol, 81%).

M.p.: 325 °C.

R_f = 0.60 (SiO$_2$, PE/CH$_2$Cl$_2$ 1:1).

^{1}H NMR (700 MHz, CDCl$_3$): δ 8.84 (s, 4H), 8.61 (d, *J* = 7.8 Hz, 4H), 7.98 (s, 4H), 7.65 (d, *J* = 7.6 Hz, 4H), 7.59 (s, 4H), 7.17 (d, *J* = 8.5 Hz, 4H), 6.98 (t, *J* = 7.2 Hz, 4H), 6.68 (t, *J* = 7.7 Hz, 4H), 4.36 (t, *J* = 6.5 Hz, 8H), 4.22 (t, *J* = 6.7 Hz, 8H), 2.15 – 2.05 (m, 8H), 2.01 – 1.92 (m, 8H), 1.26 (t, *J* = 7.3 Hz, 12H), 1.10 (t, *J* = 7.4 Hz, 12H) ppm.

^{13}C NMR (176 MHz, CDCl$_3$): δ 150.6, 147.9, 138.9, 138.2, 137.6, 136.4, 134.2, 133.7, 131.3, 129.9, 128.5, 125.8, 125.2, 124.9, 124.7, 123.5, 123.4, 123.1, 122.0, 121.9,

113.3, 106.8, 71.1, 70.9, 22.9, 22.8, 10.9, 10.8 ppm. One signal coincident or not observed.

IR (FT-ATR): $\tilde{\nu}$ = 3057 (w), 2960 (w), 2927 (w), 2872 (w), 1609 (m), 1507 (s), 1488 (m), 1453 (s), 1418 (s), 1389 (m), 1376 (m), 1307 (w), 1281 (m), 1255 (s), 1227 (s), 1205 (m), 1179 (s), 1160 (m), 1137 (m), 1102 (s), 1062 (m), 1042 (m), 1025 (m), 1006 (m), 964 (m), 876 (m), 831 (s), 805 (m), 774 (m), 748 (s), 730 (s), 663 (w), 649 (w), 521 (w), 442 (m) cm^{-1}.

UV/Vis (CH_2Cl_2, rt): λ_{max} (ε) 660 (56900), 609 (42200), 448 (37600), 355 (75000), 267 (108000) nm (M^{-1} cm^{-1}).

HRMS (MALDI, dctb): calcd. for $C_{112}H_{88}O_8S_4$: 1688.5357 [M^+]; found: 1688.5364.

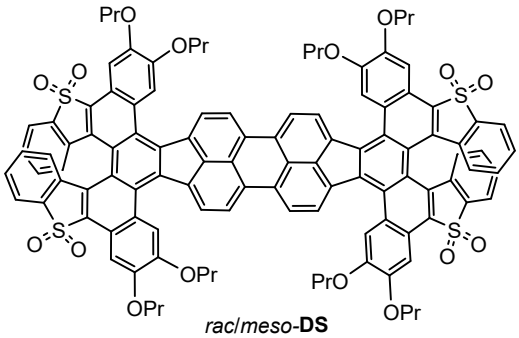

rac/*meso*-**DS**
mixture of diastereomers

Bis(2,3,12,13-tetrapropoxyacenaphtho[1',2':13,14][1]benzothieno[3',2':7,8] piceno[5,6-*b*][1]benzothiophene-7,8-ylene)-*S,S,S',S',S'',S'',S''',S'''*-octaoxide (DS). In a glove box, [Ni(COD)$_2$] (8.50 mg, 30.9 µmol, 3.00 equiv.) was placed in a heated microwave flask, which was sealed with a rubber septum crimp cap and exported from the glove box. In a heated Schlenk flask was dissolved *rac*-**HS-Br$_2$** (11.0 mg, 10.3 µmol, 1.00 equiv.) and 4-(dimethylamino)pyridine (7.50 mg, 61.8 µmol, 6.00 equiv.) in anhyd. THF (2.0 mL, degassed by N_2 bubbling). To the microwave flask was added cyclooctadiene (4.0 µL, 30.9 µmol, 3.00 equiv., dissolved in THF (40 µL)) and the prepared solution of the starting material and 4-(dimethylamino)pyridine. The flask was stirred at rt for 2 d. The contents of the flask were transferred to a round-bottom flask and the solvent was removed under reduced pressure. The product was purified by flash column chromatography (SiO_2, PE/CH_2Cl_2/EtOAc 9/9/2) and obtained as dark green solid (1.30 mg, 715 nmol, 14%) as mixture of *rac*-**DS** and *meso*-**DS**.

R_f = 0.13 (SiO_2, PE/EtOAc 7:3).

^{1}H NMR (600 MHz, $CDCl_3$): δ 8.73 (s, 4H), 8.62 (dd, *J* = 7.9, 1.3 Hz, 4H), 8.06 (d, *J* = 8.0 Hz, 4H), 7.92 (s, 4H), 7.66 – 7.61 (m, 8H), 7.26 (t, *J* = 7.6 Hz, 4H), 7.20 (t, *J* = 7.3 Hz, 4H), 4.42 – 4.30 (m, 8H), 4.27 – 4.17 (m, 8H), 2.12 – 2.02 (m, 8H), 2.03 – 1.92 (m, 8H), 1.21 (t, *J* = 7.4 Hz, 12H), 1.11 (t, *J* = 7.4 Hz, 12H) ppm.

^{13}C NMR (151 MHz, $CDCl_3$): δ 152.3, 149.7, 138.2, 136.5, 136.0, 133.9, 133.7, 133.4, 132.4, 129.6, 128.6, 128.09, 128.05, 126.6, 126.0, 125.9, 123.2, 123.0, 121.6, 112.1, 104.0, 71.0, 70.9, 22.8, 22.6, 10.8, 10.7 ppm. Two signals coincident or not observed.

UV/Vis (CH_2Cl_2, rt): λ_{max} (ε) 657 (55800), 606 (36500), 445 (24600), 379 (66800), 318 (64000), 272 (90900), 248 (104000) nm (M^{-1} cm^{-1}).

HRMS (MALDI, dctb): calcd. for $C_{112}H_{88}O_{16}S_4$: 1816.4950 [M^+]; found: 1816.4965.

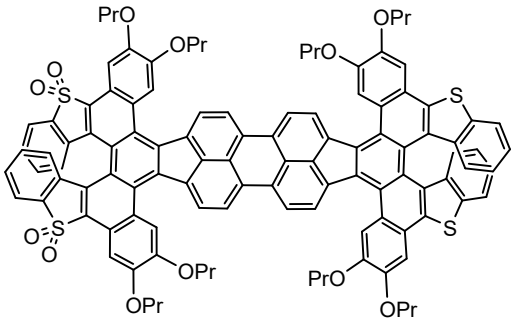

(*M*,*M*)-**DS**

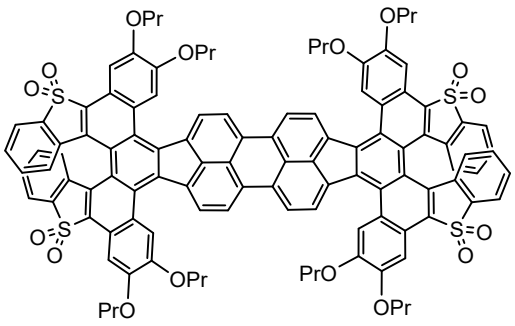

(*P*,*P*)-**DS**

Bis(2,3,12,13-tetrapropoxyacenaphtho[1',2':13,14][1]benzothieno[3',2':7,8] piceno[5,6-*b*][1]benzothiophene-7,8-ylene)-*S,S,S',S',S'',S'',S''',S'''*-octaoxide (DS). The reaction was conducted twice, once for each enantiomer. Under an N_2 atmosphere, a microwave flask (5 mL) was charged with **DT** ((*P,P*): 2.4 mg, 1.4 µmol, 1.0 equiv.; (*M,M*): 2.0 mg, 1.2 µmol, 1.0 equiv.), *m*CPBA ((*P,P*): 11.9 mg, 69.0 µmol, 48.6 equiv.; (*M,M*): 13.2 mg, 76.5 µmol, 64.6 equiv.), and CH_2Cl_2 (0.5 mL) while stirring in an ice bath (0 °C). After stirring for 7 h at 0 °C, the reaction was quenched by the addition of aq. K_2CO_3 (0.7 M, 5 mL) and diluted with CH_2Cl_2 (10 mL). Phases were separated, and the organic phase washed with aq. K_2CO_3 (0.7 M, 2 x 10 mL), dried over $MgSO_4$, and concentrated under reduced pressure. The crude product was purified by column chromatography (SiO2, PE/CH_2Cl_2/EtOAc 6/4/1) to obtain the product as dark green solid ((*P,P*): 0.9 mg, 0.50 µmol, 35%; (*M,M*): 0.5 mg, 0.27 µmol, 23%).

3. UV/Vis Absorption and Emission Data

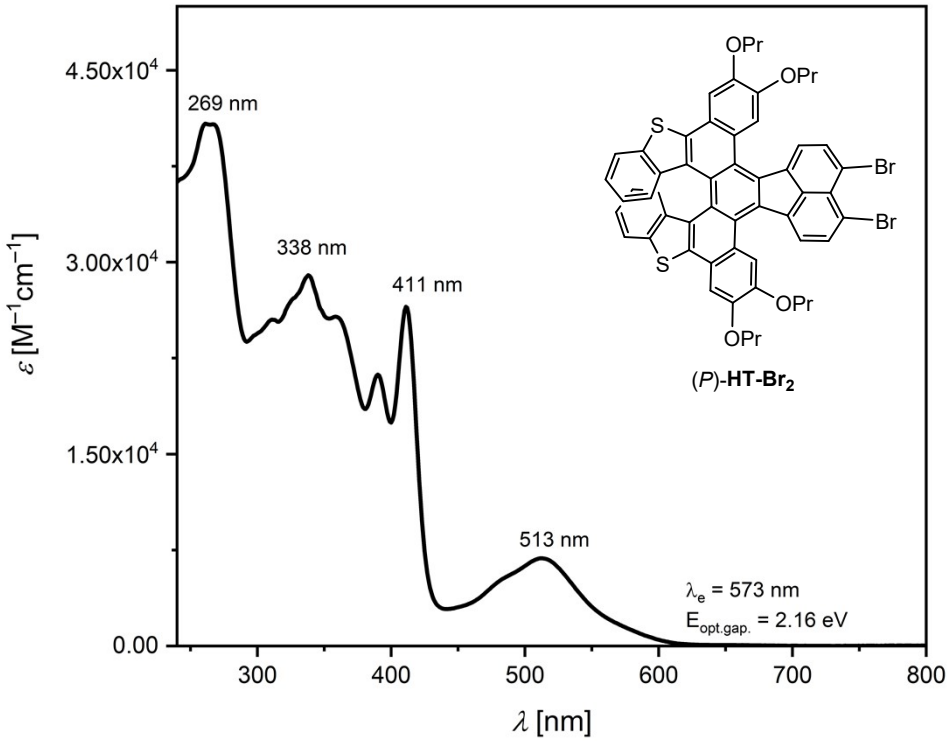

Figure S2. UV/Vis absorption spectrum of (*P*)-**HT-Br$_2$** in CH_2Cl_2 at rt.

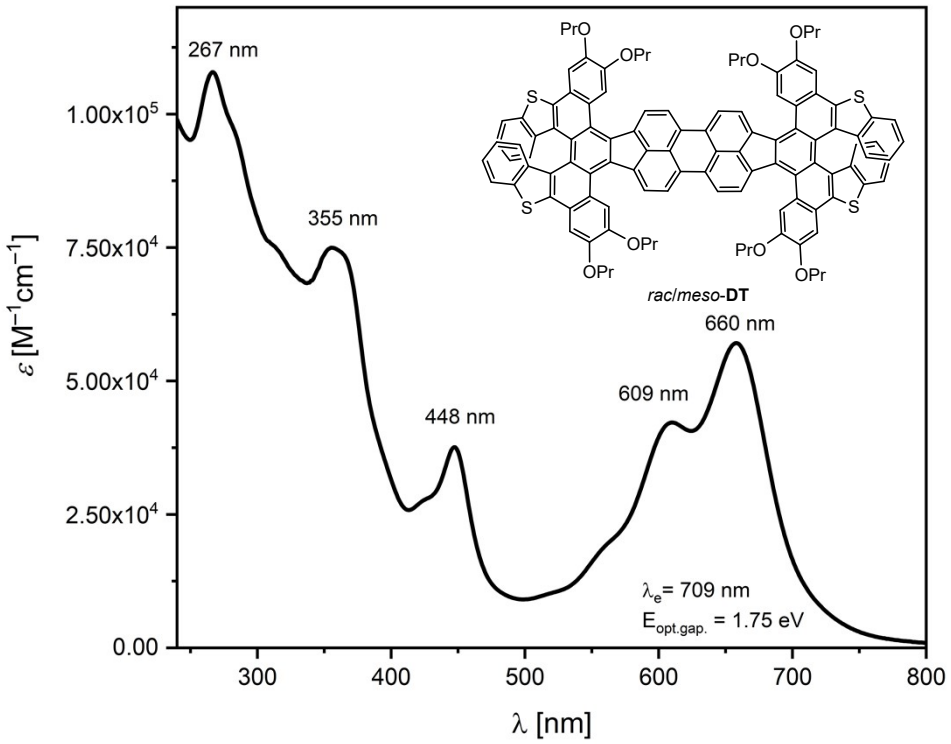

Figure S3. UV/Vis absorption spectrum of *rac*/*meso*-**DT** (mixture of diastereomers) in CH_2Cl_2 at rt.

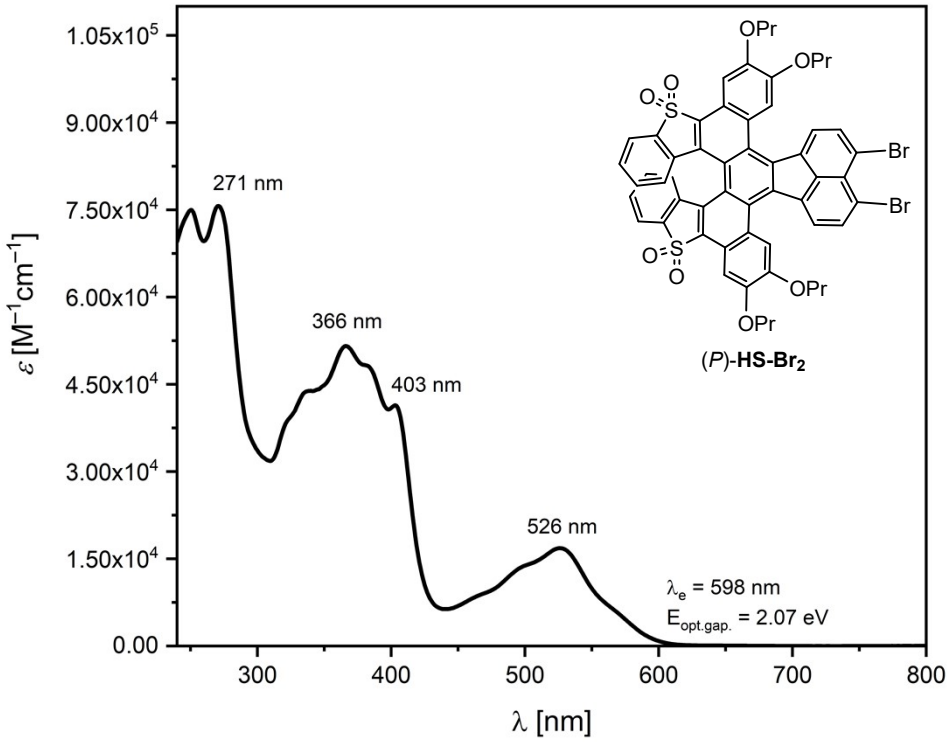

Figure S4. UV/Vis absorption spectrum of (*P*)-**HS-Br$_2$** in CH_2Cl_2 at rt.

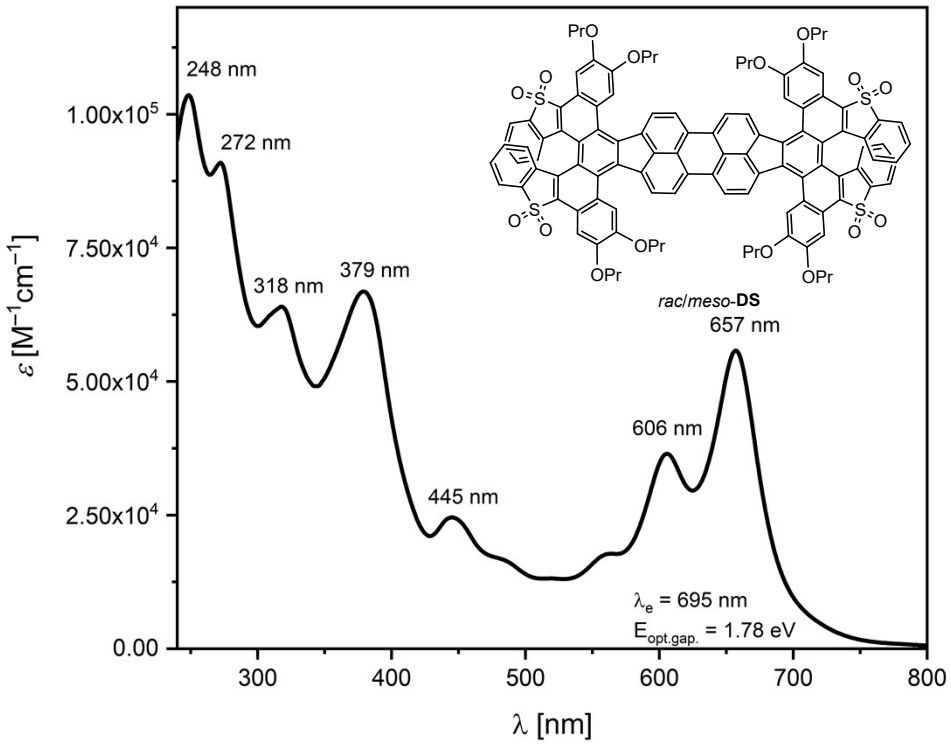

Figure S5. UV/Vis absorption spectrum of *rac*/*meso*-**DS** in CH_2Cl_2 at rt.

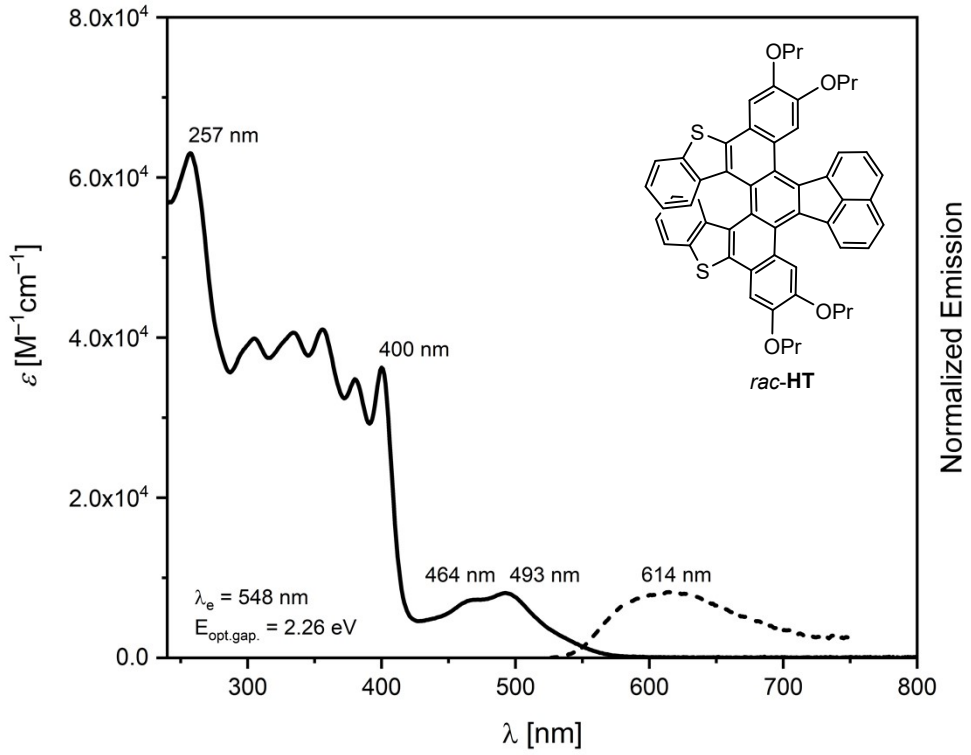

Figure S6. UV/Vis absorption spectrum of *rac*-**HT** in CH_2Cl_2 at rt. Emission with λ_{ex} = 490 nm, QY = 1.9%.

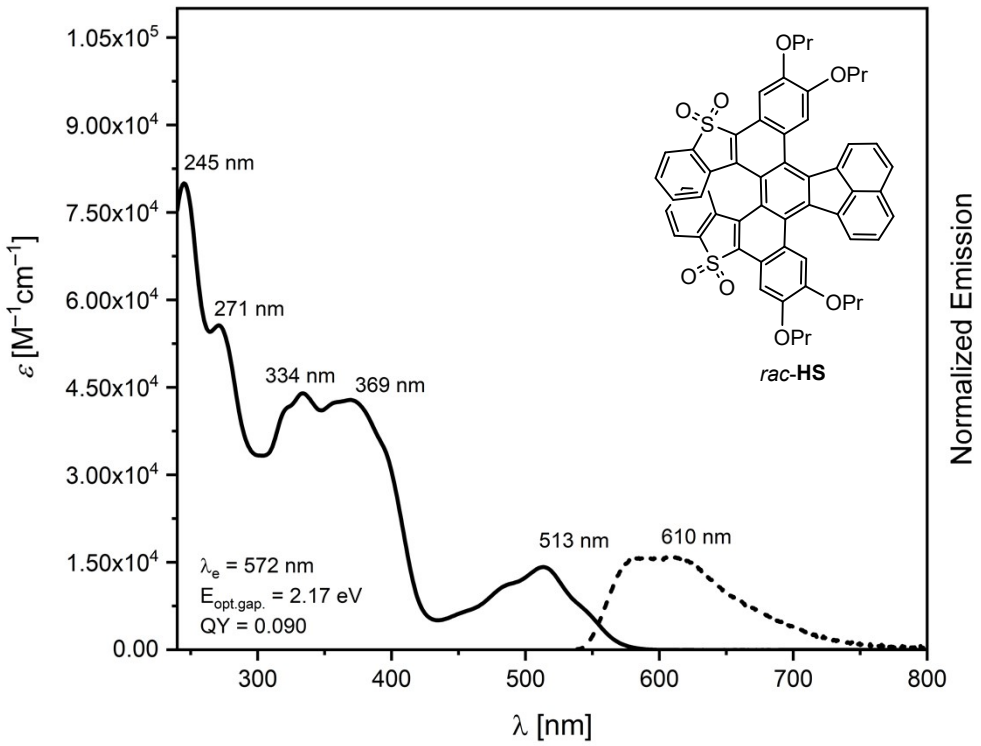

Figure S7. UV/Vis absorption spectrum of *rac*-**HS** in CH_2Cl_2 at rt. Emission with λ_{ex} = 525 nm. With λ_{ex} = 510 nm: QY = 9.0%.

4. Theoretical UV/Vis Absorption Data

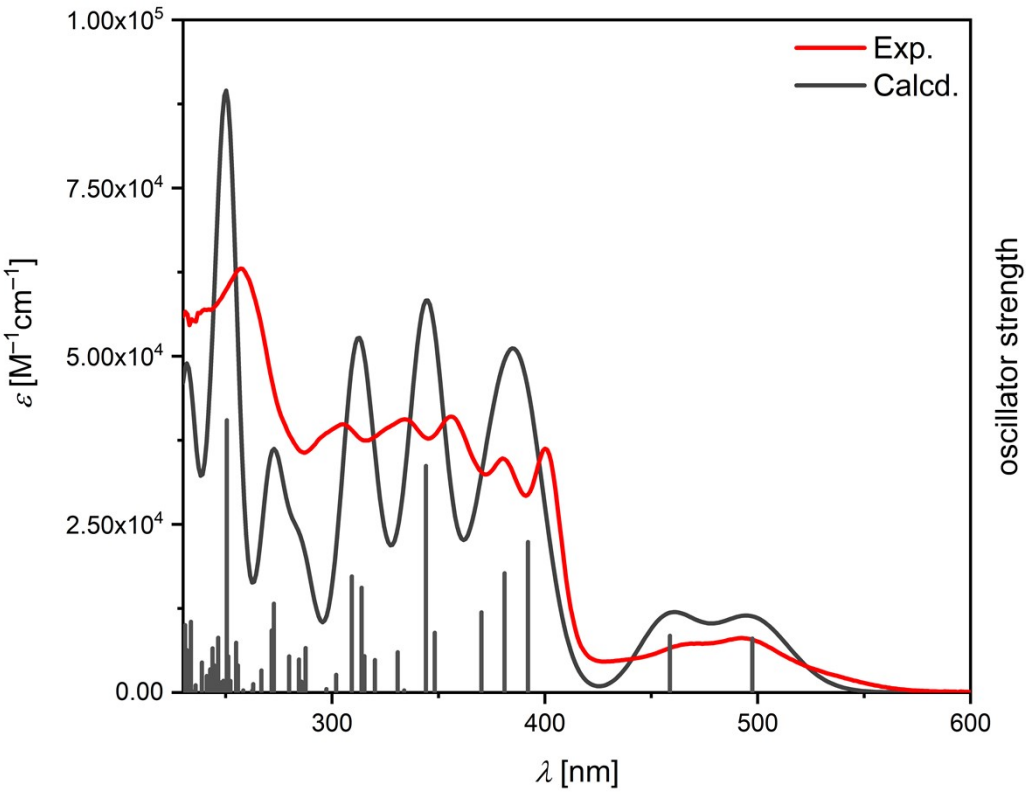

Figure S8. Theoretical UV/Vis absorption spectrum calculated by TD-DFT (CAM-B3LYP(D3BJ)/def2-TZVP/SMD(CH_2Cl_2), line width 0.10 eV) of **HT**, redshifted by 0.39 eV, compared to the experimental spectrum (CH_2Cl_2). Oscillator strength and theoretical spectrum scaled to match experimental data.

Table S1: Vertical excitations of **HT** calculated by TD-DFT (CAM-B3LYP(D3BJ)/def2-TZVP/ SMD(CH_2Cl_2)).

Excitation	*E* [eV]	λ [nm]	Type	*f*
S_1	2.88	430	HOMO → LUMO (0.66)	0.16
S_2	3.09	401	HOMO−1 → LUMO (0.58)	0.17
S_3	3.55	349	HOMO−2 → LUMO (0.44)	0.45
S_4	3.64	340	HOMO−2 → LUMO (0.44)	0.35
S_5	3.74	332	HOMO−1 → LUMO+1 (0.59)	0.24
S_6	3.95	314	HOMO−2 → LUMO+1 (0.46)	0.18
S_7	3.99	311	HOMO−3 → LUMO (0.30)	0.67
S_8	4.10	302	HOMO → LUMO+2 (0.48)	0.01
S_9	4.14	300	HOMO−3 → LUMO (0.44)	0.12
S_{10}	4.26	291	HOMO−8 → LUMO (0.45)	0.10

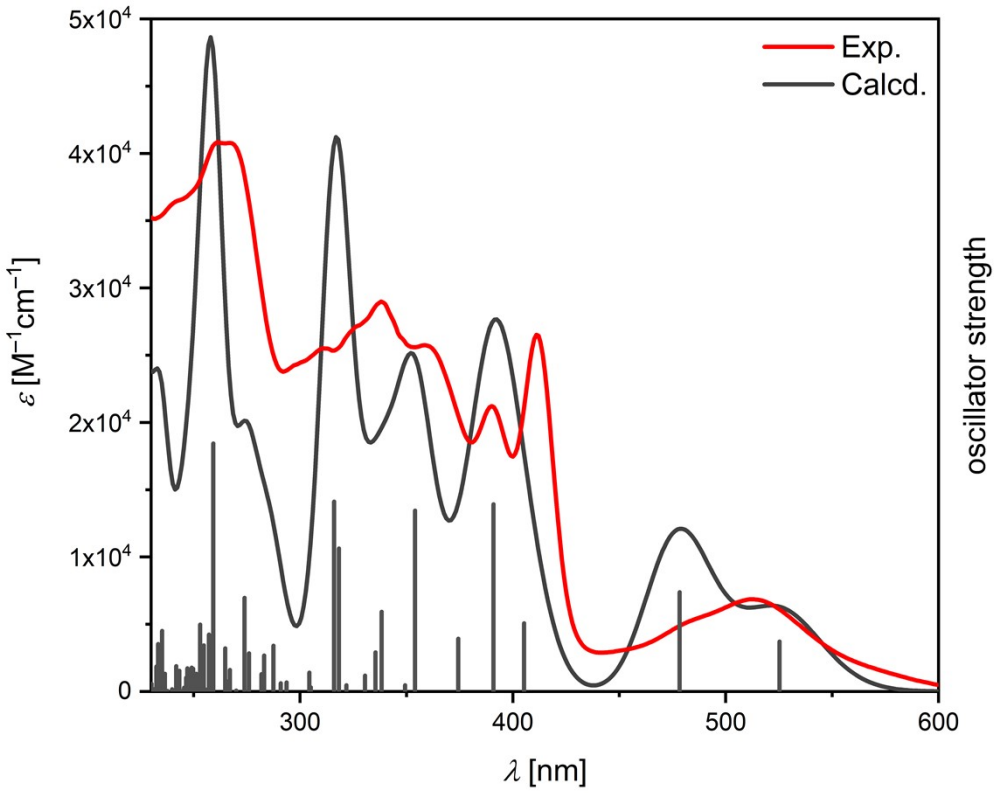

Figure S9. Theoretical UV/Vis absorption spectrum calculated by TD-DFT (CAM-B3LYP(D3BJ)/def2-TZVP/SMD(CH_2Cl_2), line width 0.10 eV) of **HT-Br$_2$**, redshifted by 0.39 eV, compared to the experimental spectrum (CH_2Cl_2). Oscillator strength and theoretical spectrum scaled to match experimental data.

Table S2: Vertical excitations of **HT-Br$_2$** calculated by TD-DFT (CAM-B3LYP(D3BJ)/def2-TZVP/ SMD(CH_2Cl_2)).

Excitation	*E* [eV]	λ [nm]	Type	*f*
S_1	2.75	451	HOMO → LUMO (0.66)	0.15
S_2	2.98	416	HOMO−1 → LUMO (0.60)	0.30
S_3	3.45	359	HOMO−2 → LUMO (0.57)	0.20
S_4	3.56	348	HOMO → LUMO+1 (0.55)	0.56
S_5	3.70	335	HOMO−1 → LUMO+1 (0.56)	0.16
S_6	3.89	319	HOMO−6 → LUMO (0.33)	0.54
S_7	3.94	315	HOMO−2 → LUMO+1 (0.43)	0.02
S_8	4.05	306	HOMO → LUMO+3 (0.37)	0.24
S_9	4.09	303	HOMO → LUMO+2 (0.49)	0.12
S_{10}	4.14	299	HOMO−5 → LUMO (0.49)	0.05

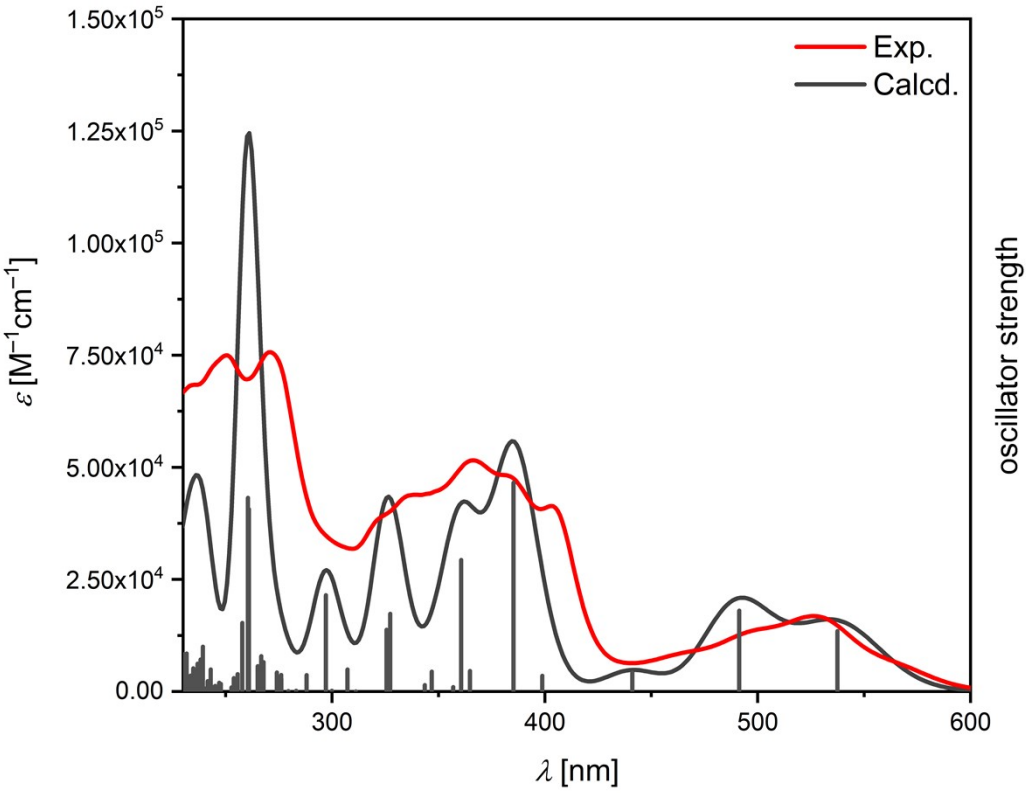

Figure S10. Theoretical UV/Vis absorption spectrum calculated by TD-DFT (CAM-B3LYP(D3BJ)/def2-TZVP/SMD(CH_2Cl_2), line width 0.10 eV) of **HS-Br$_2$**, redshifted by 0.39 eV, compared to the experimental spectrum (CH_2Cl_2). Oscillator strength and theoretical spectrum scaled to match experimental data.

Table S3: Vertical excitations of **HS-Br$_2$** calculated by TD-DFT (CAM-B3LYP(D3BJ)/def2-TZVP/ SMD(CH_2Cl_2)).

Excitation	*E* [eV]	*λ* [nm]	Type	*f*
S_1	2.70	460	HOMO → LUMO (0.66)	0.22
S_2	2.91	426	HOMO−1 → LUMO (0.61)	0.30
S_3	3.20	387	HOMO−2 → LUMO (0.63)	0.07
S_4	3.50	354	HOMO → LUMO+2 (0.45)	0.06
S_5	3.61	344	HOMO → LUMO+1 (0.54)	0.78
S_6	3.79	327	HOMO−1 → LUMO+1 (0.37)	0.08
S_7	3.83	324	HOMO−1 → LUMO+1 (0.43)	0.49
S_8	3.86	321	HOMO → LUMO+3 (0.45)	0.02
S_9	3.96	313	HOMO−4 → LUMO (0.46)	0.07
S_{10}	4.00	310	HOMO−3 → LUMO (0.35)	0.02

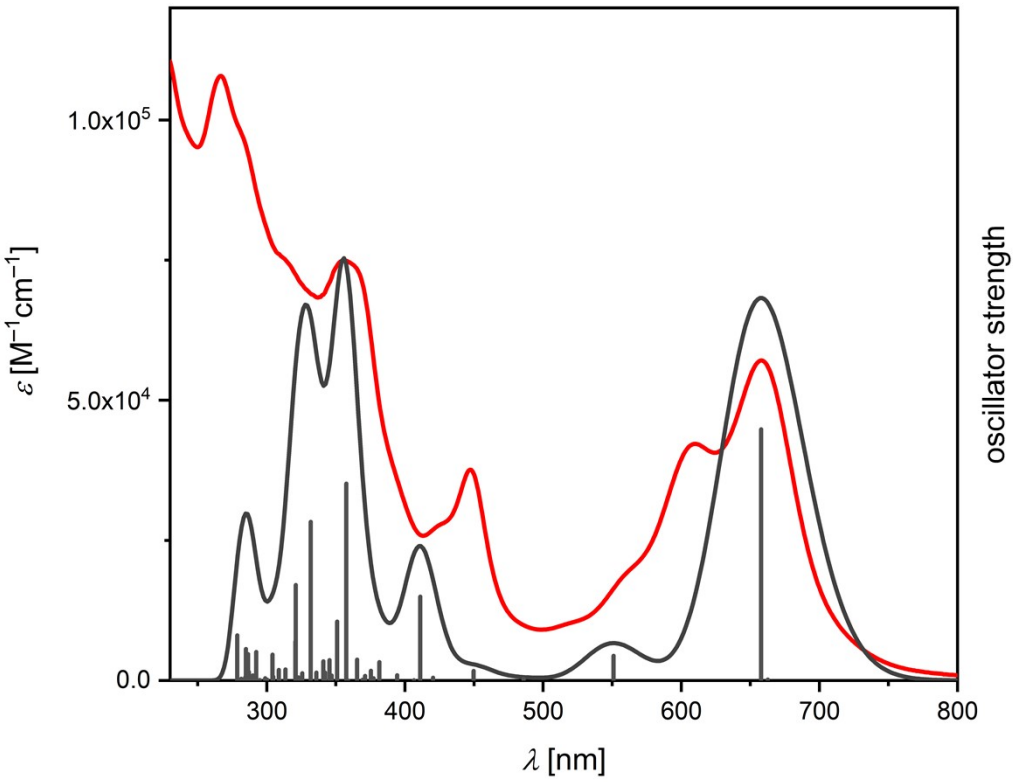

Figure S11. Theoretical UV/Vis absorption spectrum calculated by TD-DFT (CAM-B3LYP(D3BJ)/def2-TZVP/SMD(CH_2Cl_2), line width 0.10 eV) of **DT**, redshifted by 0.39 eV, compared to the experimental spectrum (CH_2Cl_2). Oscillator strength and theoretical spectrum scaled to match experimental data.

Table S4: Vertical excitations of **DT** calculated by TD-DFT (CAM-B3LYP(D3BJ)/def2-TZVP/ SMD(CH_2Cl_2)).

Excitation	***E* [eV]**	**λ [nm]**	**Type**	***f***
S_1	2.26	548	HOMO−1 → LUMO (0.64)	0.01
S_2	2.27	545	HOMO → LUMO (0.66)	1.68
S_3	2.64	470	HOMO−2 → LUMO (0.62)	0.17
S_4	2.94	421	HOMO−3 → LUMO (0.55)	0.01
S_5	3.15	394	HOMO−4 → LUMO (0.53)	0.06
S_6	3.34	371	HOMO−5 → LUMO (0.55)	0.02
S_7	3.41	364	HOMO−1 → LUMO+2 (0.37)	0.56
S_8	3.44	360	HOMO−6 → LUMO (0.39)	0.00
S_9	3.53	351	HOMO−1 → LUMO+3 (0.39)	0.04
S_{10}	3.64	341	HOMO → LUMO+3 (0.34)	0.12

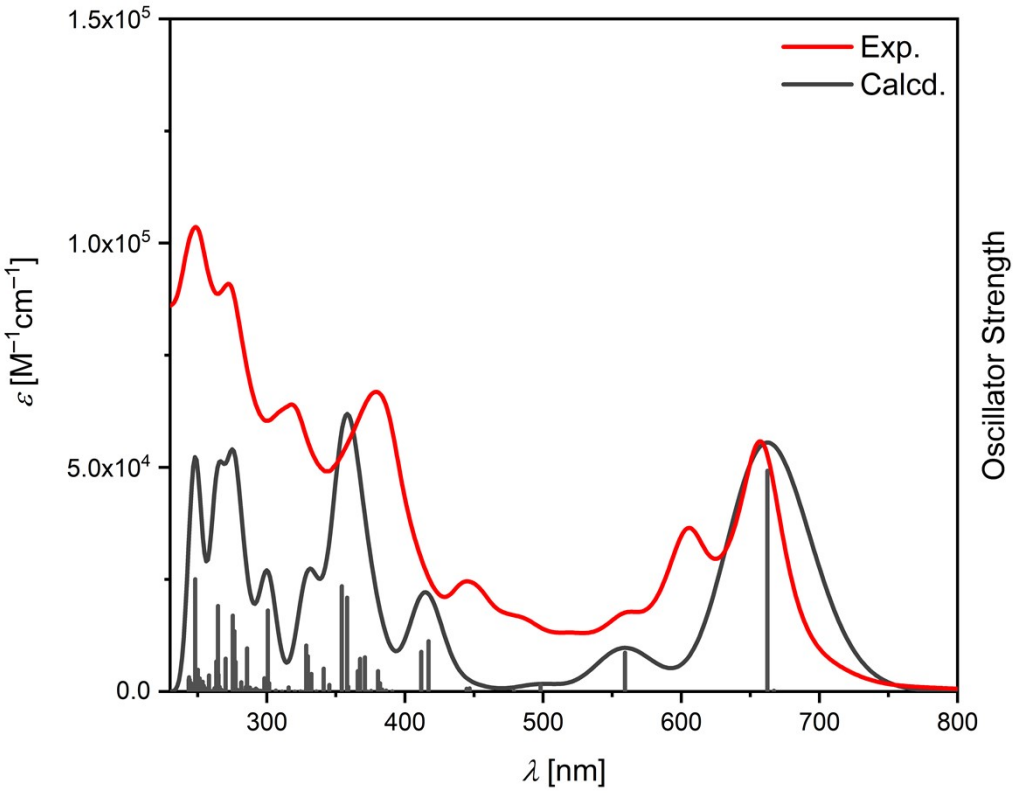

Figure S12. Theoretical UV/Vis absorption spectrum calculated by TD-DFT (CAM-B3LYP(D3BJ)/def2-TZVP/SMD(CH_2Cl_2), line width 0.10 eV) of **DS**, redshifted by 0.39 eV, compared to the experimental spectrum (CH_2Cl_2). Oscillator strength and theoretical spectrum scaled to match experimental data.

Table S5: Vertical excitations of **DS** calculated by TD-DFT (CAM-B3LYP(D3BJ)/def2-TZVP/ SMD(CH_2Cl_2)).

Excitation	***E* [eV]**	**λ [nm]**	**Type**	***f***
S_1	2.25	551	HOMO−1 → LUMO (0.64)	0.01
S_2	2.26	548	HOMO → LUMO (0.67)	1.64
S_3	2.61	476	HOMO−2 → LUMO (0.59)	0.29
S_4	2.88	431	HOMO−3 → LUMO (0.51)	0.05
S_5	2.98	416	HOMO−4 → LUMO (0.54)	0.00
S_6	3.17	392	HOMO−5 → LUMO (0.39)	0.02
S_7	3.18	390	HOMO−2 → LUMO+1 (0.34)	0.02
S_8	3.36	369	HOMO−6 → LUMO (0.40)	0.37
S_9	3.40	365	HOMO−1 → LUMO+1 (0.39)	0.29
S_{10}	3.56	348	HOMO → LUMO+1 (0.38)	0.00

5. Separation of Enantiomers by Chiral HPLC

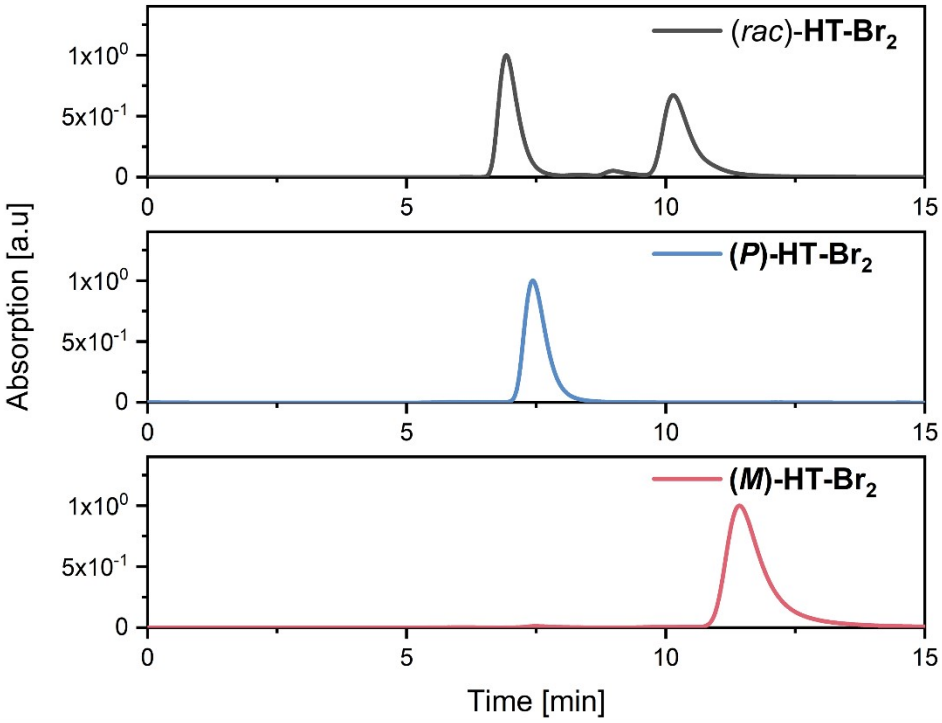

Figure S13. Analytical chiral HPLC chromatograph at 412 nm of the separation of enantiomers of **HT-Br$_2$** using a mixture of *n*-heptane and isopropanol (98:2 v/v) as the mobile phase and ChiralPak IA-3 as the stationary phase. Top: Racemate (black); Middle: First fraction of enantiopure sample (blue); Bottom: Second fraction of enantiopure sample (red).

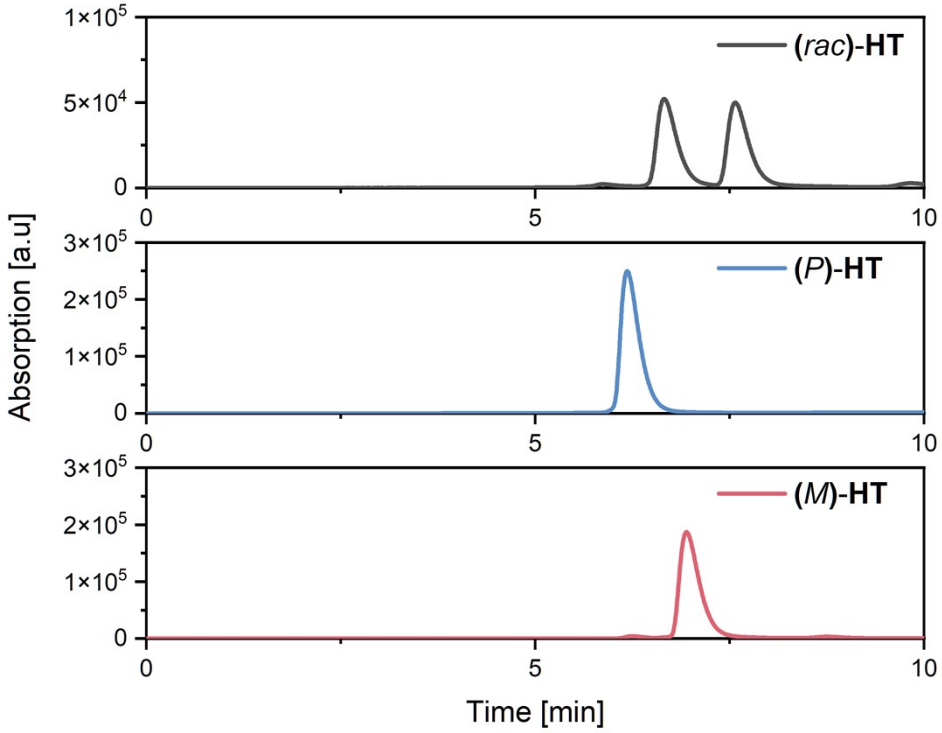

Figure S14. Analytical chiral HPLC chromatograph at 493 nm of the separation of enantiomers of **HT** using a mixture of *n*-heptane and CH_2Cl_2 (5:1 v/v) as the mobile phase and ChiralPak IA-3 as the stationary phase. Top: Racemate (black); Middle: First fraction of enantiopure sample (blue); Bottom: Second fraction of enantiopure sample (red).

6. Experimental and Simulated Electronic Circular Dichroism Data

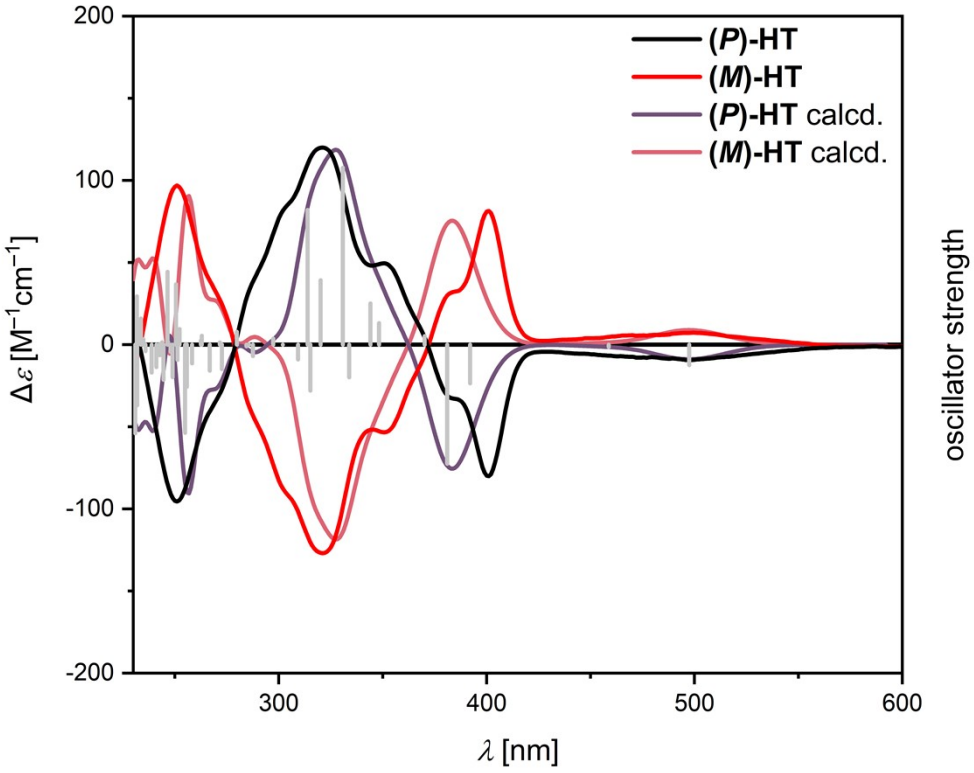

Figure S15. Experimental CD spectra of (*M*)-**HT** and (*P*)-**HT** in CH_2Cl_2 at ca. 2×10^{-5} M. Calculated oscillator strength of (*P*)-enantiomer (grey bars) and CD spectra at CAM-B3LYP(D3BJ)/def2-TZVP/SMD(CH_2Cl_2) level of theory (redshifted by 0.39 eV for comparison, line width 0.10 eV).

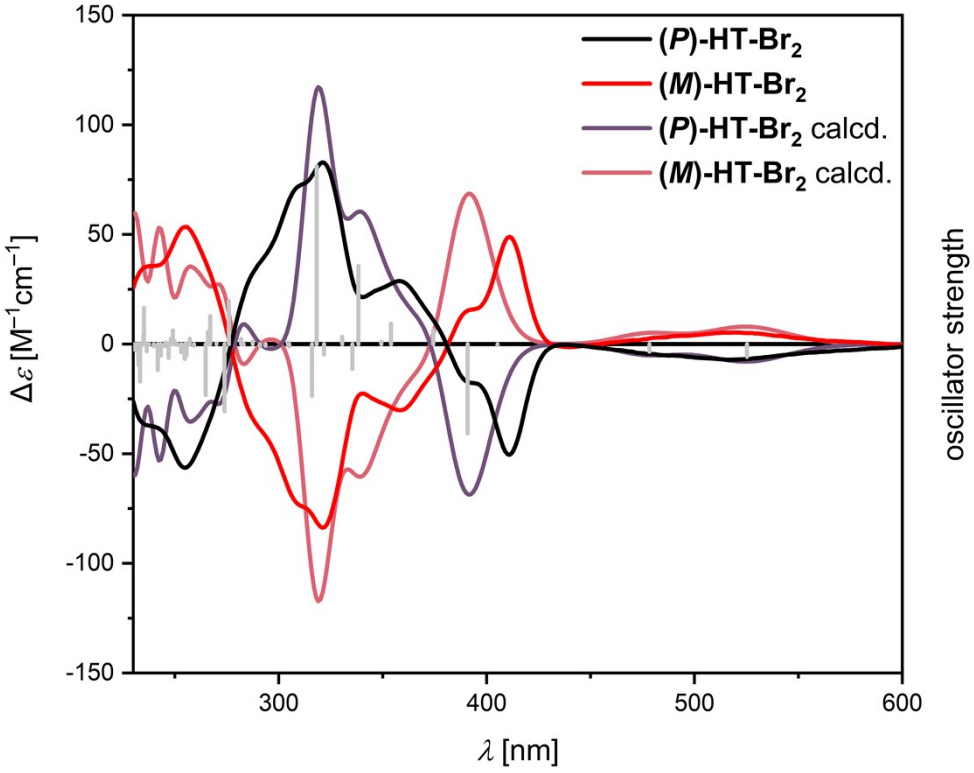

Figure S16. Experimental CD spectra of (*M*)-**HT-Br$_2$** and (*P*)-**HT-Br$_2$** in CH_2Cl_2 at ca. 3 × 10^{-5} M. Calculated oscillator strength of (*P*)-enantiomer (grey bars) and CD spectra at CAM-B3LYP(D3BJ)/def2-TZVP/SMD(CH_2Cl_2) level of theory (scaled arbitrarily and redshifted by 0.39 eV for comparison, line width 0.10 eV).

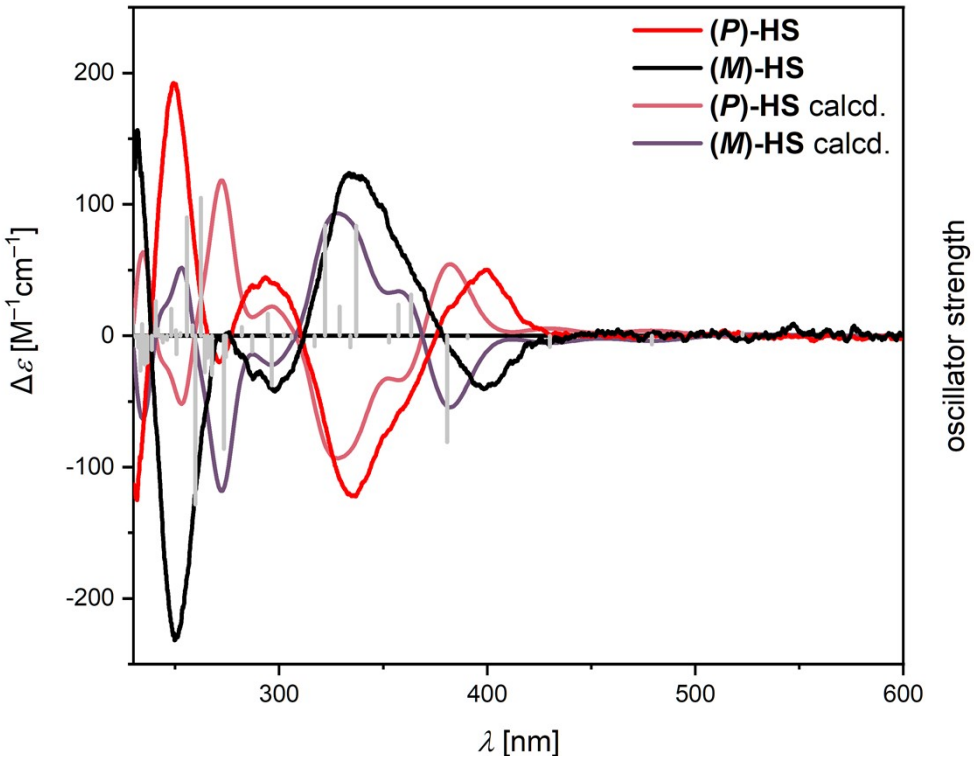

Figure S17. Experimental CD spectra of (*M*)-**HS** and (*P*)-**HS** in CH_2Cl_2 at ca. 1 × 10^{-5} M. Calculated oscillator strength of (*P*)-enantiomer (grey bars) and CD spectra at CAM-B3LYP(D3BJ)/def2-TZVP/SMD(CH_2Cl_2) level of theory (redshifted by 0.39 eV for comparison, line width 0.10 eV).

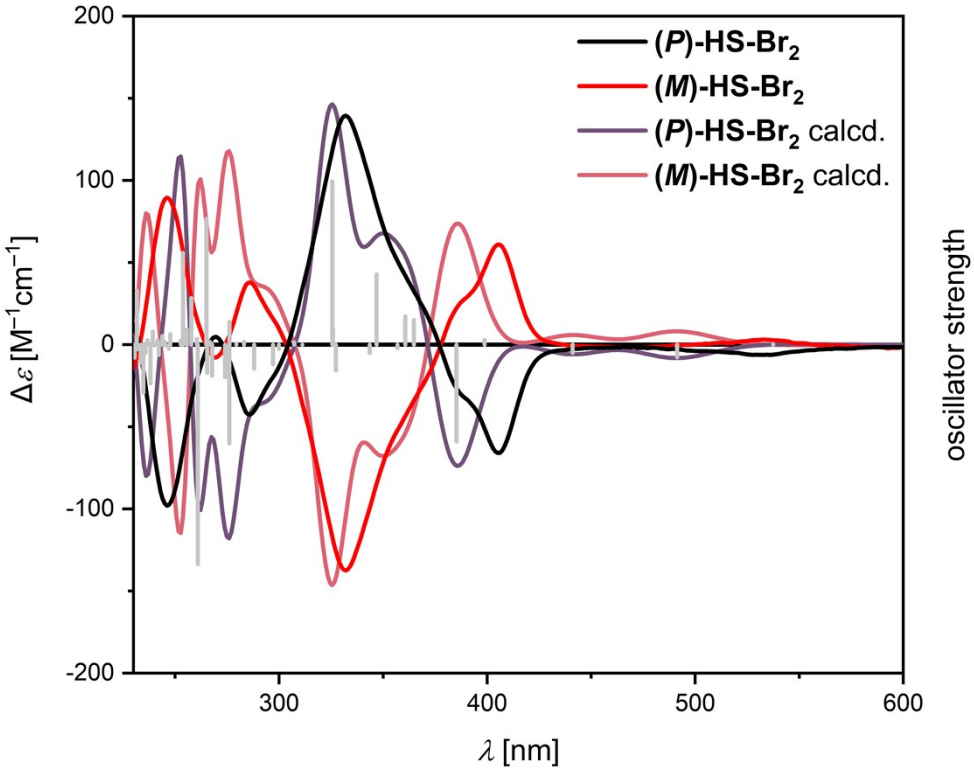

Figure S18. Experimental CD spectra of (*M*)-**HS-Br$_2$** and (*P*)-**HS-Br$_2$** in CH_2Cl_2 at ca. 1.4×10^{-5} M. Calculated oscillator strength of (*P*)-enantiomer (grey bars) and CD spectra at CAM-B3LYP(D3BJ)/def2-TZVP/SMD(CH_2Cl_2) level of theory (scaled arbitrarily and redshifted by 0.39 eV for comparison, line width 0.10 eV).

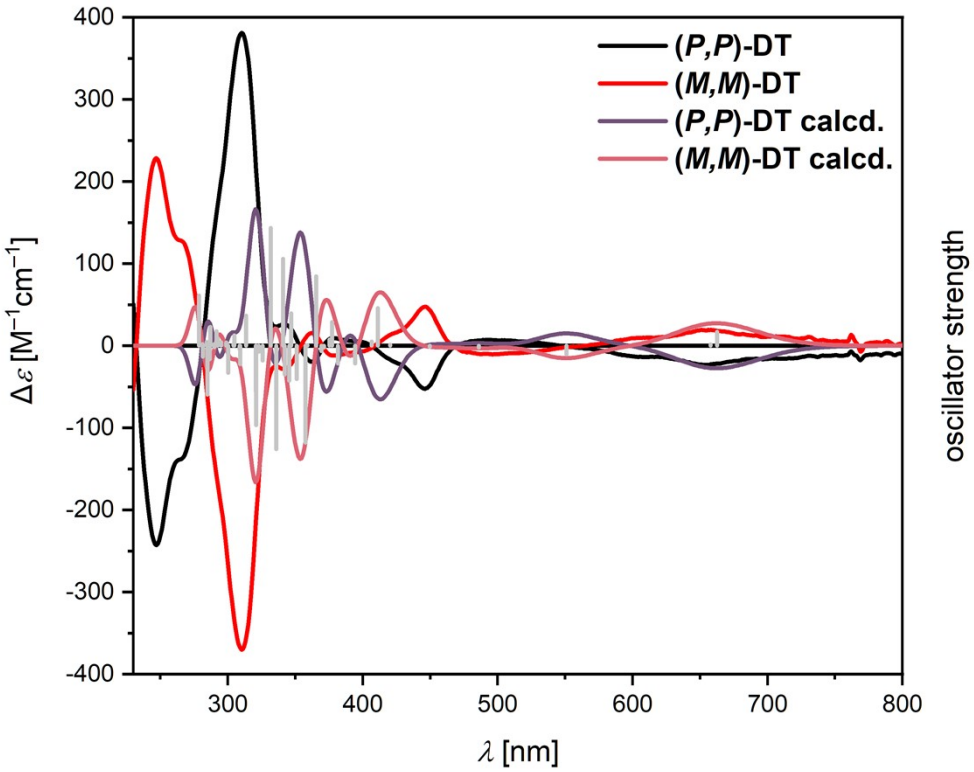

Figure S19. Experimental CD spectra of (*M,M*)-**DT** and (*P,P*)-**DT** in CH_2Cl_2 at ca. 1.3×10^{-5} M. Calculated oscillator strength of (*P*)-enantiomer (grey bars) and CD spectra at CAM-B3LYP(D3BJ)/def2-TZVP/SMD(CH_2Cl_2) level of theory (scaled arbitrarily and redshifted by 0.39 eV for comparison, line width 0.10 eV).

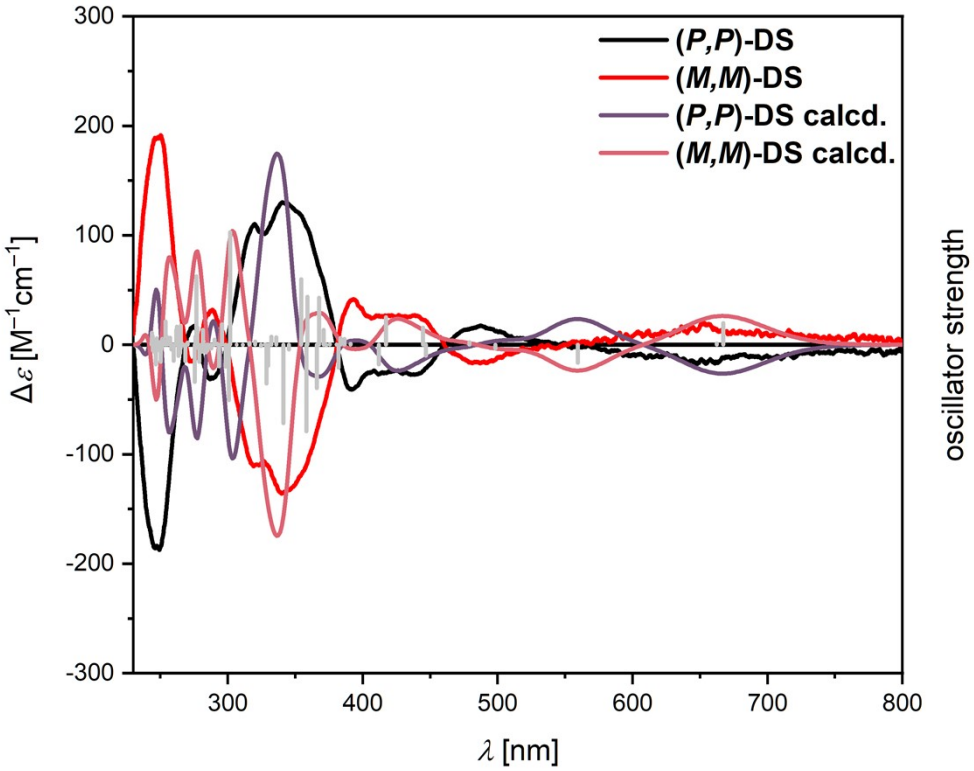

Figure S20. Experimental CD spectra of (*M,M*)-**DS** and (*P,P*)-**DS** in CH_2Cl_2 at ca. 0.7×10^{-5} M. Calculated oscillator strength of (*P*)-enantiomer (grey bars) and CD spectra at CAM-B3LYP(D3BJ)/def2-TZVP/SMD(CH_2Cl_2) level of theory (scaled arbitrarily and redshifted by 0.39 eV for comparison, line width 0.10 eV).

7. Plots of Frontier Molecular Orbitals

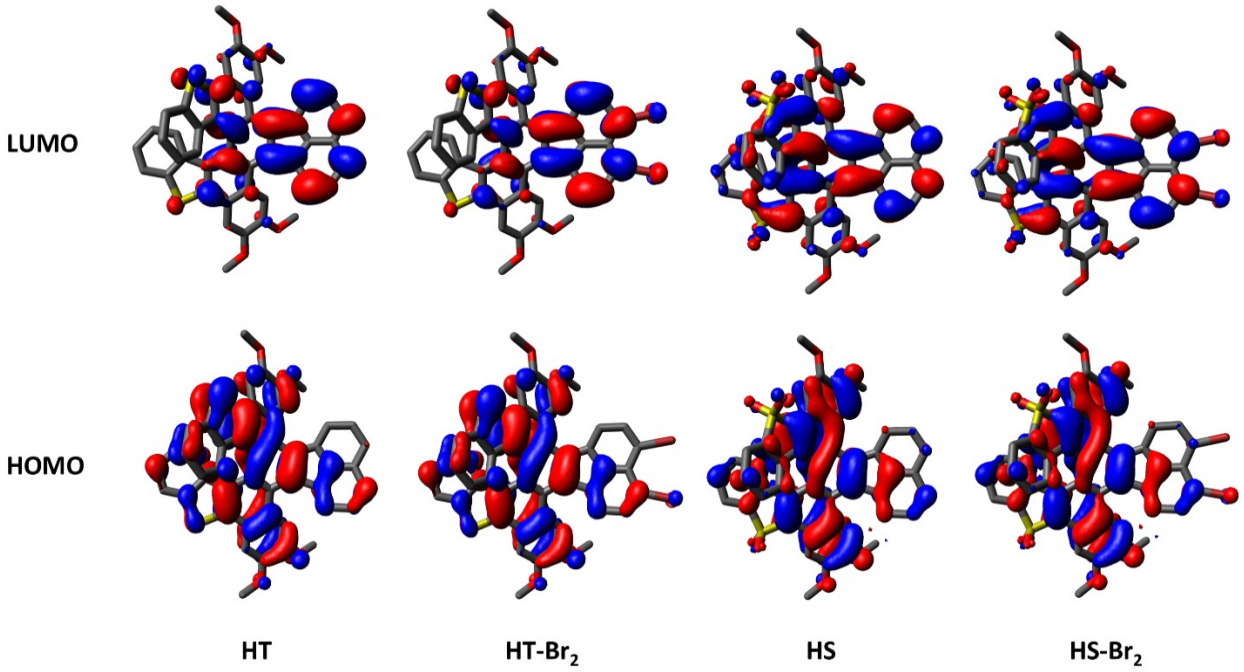

Figure S21. Visual representations of highest occupied molecular orbitals (HOMO) and lowest unoccupied molecular orbitals (LUMO) of monohelicenes at the CAM-B3LYP(D3BJ)/def2-TZVP/SMD(CH_2Cl_2) level of theory (isovalue = 0.02). *n*-Propoxy groups were shortened to methoxy groups. Hydrogen atoms are omitted for clarity.

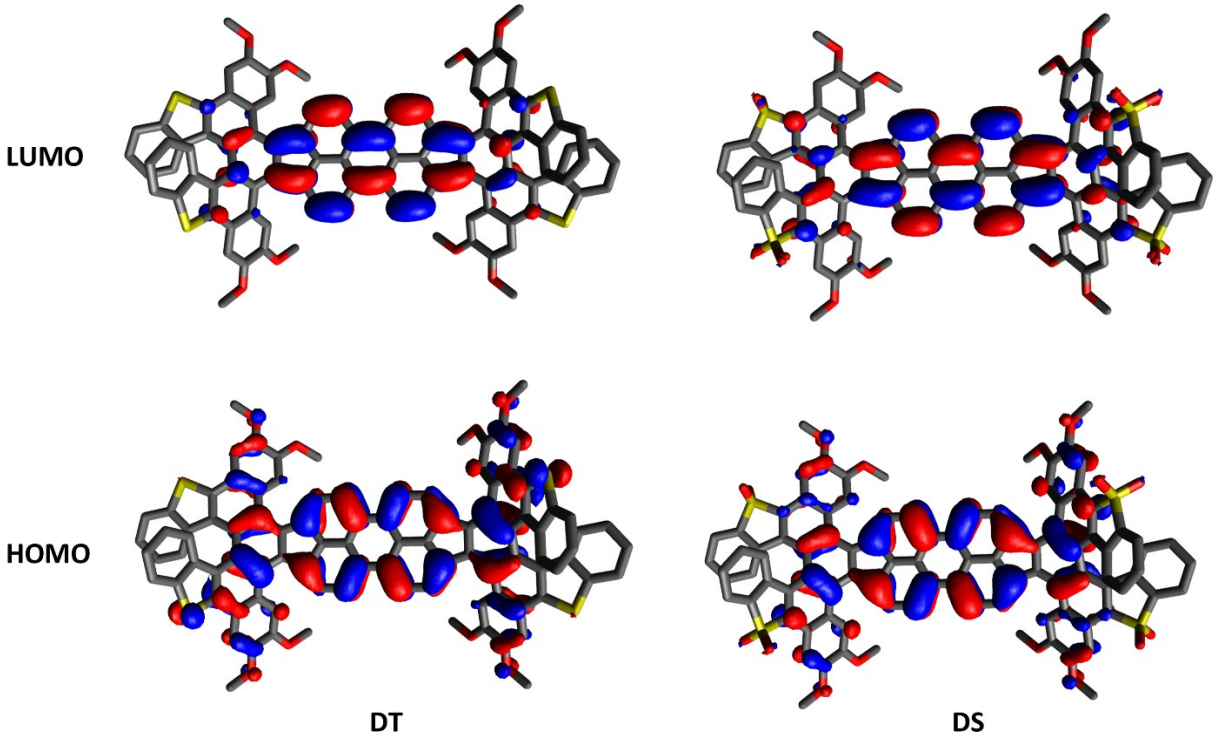

Figure S22. Visual representations of highest occupied molecular orbitals (HOMO) and lowest unoccupied molecular orbitals (LUMO) of **DT** and **DS** at the CAM-B3LYP(D3BJ)/def2-TZVP/SMD(CH_2Cl_2) level of theory (isovalue = 0.02). *n*-Propoxy groups were shortened to methoxy groups. Hydrogen atoms are omitted for clarity.

8. Theoretical Investigation of Configurational Energy Barriers

8.1. Inversion Barrier of Dithia[7]helicenes

The enantiomers of all isolated helicenes seem to be configurationally stable at room temperature, racemization has not been observed. To confirm this observation and to ensure that no racemization would occur during the subsequent reaction steps, computational analysis of the racemization process was conducted. To minimize computational effort, only monohelicene **HT** was investigated. The helicenes do not differ in any way that should significantly influence the isomerization barrier, therefore, the results should be transferable to the other dithia[7]helicenes in this work. Bromo substituents or a dimerization to the perylene should not impact the barrier significantly, as their steric influence should be minimal due to their location at the naphthylene unit opposite to the investigated helicene unit. To minimize computational effort, *n*-propoxy side chains were shortened to methoxy side chains. The *ortho*-positioned methoxy groups were rotated opposing each other, as observed in the crystal structure of **HT**. The r^{2}SCAN-3c method[34] was utilized. Minima were found by geometric optimization of appropriate guess structures; the transition state was found by constrained optimization of an appropriate guess structure, followed by saddle point optimization (Figure S23). With vibrational frequency analyses, the two minima and the transition state were verified to show 0 and 1 imaginary frequencies, respectively.

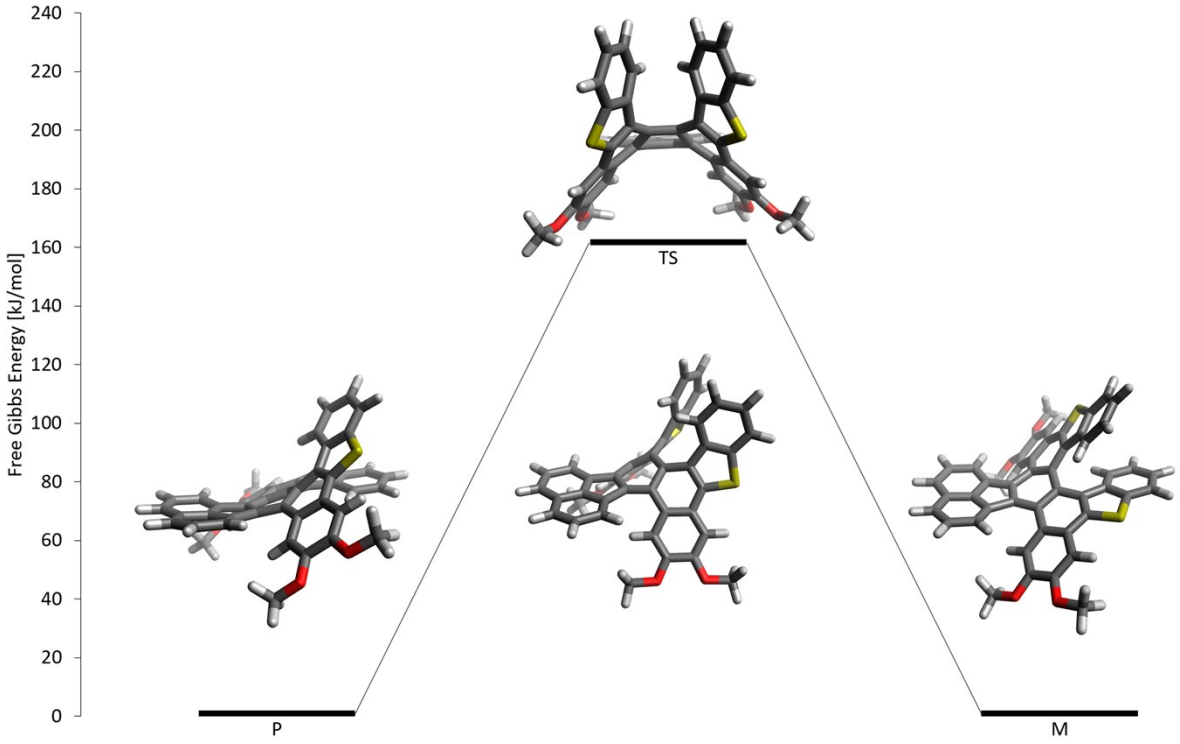

Figure S23: Energy diagram of the interconversion of the (*P*) and (*M*) enantiomers of **HT** (r^{2}SCAN-3c).[34] The C_s symmetrical transition state is highlighted. To minimize computational effort and avoid issues involving multiple conformers, the propyl groups were shortened to methyl groups.

The calculated transition state has C_s symmetry, with the terminal rings of the helicene unit bent almost perpendicular to the naphthalene core (Figure S23).

The rate constant of the inversion can be estimated using the transition state theory:[37,38]

$$k = \frac{\kappa k_B T}{h} e^{-\frac{\Delta G^{\ddagger}}{RT}}$$

k: Reaction rate constant, κ: Transmission coefficient estimated to be 1, k_B: Boltzmann constant; T: Temperature, h: Planck constant, $\Delta G^{\ddagger}$ Gibbs Free Activation Enthalpy estimated to be equal to Gibbs Free Activation Energy, R: Ideal gas constant.

The Gibbs free activation enthalpy of the interconversion was estimated to be around 159 kJ mol^{-1}, which corresponds to an estimated half-life of approximately 10^5 years at 300 K, or approximately one year at 373 K. Based on this estimation, racemization should not occur to any significant extent under the conditions employed in the subsequent reactions.

8.2. Inversion Barrier of [5]helicenes

Next to each dithia[7]helicene unit, the molecule features two [5]helicene units. In the global energy minima, these two [5]helicene units are heterochiral (Figure 3A, Figure S25), leading to a “tilt” of the dithia[7]helicene unit relative to the perylene backbone. In consequence, two diastereomeric forms, one “boat-shaped” and one “armchair-shaped” form of double dithia[7]helicene **DT** exist (Figure S24). Their isomerization barrier was investigated in this section.

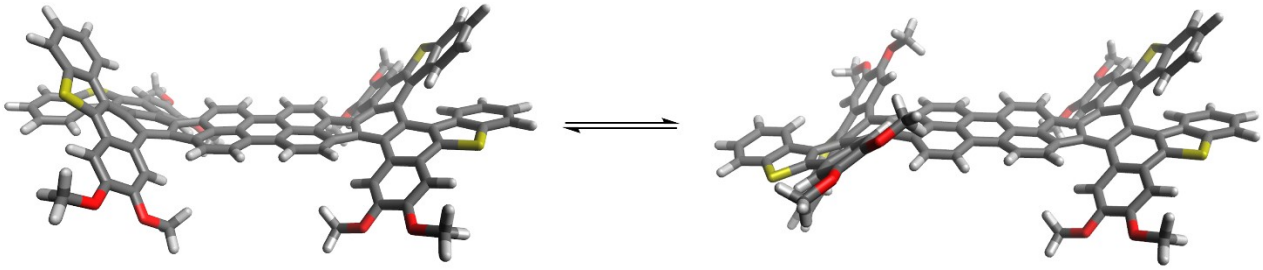

Figure S24: Equilibrium of "boat" (left) and "armchair" (right) isomers of **DT**.

The calculation employed the r^{2}SCAN-3c method. Using this method, the energies of both isomers differ insignificantly by <1 kJ mol^{-1}. Therefore, both halves of the molecule were considered independently, and one half of the molecule is used as model compound. To further reduce the computational effort, the *n*-propoxy groups were replaced by methoxy groups. The interconversion was assumed to proceed through the C_2-symmetric intermediate **I1** (Figure S25). For symmetry reasons, both transition states connecting **I1** with both C_1 symmetric lowest-energy conformers have the same energy, as they can be mapped through a rotation.

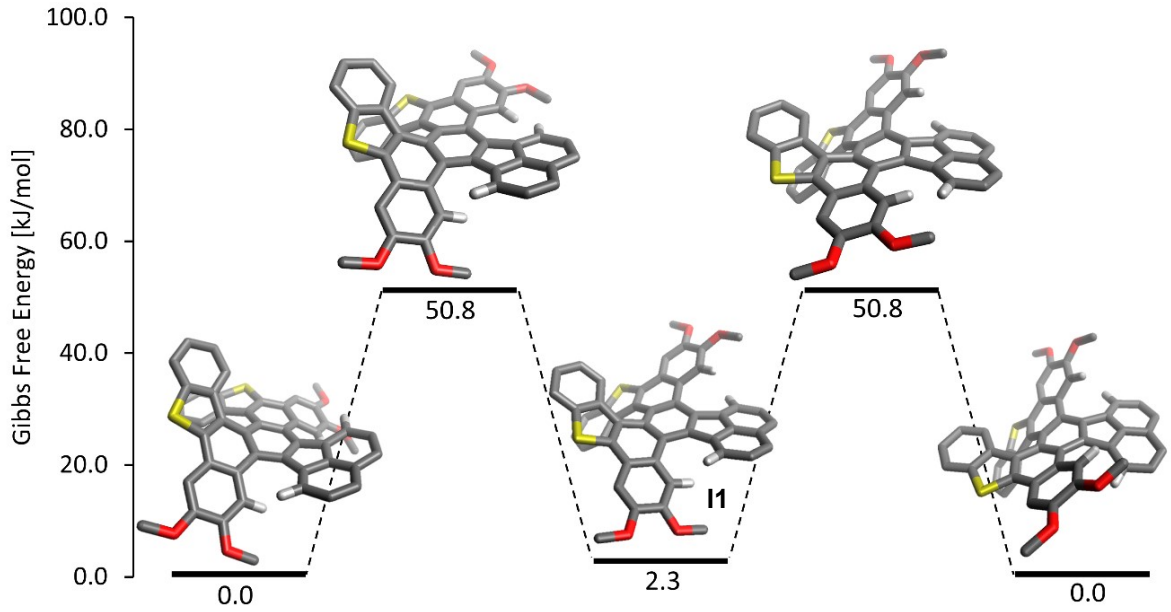

Figure S25: Energy diagram for the flip of the helicene unit relative to the naphthalene unit (r2SCAN-3c). Hydrogen aroms, except those especially relevant to the conversion, were omitted.

The rate constant of the inversion can be estimated using the transition state theory:[37,38]

$$k = 2\frac{\kappa k_B T}{h} e^{-\frac{\Delta G^{\ddagger}}{RT}}$$

k: Reaction rate constant, κ: Transmission coefficient estimated to be 1, k_B: Boltzmann constant; T: Temperature, h: Planck constant, $\Delta G^{\ddagger}$ Gibbs Free Activation Enthalpy estimated to be equal to Gibbs Free Activation Energy, R: Ideal gas constant. The factor of 2 accounts for **DT** comprising two of the modeled helicene units.

The Gibbs Free Activation Enthalpy of the interconversion was estimated to be around 51 kJ/mol, which corresponds to a rate constant of 1.6×10^4 s^{-1} at 298 K. Therefore, interconversion between “boat” and “armchair” form should proceed rapidly at and even below room temperature. This agrees with NMR observations, where both arms of all investigated helicenes are equivalent, indicating a rapid flip between the conformations.

9. Electrochemical Data

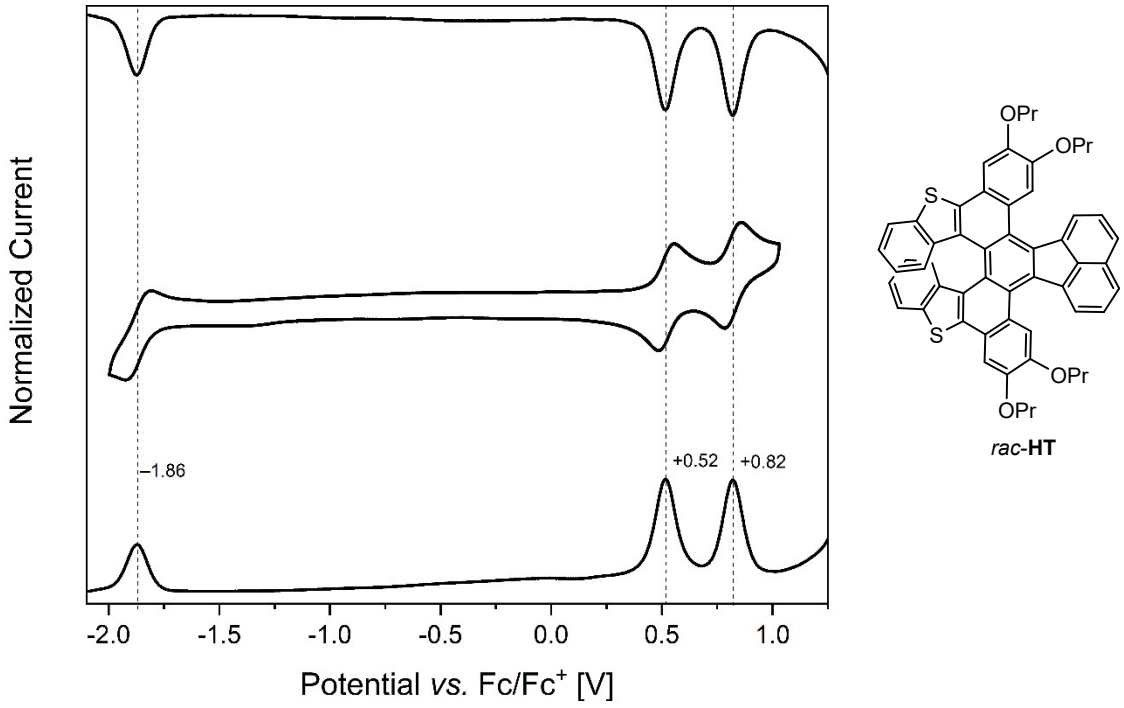

Figure S26. CV (middle), DPV (top) and SWV (bottom) measurement of *rac*-**HT** versus Fc/Fc$^+$ in CH_2Cl_2 at rt (2 mM, scan rate of 149 mVs^{-1}, *n*-Bu_4NPF_6 as supporting electrolyte).

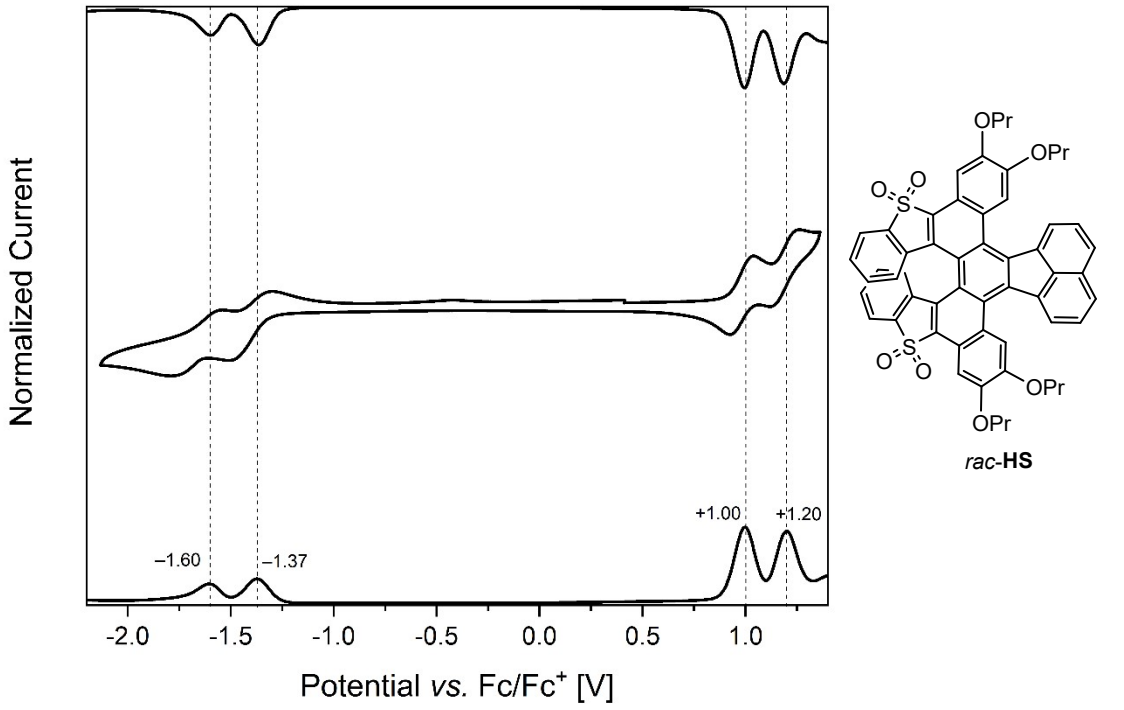

Figure S27. CV (middle), DPV (top) and SWV (bottom) measurement of *rac*-**HS** versus Fc/Fc$^+$ in CH_2Cl_2 at rt (2 mM, scan rate of 149 mVs^{-1}, *n*-Bu_4NPF_6 as supporting electrolyte).

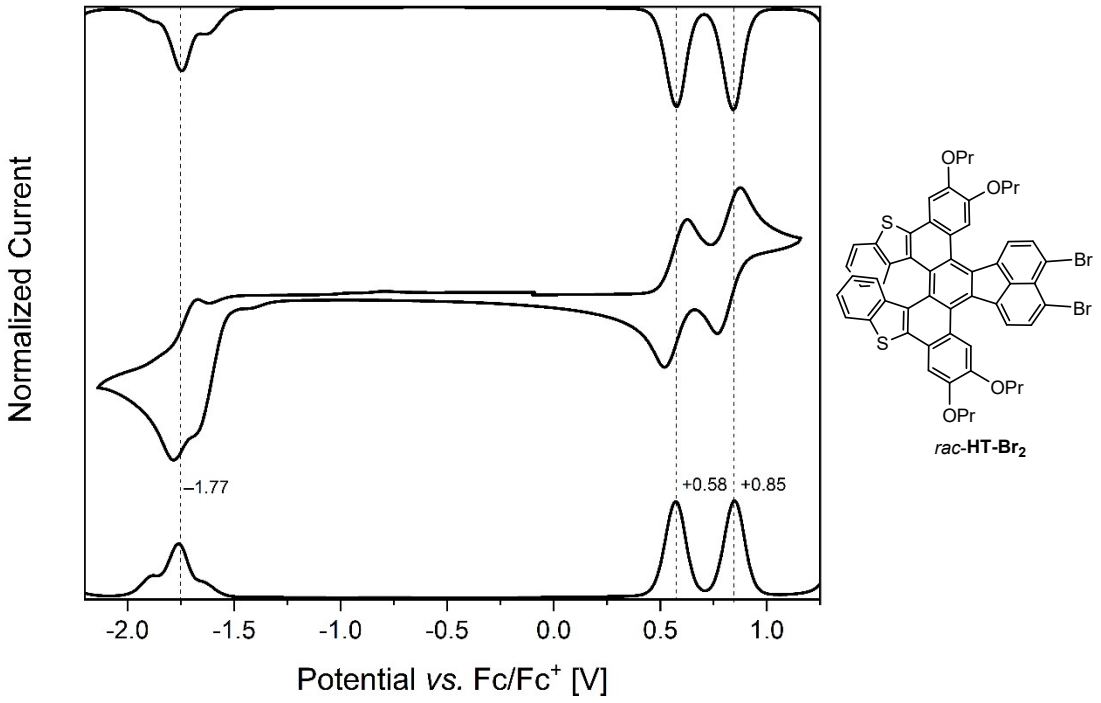

Figure S28. CV (middle), DPV (top) and SWV (bottom) measurement of *rac*-**HT-Br$_2$** versus Fc/Fc$^+$ in CH_2Cl_2 at rt (2 mM, scan rate of 149 mVs^{-1}, *n*-Bu_4NPF_6 as supporting electrolyte).

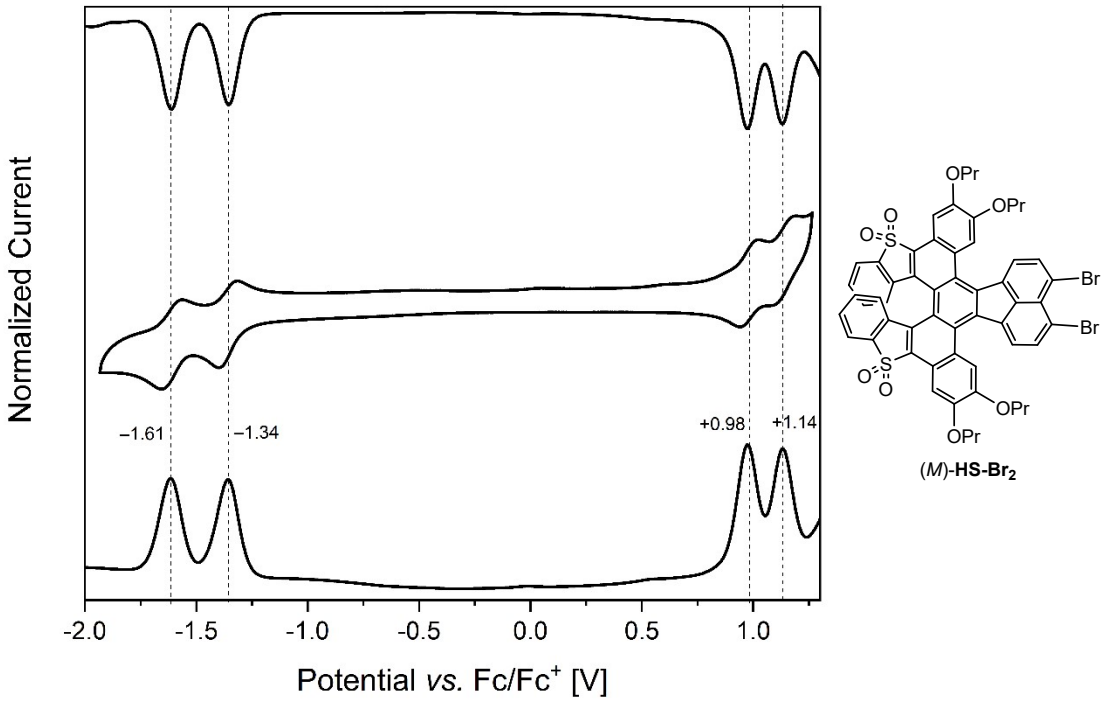

Figure S29. CV (middle), DPV (top) and SWV (bottom) measurement of (*M*)-**HS-Br$_2$** versus Fc/Fc$^+$ in CH_2Cl_2 at rt (2 mM, scan rate of 149 mVs^{-1}, *n*-Bu_4NPF_6 as supporting electrolyte).

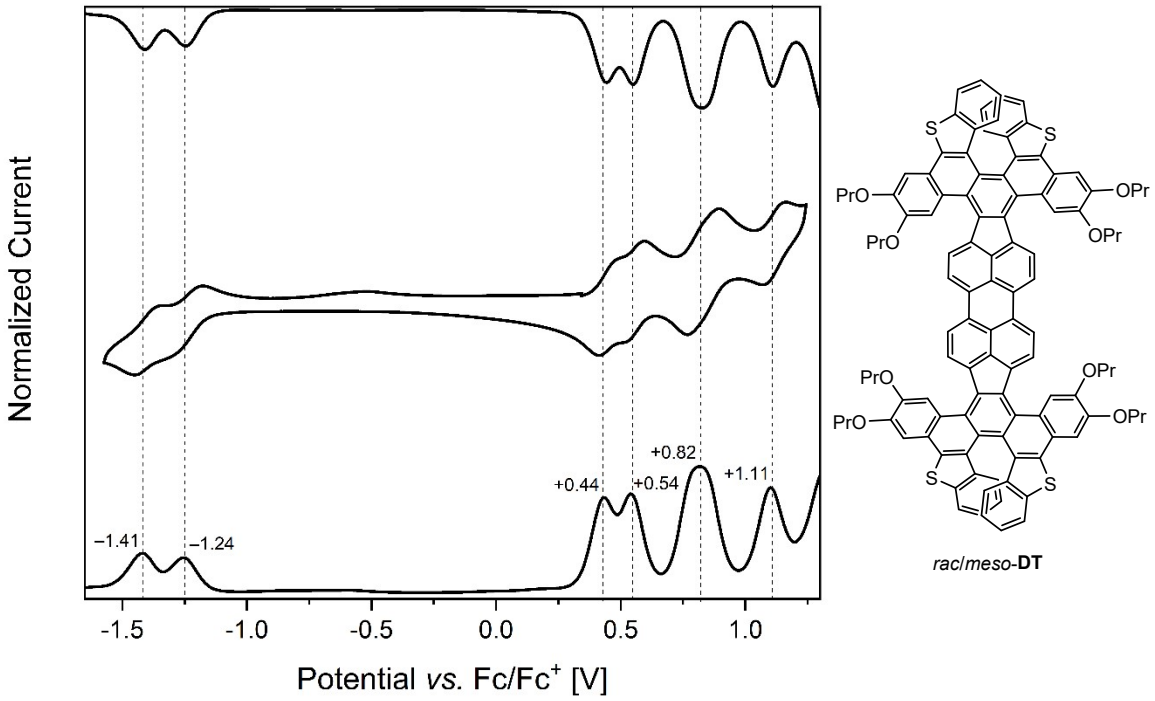

Figure S30. CV (middle), DPV (top) and SWV (bottom) measurement of *rac/meso*-**DT** versus Fc/Fc^+ in CH_2Cl_2 at rt (2 mM, scan rate of 149 mVs^{-1}, *n*-Bu_4NPF_6 as supporting electrolyte).

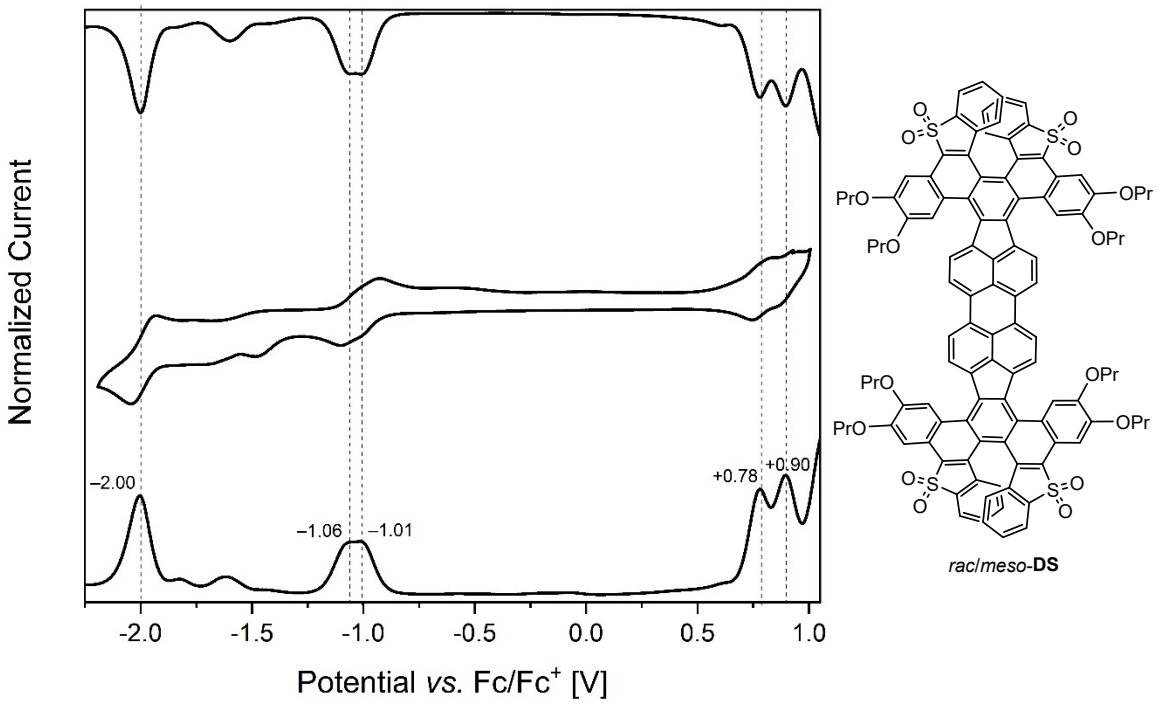

Figure S31. CV (middle), DPV (top) and SWV (bottom) measurement of *rac/meso*-**DS** versus Fc/Fc^+ in CH_2Cl_2 at rt (2 mM, scan rate of 149 mVs^{-1}, *n*-Bu_4NPF_6 as supporting electrolyte).

10. Nucleus Independent Chemical Shift

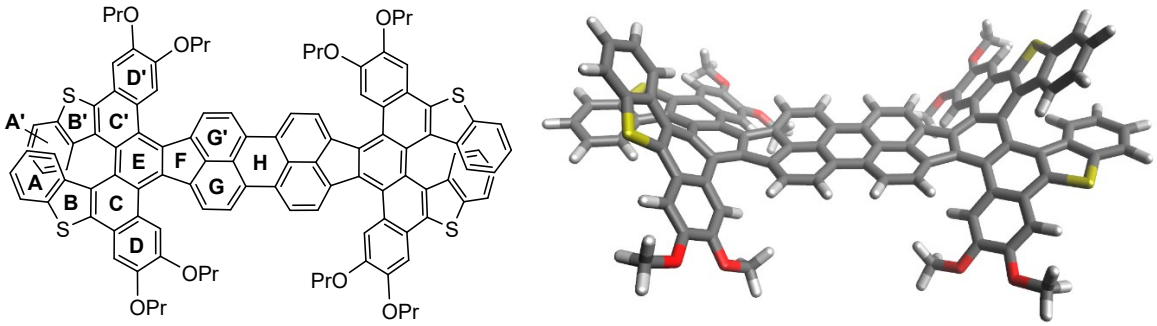

Figure S32. Left: Ring naming scheme for **DT**. Right: Optimized geometry at the CAM-B3LYP/D3BJ/def2-TZVP/SMD(CH_2Cl_2) level of theory.

Table S6. Calculated $NICS(1)_{zz}$ and $NICS(-1)_{zz}$ values for compound **DT** at the GIAO/CAM-B3LYP/D3BJ/def2-TZVP/SMD(CH_2Cl_2) level of theory, averaged over approximately symmetry-equivalent rings. The z-direction is defined orthogonal to the respective ring.

Ring	$NICS(1)_{zz}$	$NICS(-1)_{zz}$	$NICS(1)_{zz,av}$
A	–29.4	–29.5	–29.5
A'	–28.9	–29.7	–29.3
B	–15.4	–13.7	–14.5
B'	–12.0	–14.0	–13.0
C	–12.0	–10.1	–11.0
C'	–9.8	–15.2	–12.5
D	–19.3	–22.4	–20.8
D'	–17.9	–21.5	–19.7
E	–15.7	–12.3	–14.0
F	+15.9	+19.5	+17.7
G	–13.9	–11.6	–12.8
G'	–13.9	–11.2	–12.6
H	+15.8	+17.1	+16.4

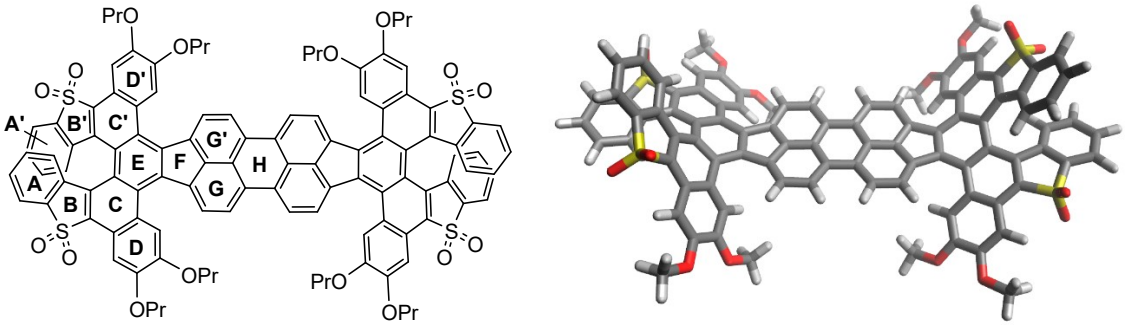

Figure S33. Left: Ring naming scheme for **DS**. Right: Optimized geometry at the CAM-B3LYP/D3BJ/def2-TZVP/SMD(CH_2Cl_2) level of theory.

Table S7. Calculated NICS(1)$_{zz}$ and NICS(–1)$_{zz}$ values for compound **DS** at the GIAO/CAM-B3LYP/D3BJ/def2-TZVP/SMD(CH_2Cl_2) level of theory, averaged over approximately symmetry-equivalent rings. The z-direction is defined orthogonal to the respective ring.

Ring	NICS(1)$_{zz}$	NICS(–1)$_{zz}$	NICS(1)$_{zz,av}$
A	–24.6	–24.9	–24.7
A'	–24.1	–24.7	–24.4
B	+10.4	+11.1	+10.8
B'	+11.7	+11.8	+11.7
C	–14.7	–12.2	–13.5
C'	–11.9	–17.5	–14.7
D	–20.2	–23.1	–21.6
D'	–19.1	–22.5	–20.8
E	–13.4	–10.0	–11.7
F	+14.4	+18.0	+16.2
G	–14.1	–11.7	–12.9
G'	–14.2	–11.4	–12.8
H	+16.0	+17.4	+16.7

11. Crystallographic Data

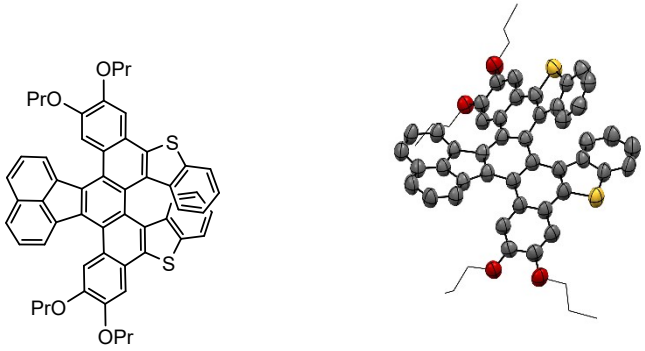

Figure S34. Structure of *rac*-**HT** determined by X-ray crystallographic analysis.

Single crystals of *rac*-**HT** suitable for X-ray crystallographic analysis were grown by slow gas phase diffusion of MeOH into a solution of the compound in $CDCl_3$ at rt.

Table S8: X-ray crystallographic data and structure refinement of compound *rac*-**HT**.

CCDC	2516116
Empirical formula	$C_{56}H_{46}O_4S_2$
Formula weight	847.05
Temperature / K	200(2)
Wavelength / Å	1.54178
Crystal system	triclinic
Space group	$P\bar{1}$
Z	2
a / Å	8.2676(8)
b / Å	12.6838(11)
c / Å	20.8608(18)
α / deg.	86.671(7)
β / deg.	79.295(7)
γ / deg.	76.915(7)
Volume / Å^3	2093.4(3)
Density (calculated) / gcm^{-3}	1.34
Absorption coefficient / mm^{-1}	1.55
Crystal shape	conoid
Crystal size / mm^3	0.076 × 0.026 × 0.023
Crystal color	orange
Theta range for data collection / deg.	3.6 to 49.7
Index ranges	$-7 \le h \le 8$, $-12 \le k \le 9$, $-20 \le l \le 20$
Reflections collected	11618
Independent reflections	4216 (R(int) = 0.00670)
Observed reflections	2358 ($I > 2\sigma(I)$)
Absorption correction	Semi-empirical from equivalents
Max. and min. transmission	0.98 and 0.74
Refinement method	Full-matrix least-squares on F^2
Data/restraints/parameters	4216 / 626 / 563
Goodness-of-fit on F^2	1.13
Final R indices ($I > 2\sigma(I)$)	R_1 = 0.103, wR_2 = 0.215
Largest diff. peak and hole / eÅ^{-3}	0.244 and –0.26

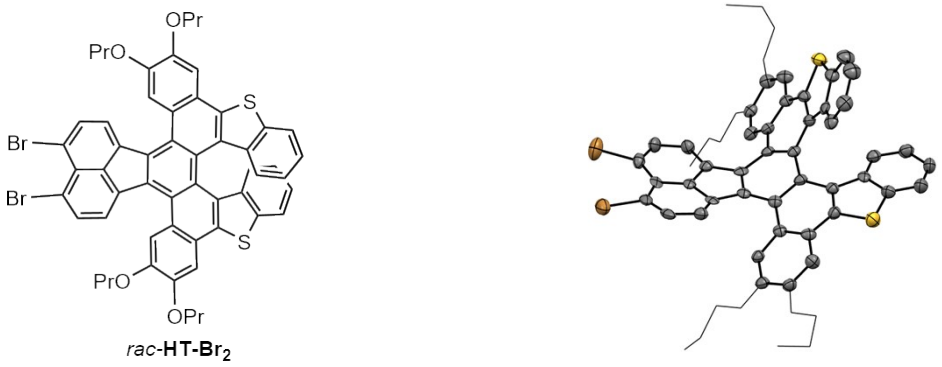

rac-**HT-Br$_2$**

Figure S35. Structure of *rac*-**HT-Br$_2$** determined by X-ray crystallographic analysis.

Single crystals of *rac*-**HT-Br$_2$** suitable for X-ray crystallographic analysis were grown by slow gas phase diffusion of MeCN into a solution of the compound in 1,2-DCE at rt.

Table S9. Crystallographic data and structure refinement for *rac*-**HT-Br$_2$**.

CCDC	2516117
Empirical formula	$C_{56}H_{44}Br_2O_4S_2$
Formula weight	1004.85
Temperature / K	200(2)
Wavelength / Å	0.71073
Crystal system	monoclinic
Space group	$P2_1/c$
Z	4
a / Å	18.4166(19)
b / Å	7.9978(7)
c / Å	32.160(3)
α / deg.	90
β / deg.	104.589(3)
γ / deg.	90
Volume / Å^3	4584.2(8)
Density (calculated) / gcm^{-3}	1.456
Absorption coefficient / mm^{-1}	1.908
Crystal shape	needle
Crystal size / mm^3	0.245 x 0.018 x 0.012
Crystal color	orange
Theta range for data collection / deg.	1.309 to 19.359
Index ranges	$-17\leq h\leq 17$, $-7\leq k\leq 7$, $-29\leq l\leq 29$
Reflections collected	35881
Independent reflections	3910 (R(int) = 0.1182)
Observed reflections	2757 ($I > 2\sigma(I)$)
Absorption correction	Semi-empirical from equivalents
Max. and min. transmission	0.96 and 0.86
Refinement method	Full-matrix least-squares on F^2
Data/restraints/parameters	3901 / 677 / 581
Goodness-of-fit on F^2	1.13
Final R indices ($I > 2\sigma(I)$)	R_1 = 0.051, wR_2 = 0.115
Largest diff. peak and hole / eÅ^{-3}	0.53 and –0.40

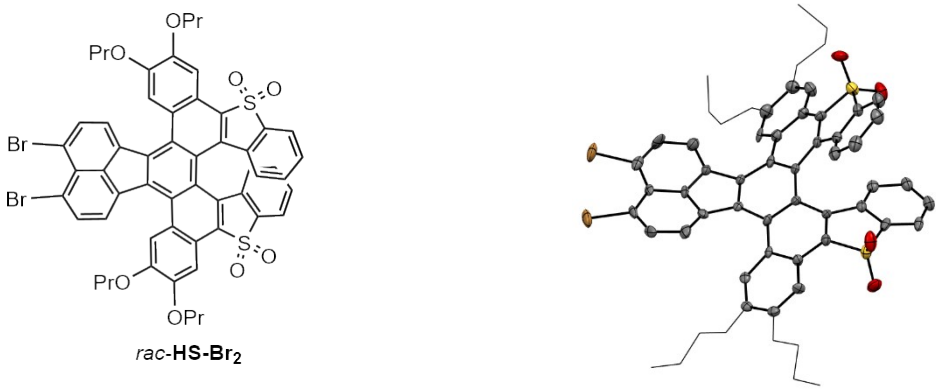

rac-**HS-Br$_2$**

Figure S36. Structure of *rac*-**HS-Br$_2$** determined by X-ray crystallographic analysis.

Single crystals of *rac*-**HS-Br$_2$** suitable for X-ray crystallographic analysis were grown by slow gas phase diffusion of MeOH into a solution of the compound in 1,2-dichlorobenzene at rt.

Table S10. Crystallographic data and structure refinement for *rac*-**HS-Br$_2$**.

CCDC	2516118
Empirical formula	$C_{62}H_{48}Br_2Cl_2O_8S_2$
Formula weight	1215.84
Temperature / K	200(2)
Wavelength / Å	0.71073
Crystal system	orthorhombic
Space group	$P2_12_12$
Z	4
a / Å	27.6680(17)
b / Å	8.9745(5)
c / Å	22.7136(13)
α / deg.	90
β / deg.	90
γ / deg.	90
Volume / Å^3	5639.9(6)
Density (calculated) / gcm^{-3}	1.43
Absorption coefficient / mm^{-1}	1.66
Crystal shape	plate
Crystal size / mm^3	0.094 x 0.067 x 0.020
Crystal color	red
Theta range for data collection / deg.	1.7 to 25.7
Index ranges	$-33\leq h\leq 33$, $-10\leq k\leq 9$, $-21\leq l\leq 27$
Reflections collected	35736
Independent reflections	10254 (R(int) = 0.0774)
Observed reflections	6960 ($I > 2\sigma(I)$)
Absorption correction	Semi-empirical from equivalents
Max. and min. transmission	0.97 and 0.78
Refinement method	Full-matrix least-squares on F^2
Data/restraints/parameters	10254 / 635 / 690
Goodness-of-fit on F^2	1.01
Final R indices ($I > 2\ \sigma(I)$)	$R_1 = 0.067$, $wR_2 = 0.162$
Largest diff. peak and hole / eÅ^{-3}	1.07 and –0.66

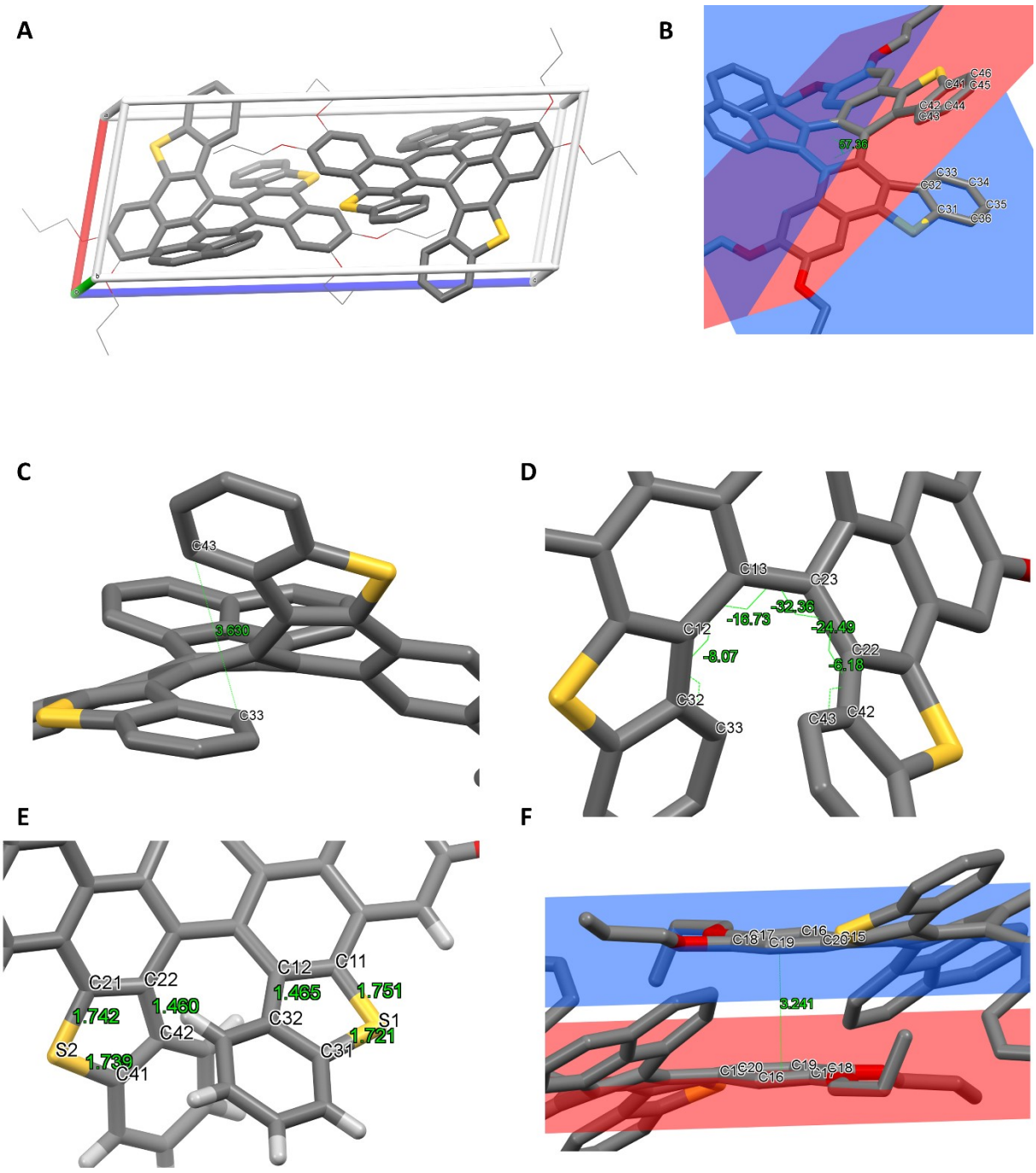

Figure S37: Measurements in the crystal structure of **HT**. A) Unit cell. B) Dihedral angle. The planes represent the mean plane of the annotate carbon atoms of the terminal rings, respectively. C) Helical pitch. D) Torsion angles to calculate the average torsion angle. E) Selected bond lengths in the thiophene units. F) Distance of mean planes of benzenoid rings of adjacent molecules.

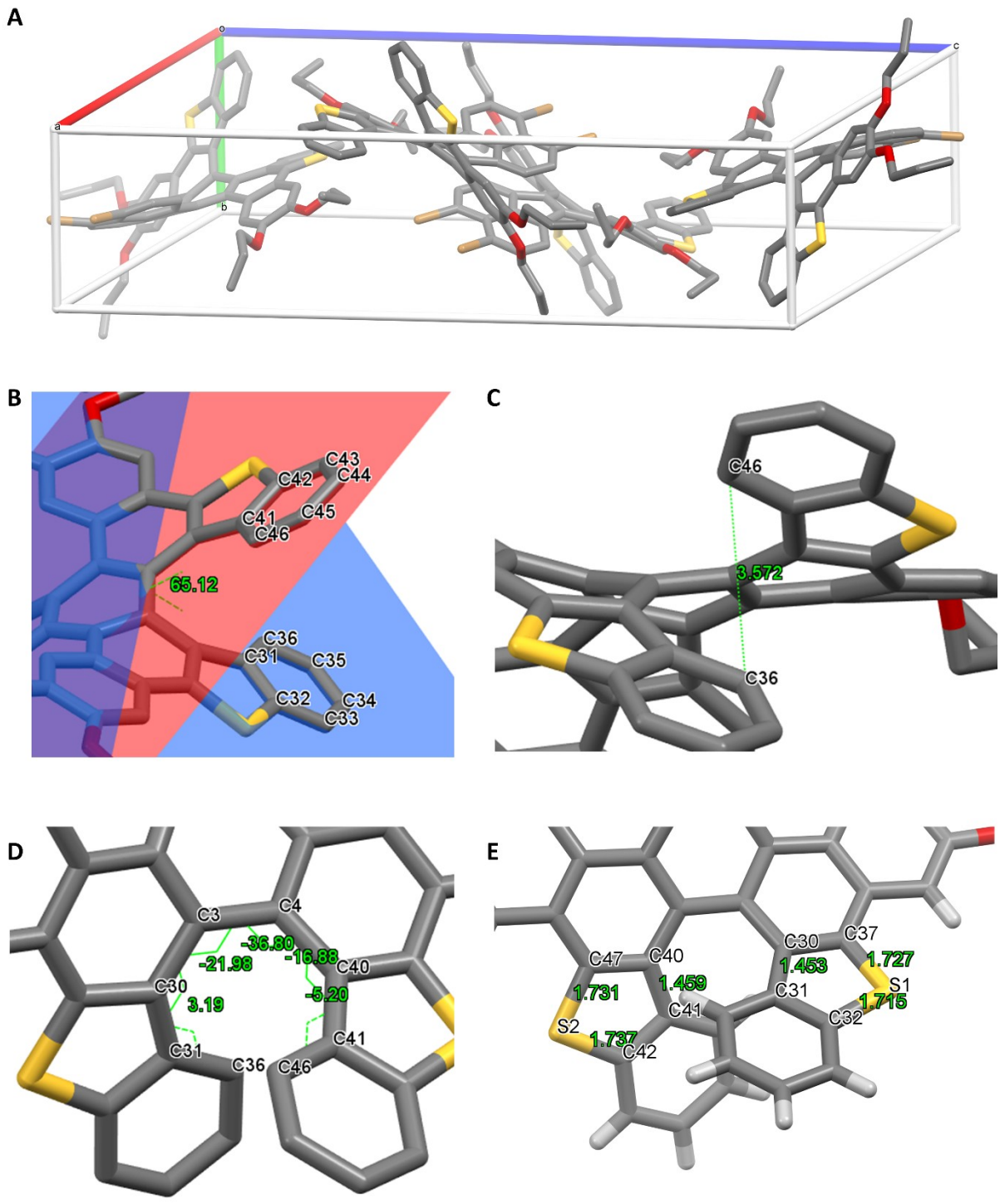

Figure S38: Measurements in the crystal structure of **HT-Br$_2$**. A) Unit cell. B) Dihedral angle. The planes represent the mean plane of the annotate carbon atoms of the terminal rings, respectively. C) Helical pitch. D) Torsion angles to calculate the average torsion angle. E) Selected bond lengths in the thiophene units.

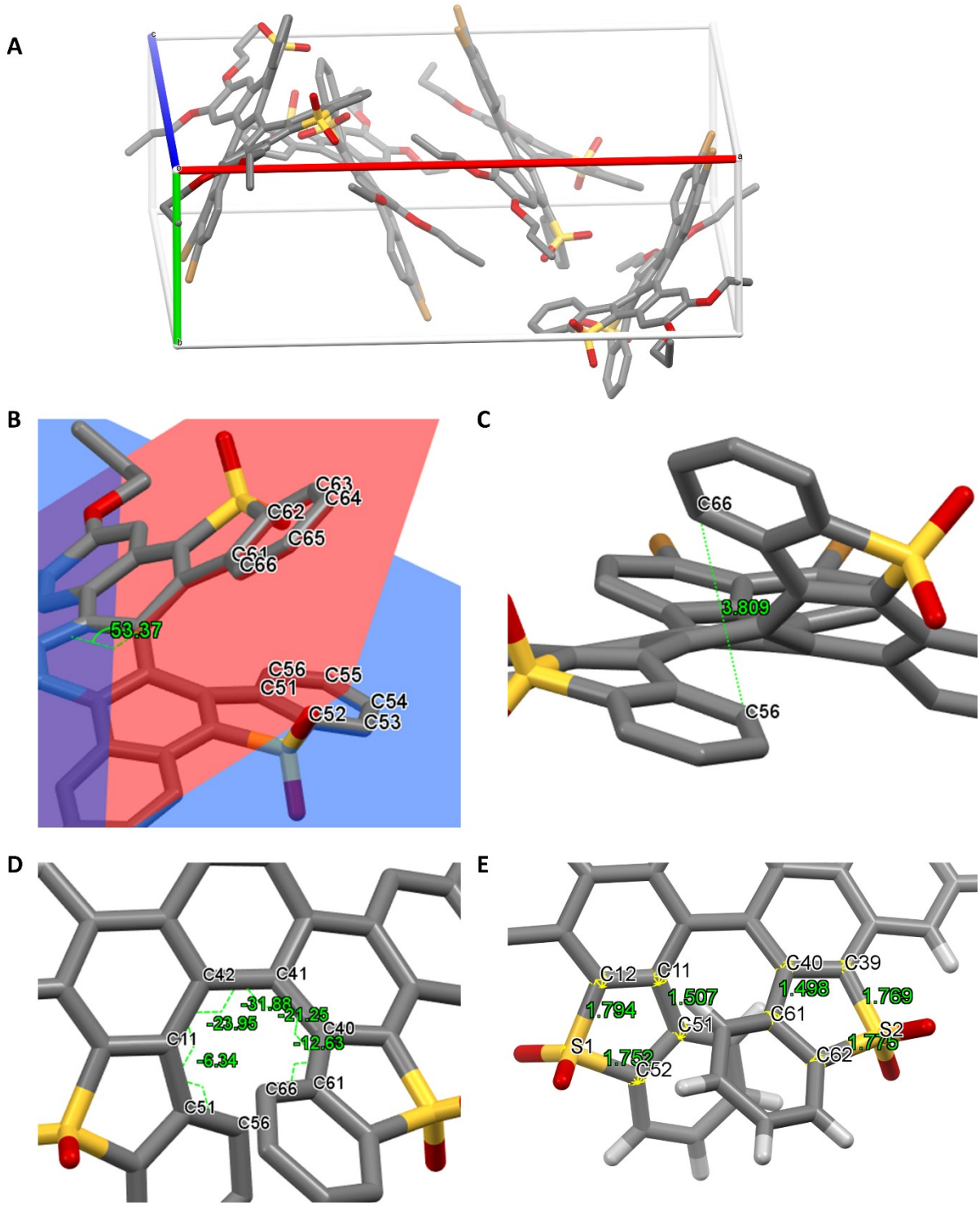

Figure S39: Measurements in the crystal structure of **HS-Br$_2$**. A) Unit cell. B) Dihedral angle. The planes represent the mean plane of the annotate carbon atoms of the terminal rings, respectively. C) Helical pitch. D) Torsion angles to calculate the average torsion angle. E) Selected bond lengths in the thiophene units.

12. NMR Data

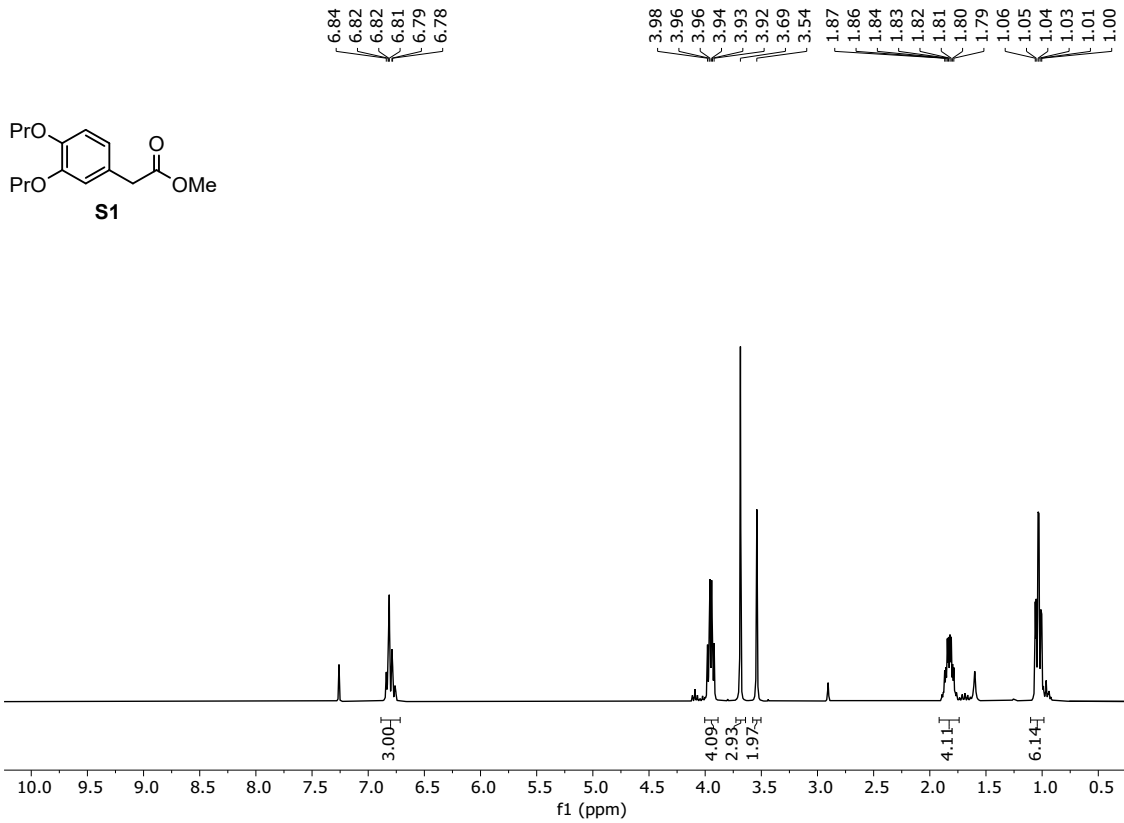

Figure S40. ^{1}H NMR spectrum of **S1** (300 MHz, $CDCl_3$).

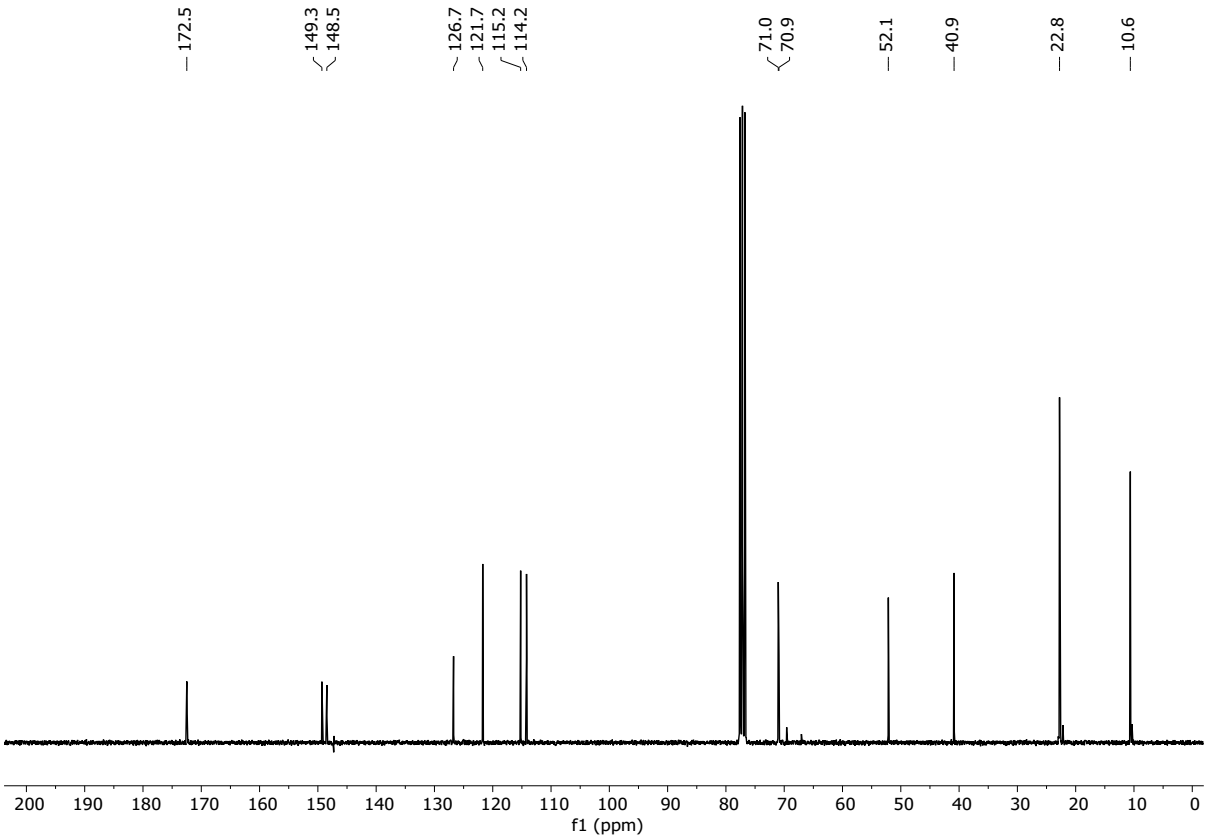

Figure S41. ^{13}C NMR spectrum of **S1** (75 MHz, $CDCl_3$).

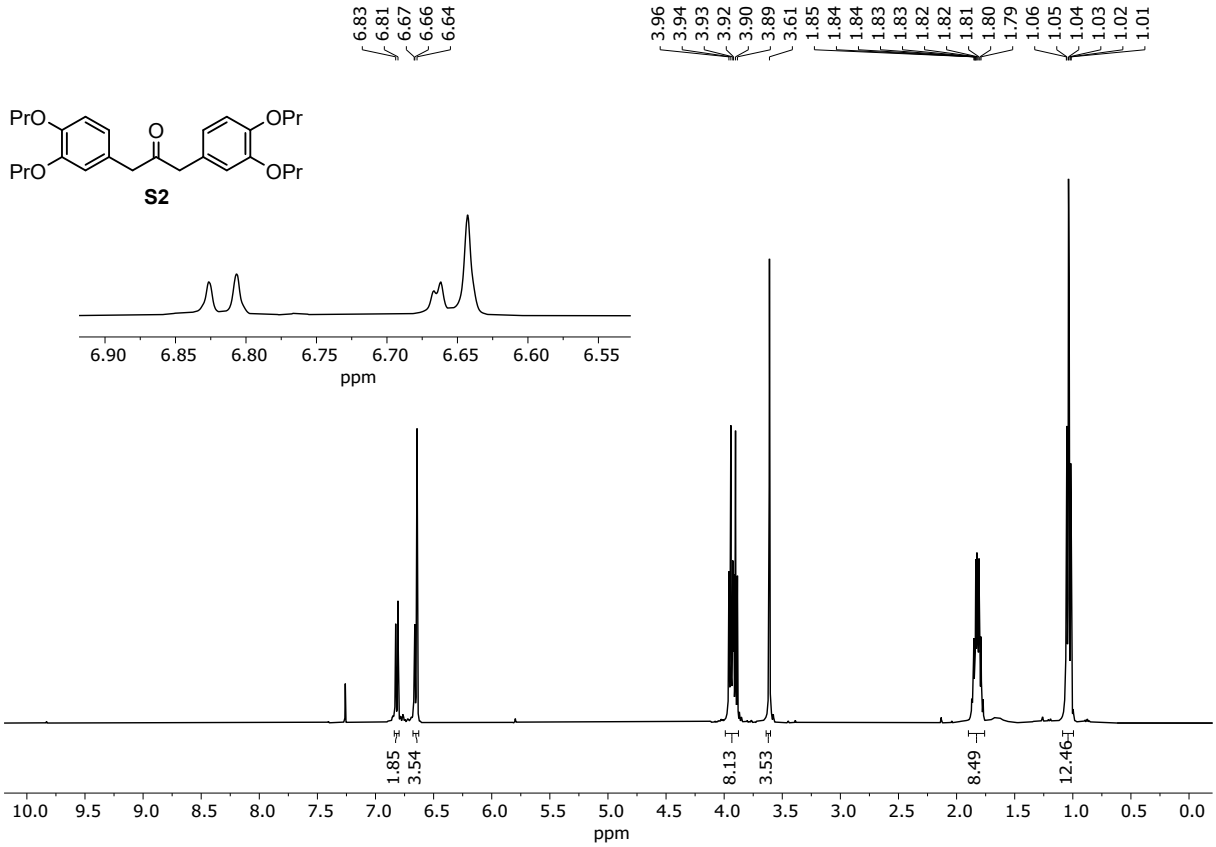

Figure S42. ^{1}H NMR spectrum of **S2** (400 MHz, $CDCl_3$).

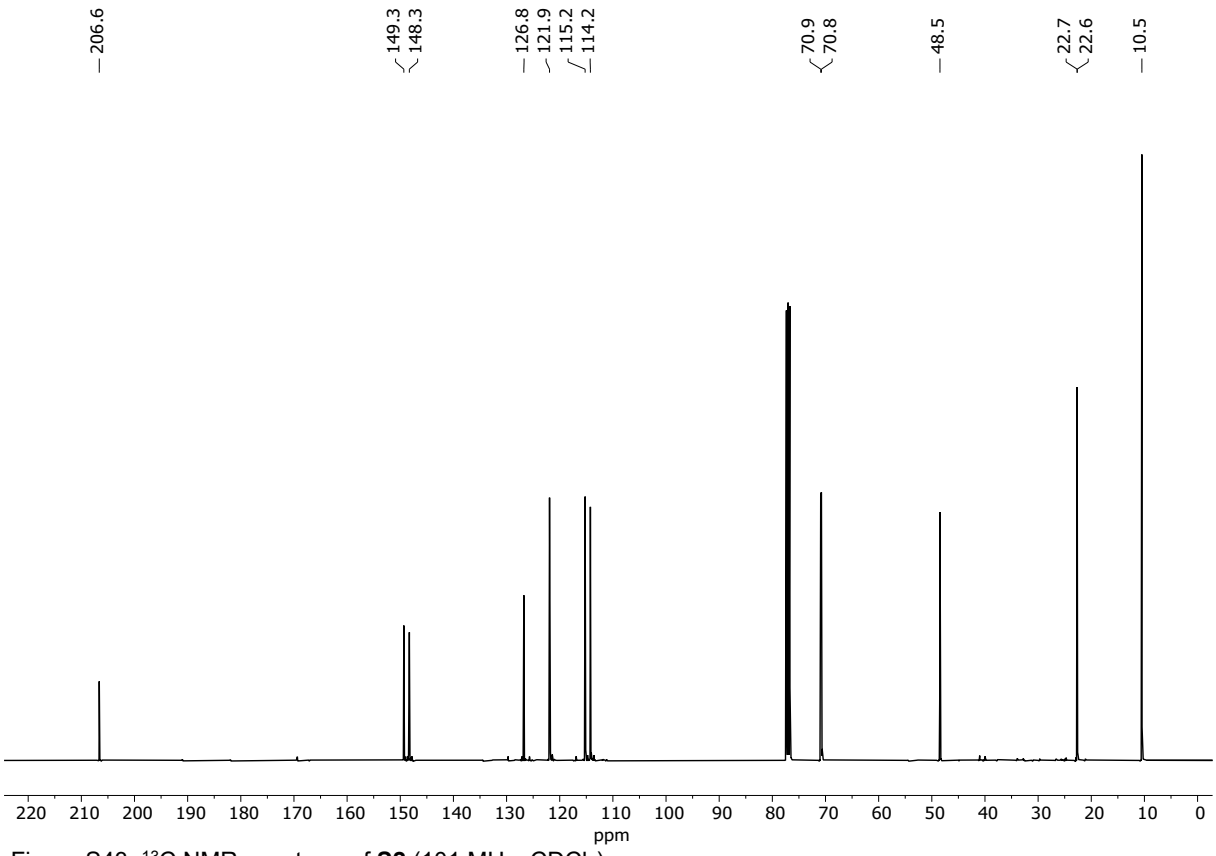

Figure S43. ^{13}C NMR spectrum of **S2** (101 MHz, $CDCl_3$).

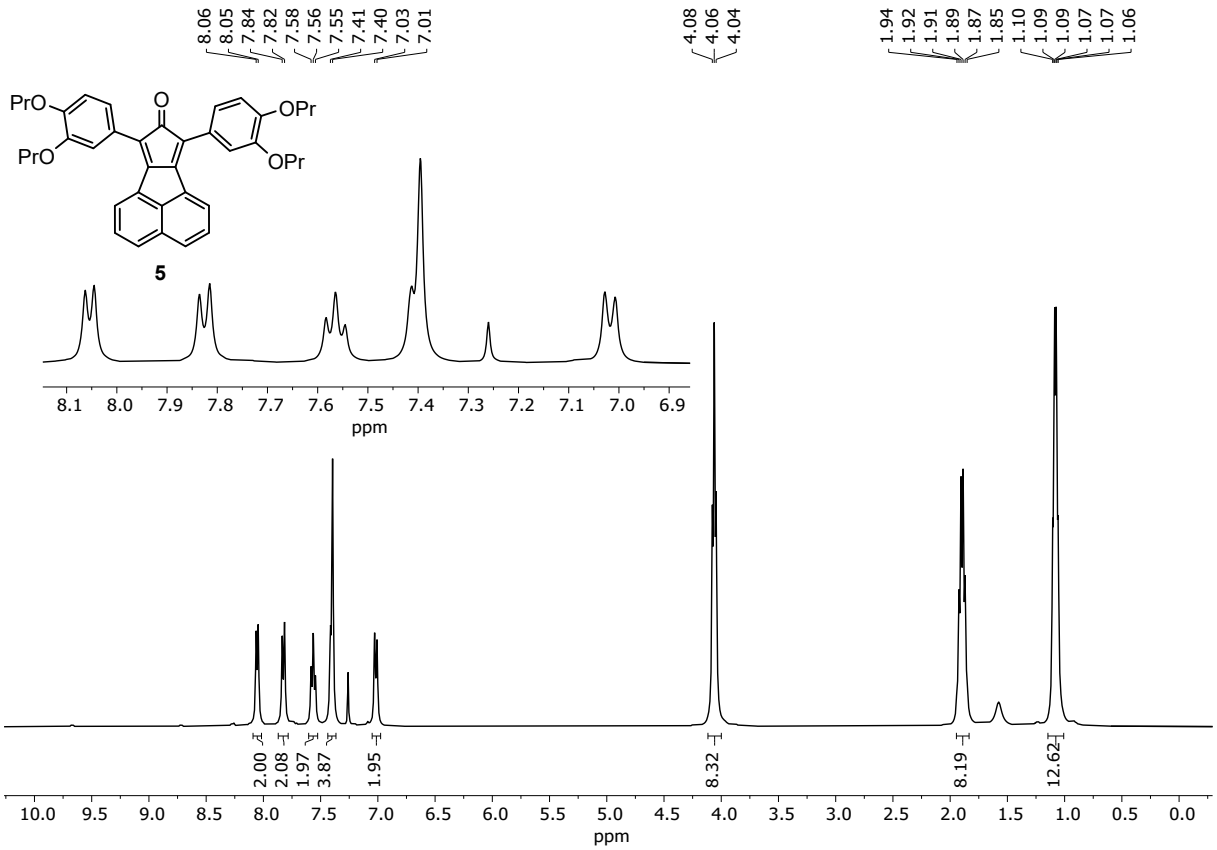

Figure S44. ^{1}H NMR spectrum of **5** (400 MHz, $CDCl_3$).

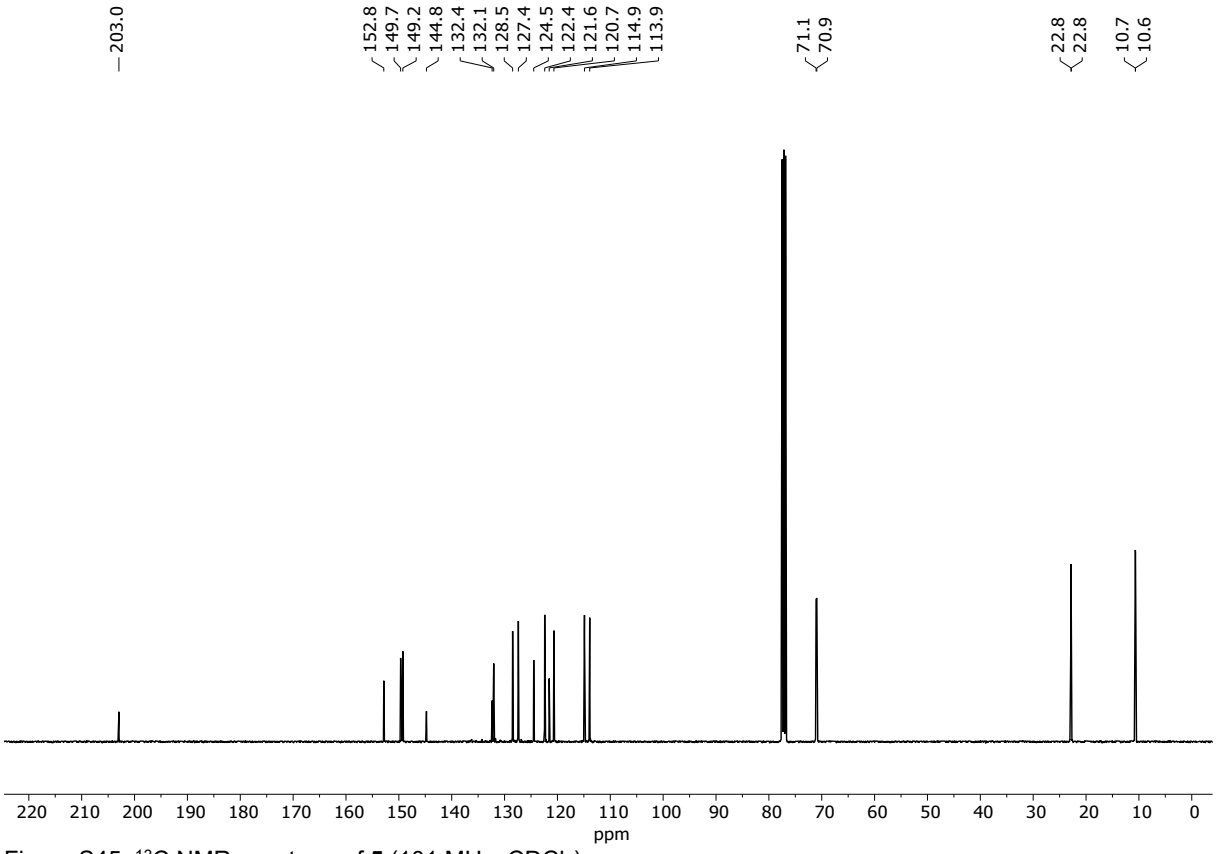

Figure S45. ^{13}C NMR spectrum of **5** (101 MHz, $CDCl_3$).

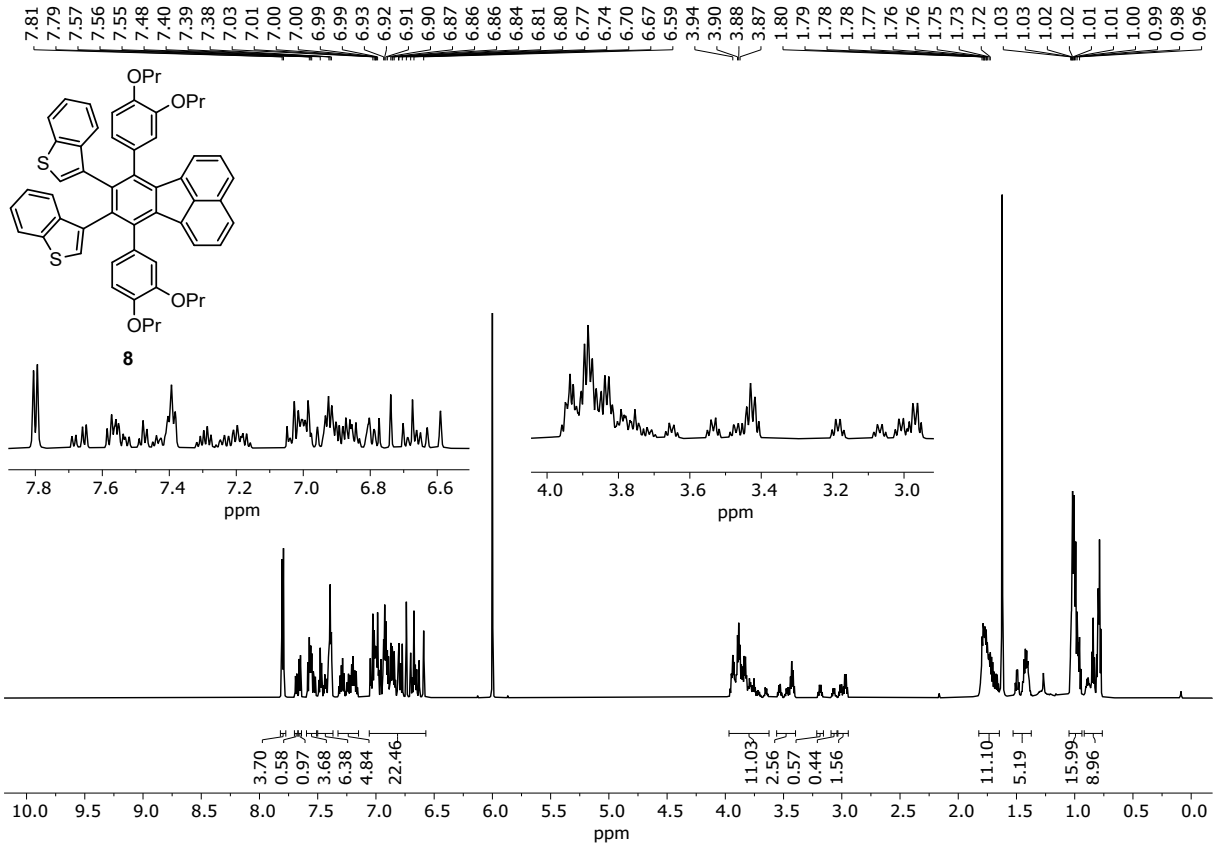

Figure S46. ^{1}H NMR spectrum of **8** (700 MHz, $C_2D_2Cl_4$).

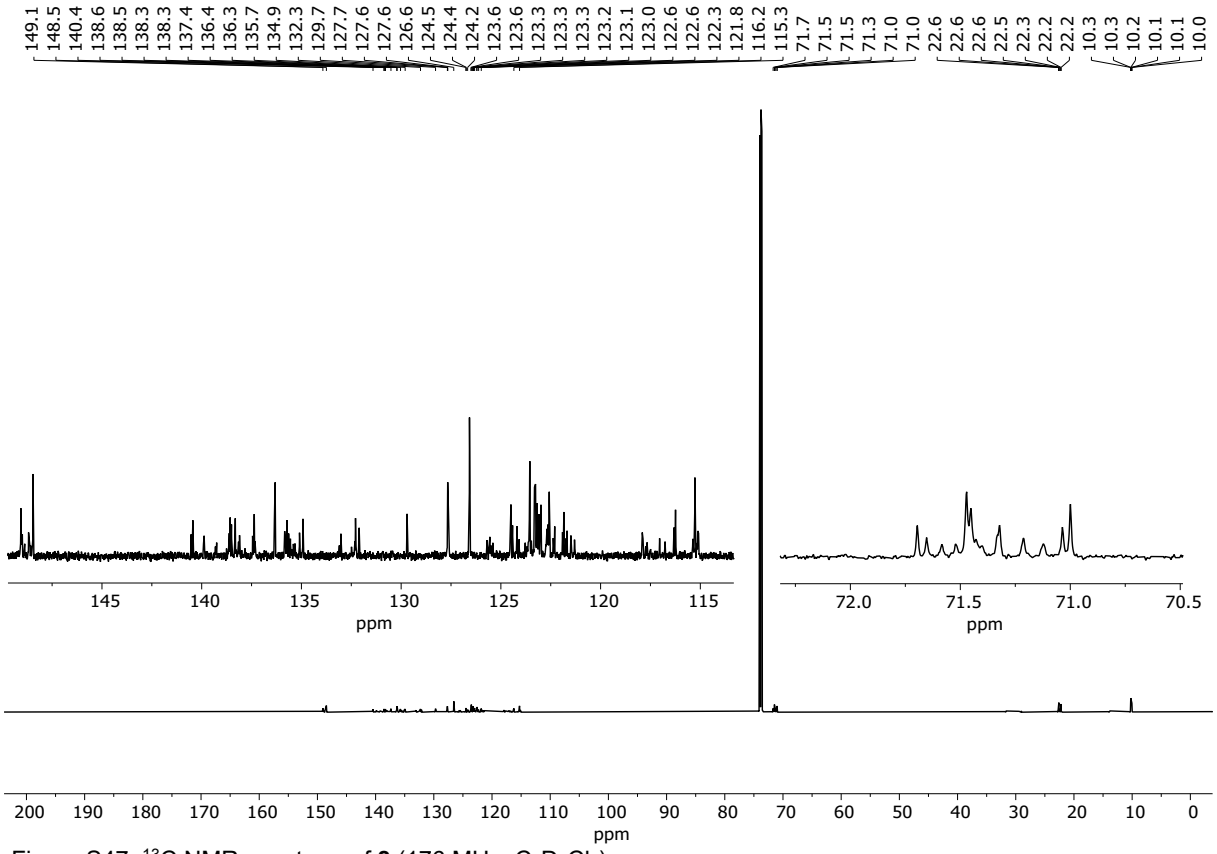

Figure S47. ^{13}C NMR spectrum of **8** (176 MHz, $C_2D_2Cl_4$).

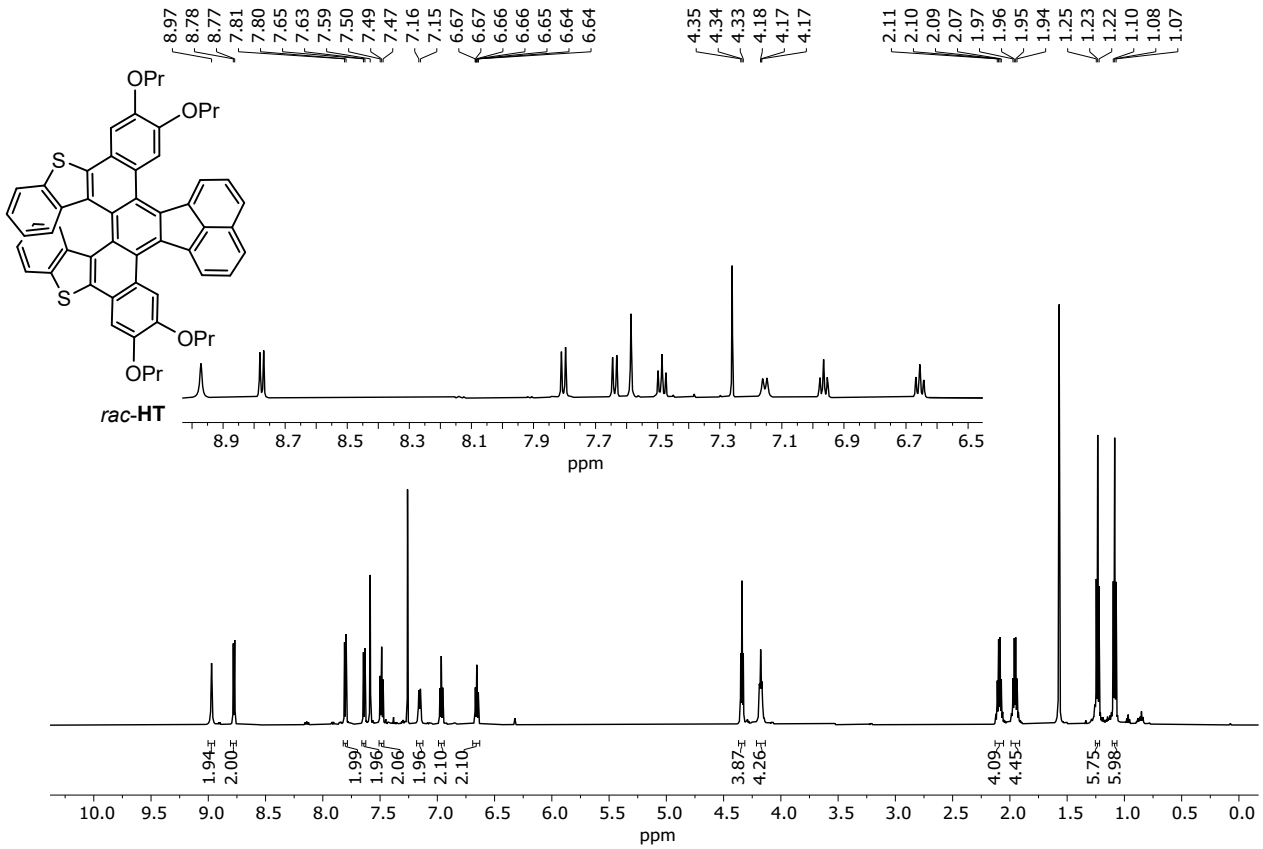

Figure S48. ^{1}H NMR spectrum of *rac*-**HT** (600 MHz, $CDCl_3$).

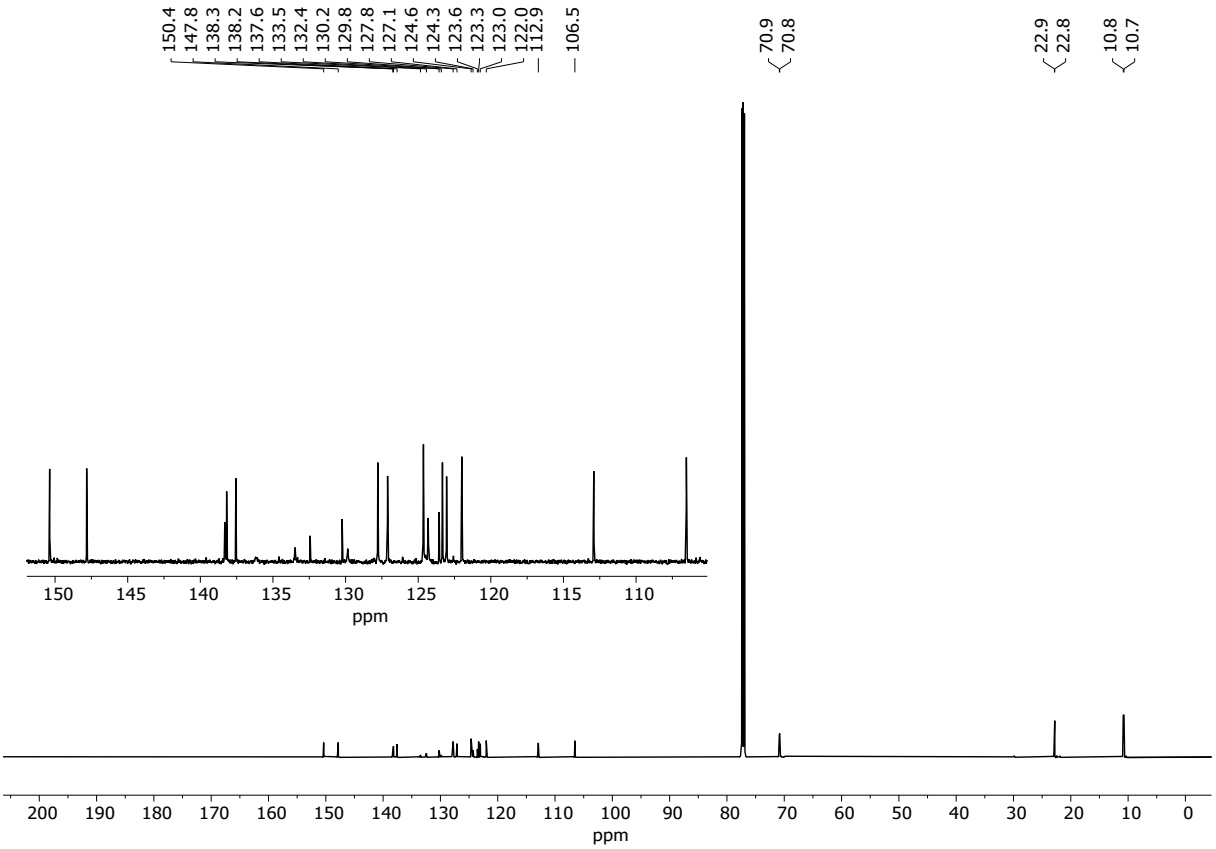

Figure S49. ^{13}C NMR spectrum of *rac*-**HT** (151 MHz, $CDCl_3$).

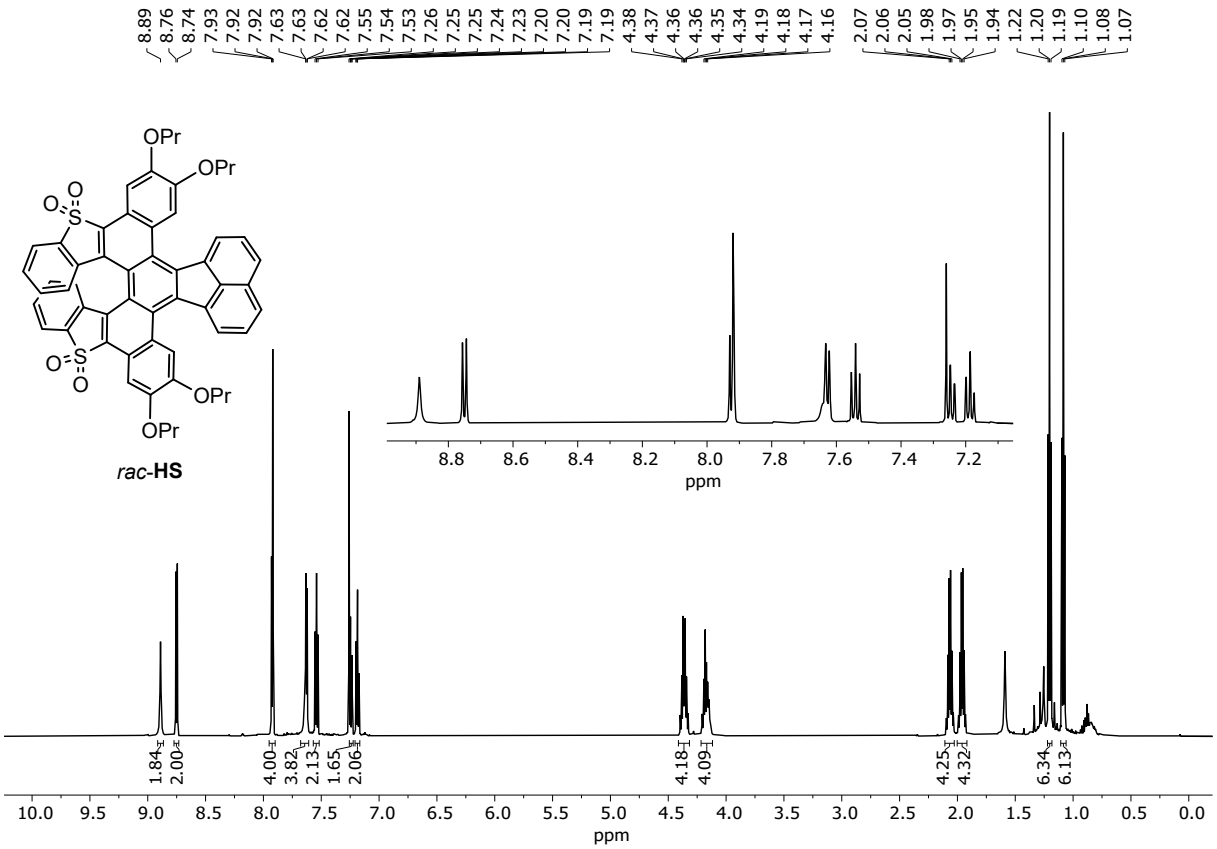

Figure S50. ^{1}H NMR spectrum of *rac*-**HS** (600 MHz, $CDCl_3$).

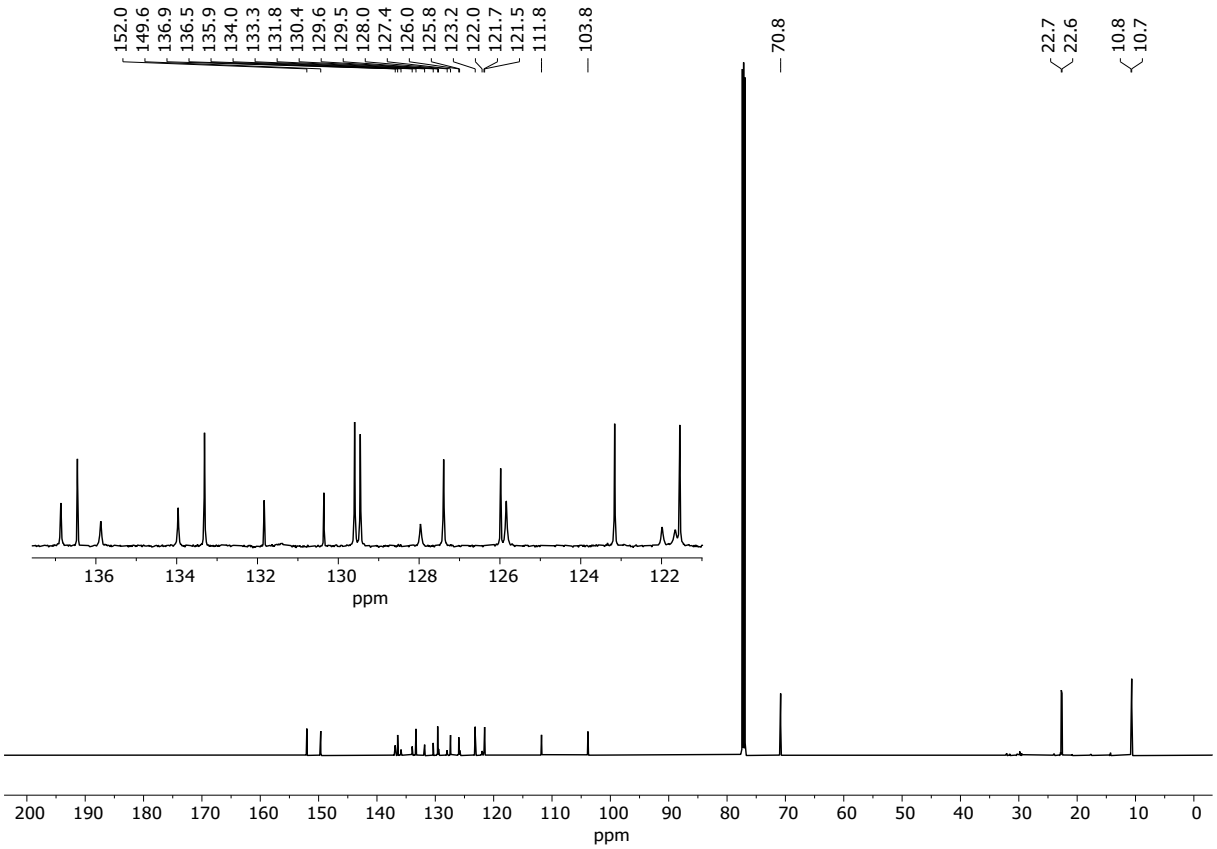

Figure S51. ^{13}C NMR spectrum of *rac*-**HS** (151 MHz, $CDCl_3$).

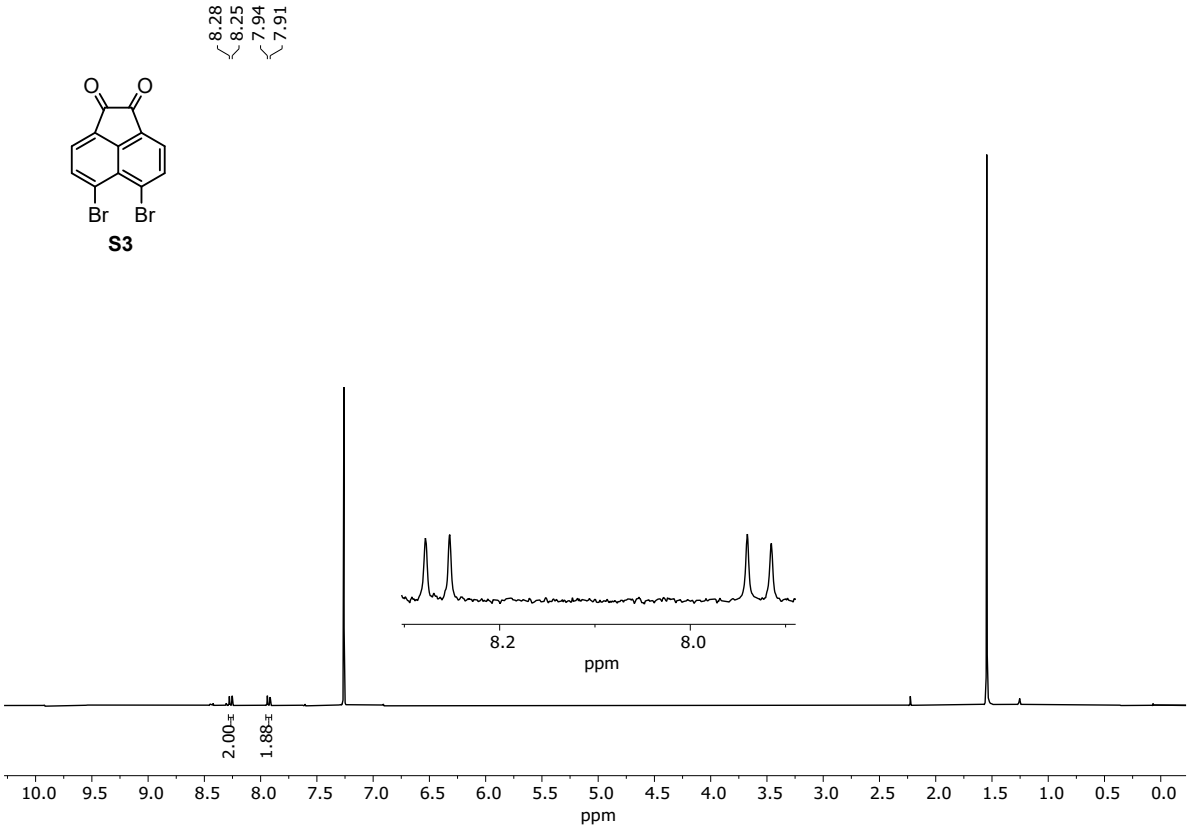

Figure S52. ^{1}H NMR spectrum of **S3** (300 MHz, $CDCl_3$).

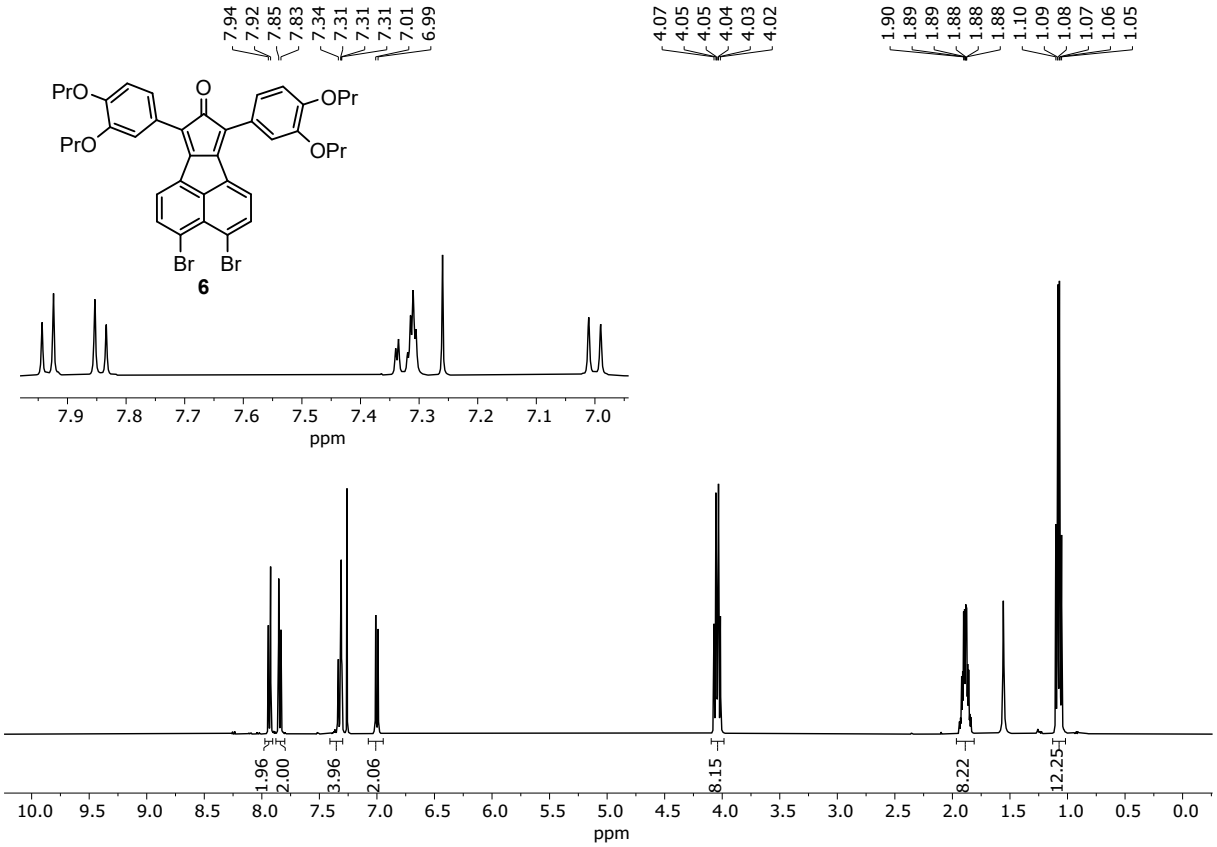

Figure S53. ^{1}H NMR spectrum of **6** (400 MHz, $CDCl_3$).

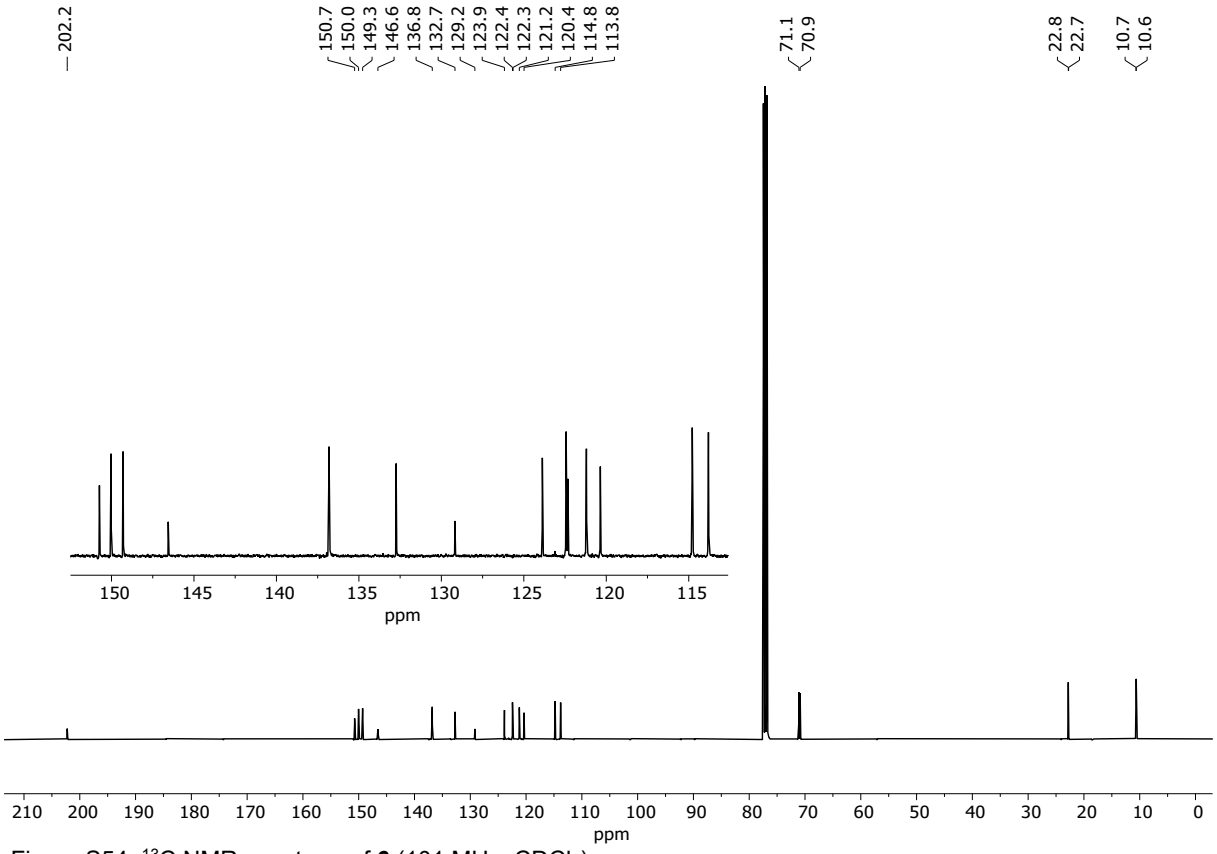

Figure S54. ^{13}C NMR spectrum of **6** (101 MHz, $CDCl_3$).

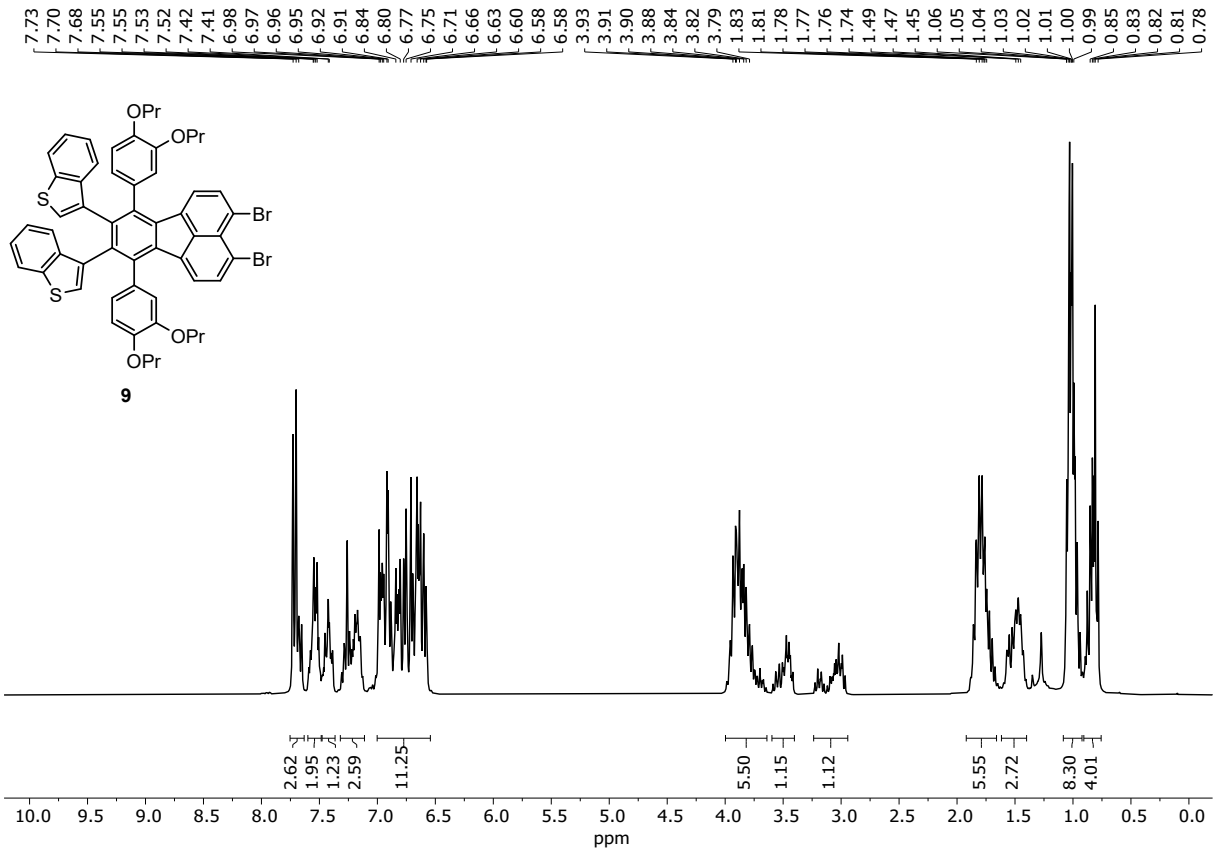

Figure S55. ^{1}H NMR spectrum of **9** (300 MHz, $CDCl_3$).

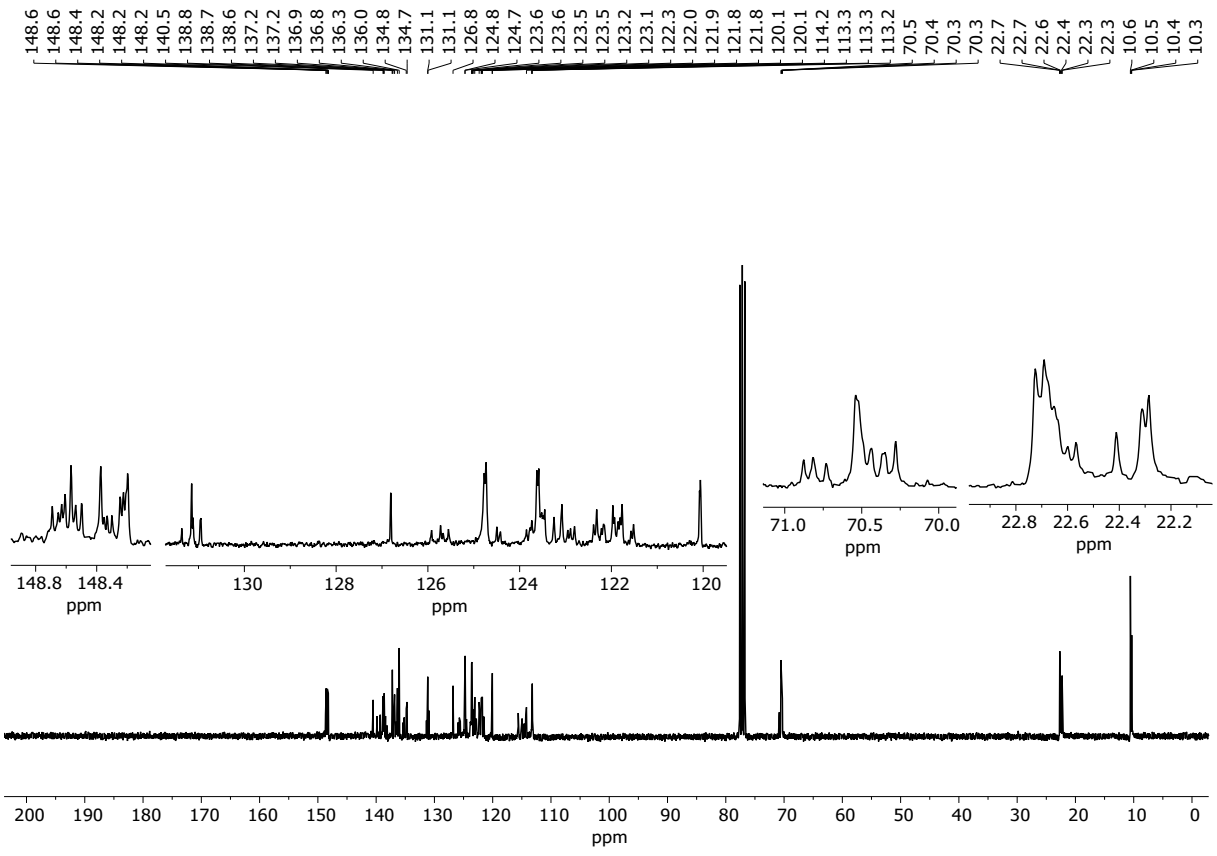

Figure S56. ^{13}C NMR spectrum of **9** (75 MHz, $CDCl_3$).

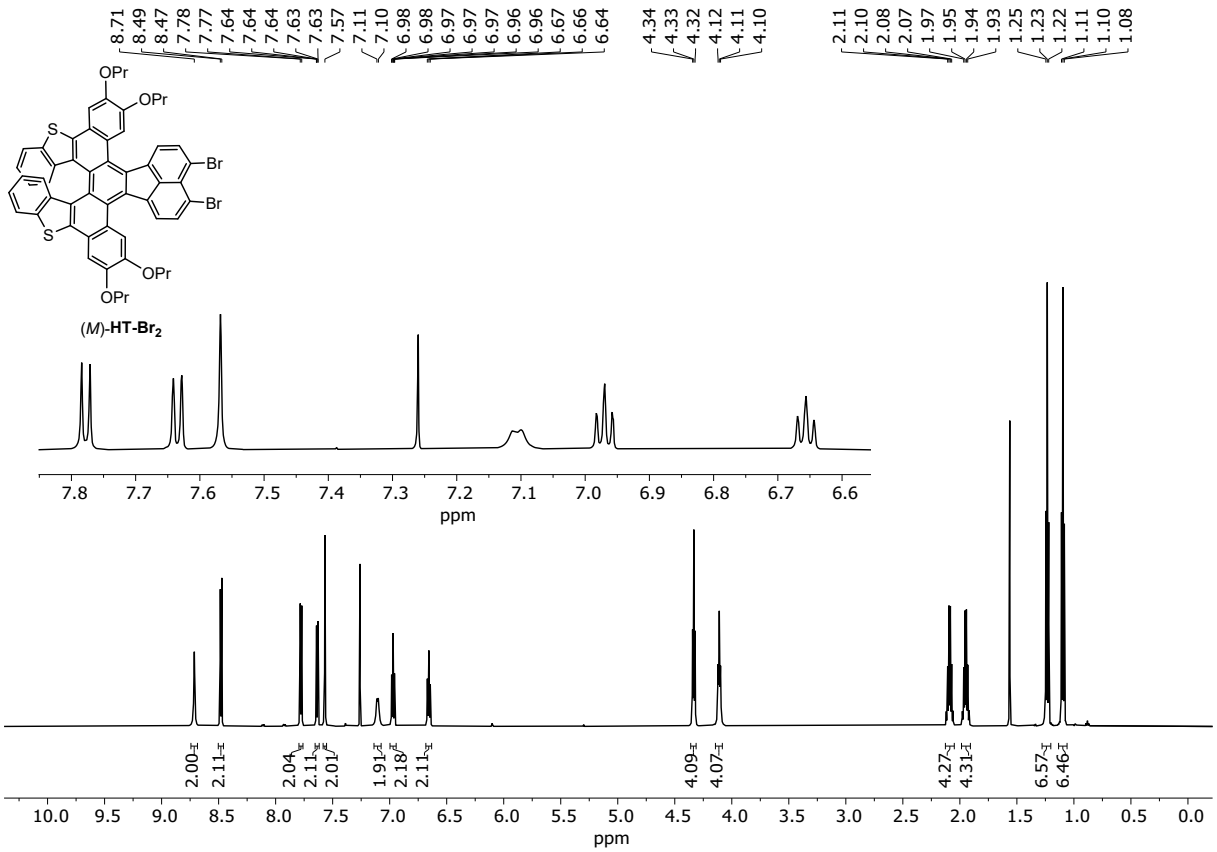

Figure S57. ^{1}H NMR spectrum of (*M*)-**HT-Br$_2$** (600 MHz, $CDCl_3$).

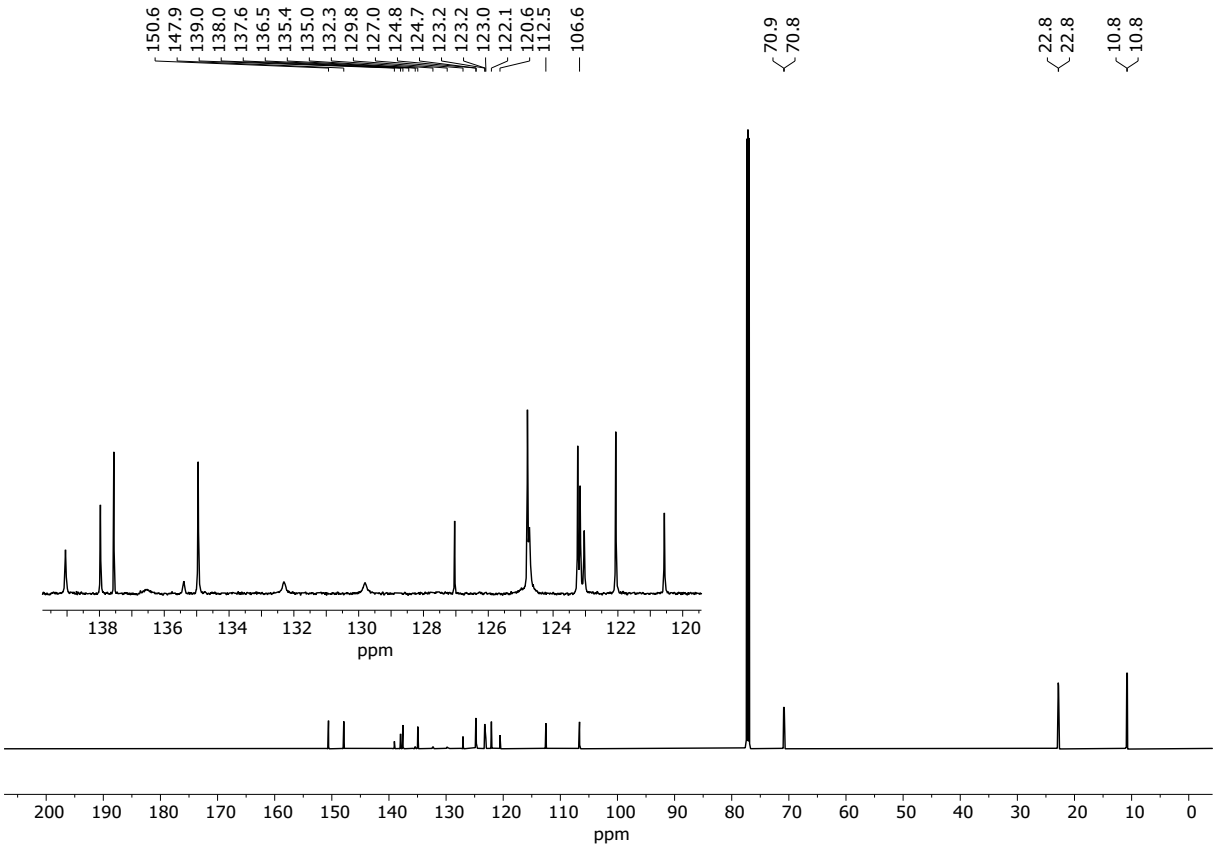

Figure S58. ^{13}C NMR spectrum of (*M*)-**HT-Br$_2$** (151 MHz, $CDCl_3$).

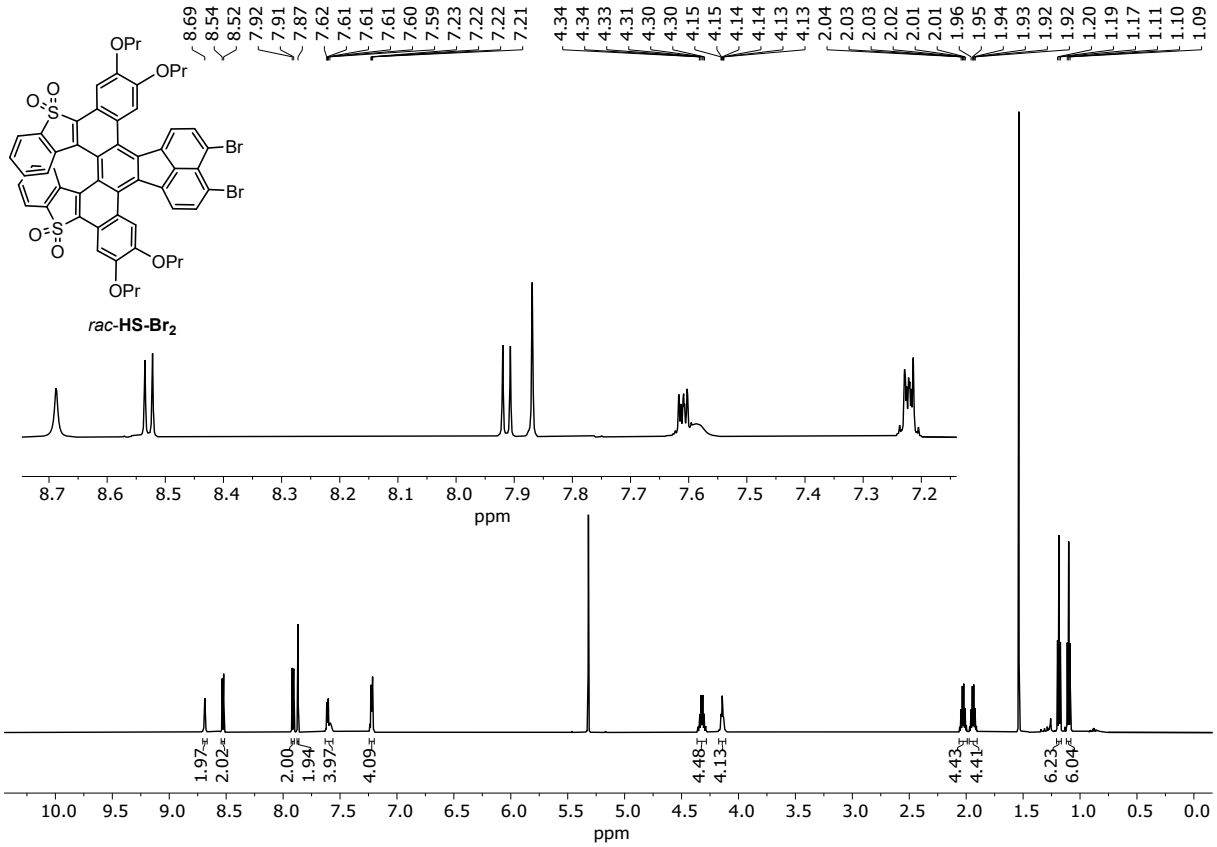

Figure S59. ^{1}H NMR spectrum of *rac*-**HS-Br$_2$** (600 MHz, CD_2Cl_2).

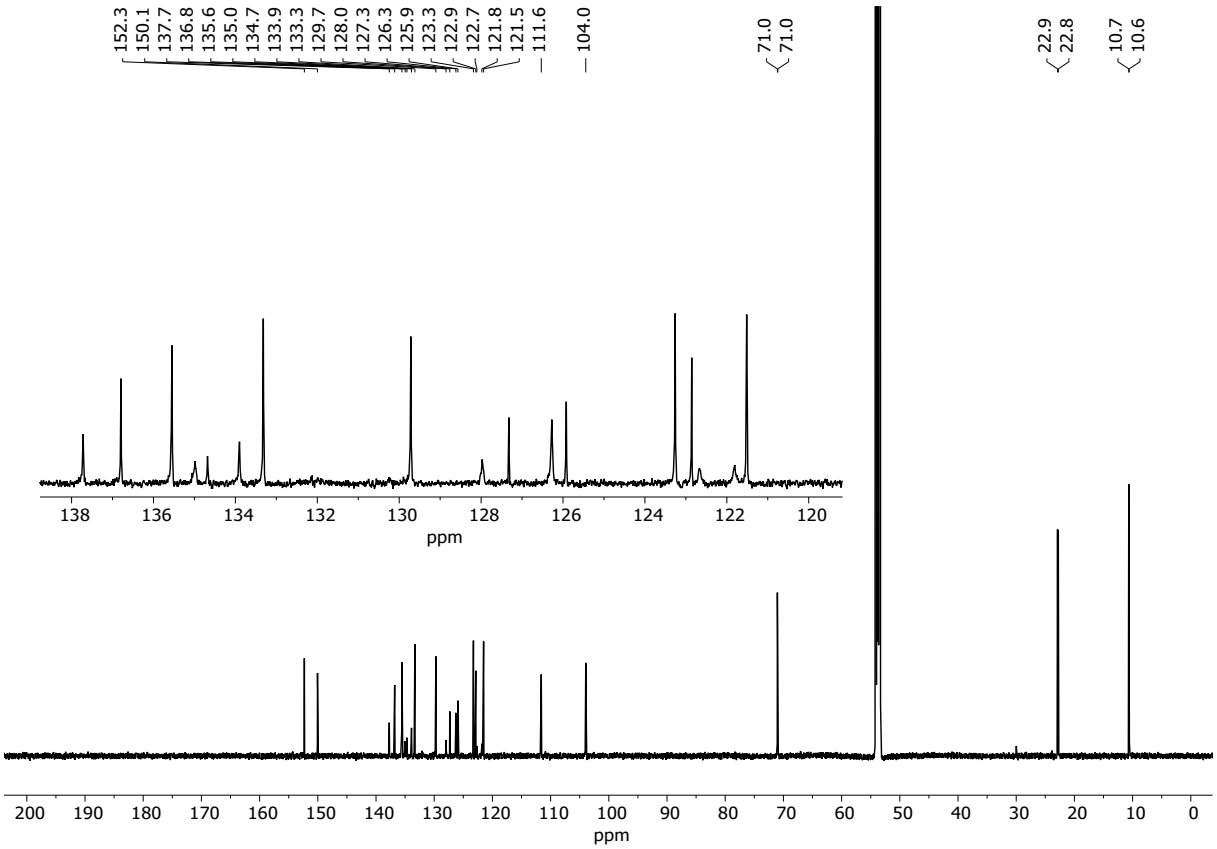

Figure S60. ^{13}C NMR spectrum of *rac*-**HS-Br$_2$** (151 MHz, CD_2Cl_2).

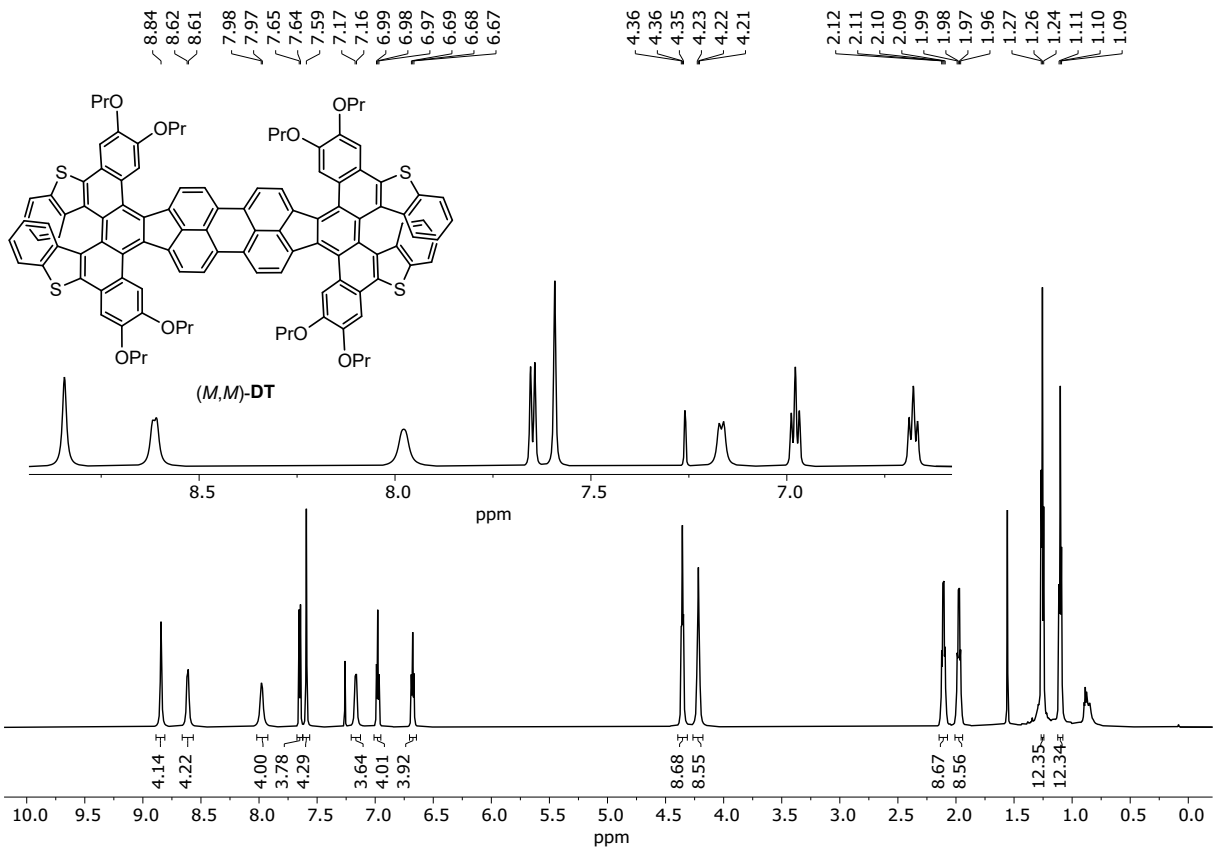

Figure S61. ^{1}H NMR spectrum of (*M*,*M*)-**DT** (700 MHz, $CDCl_3$).

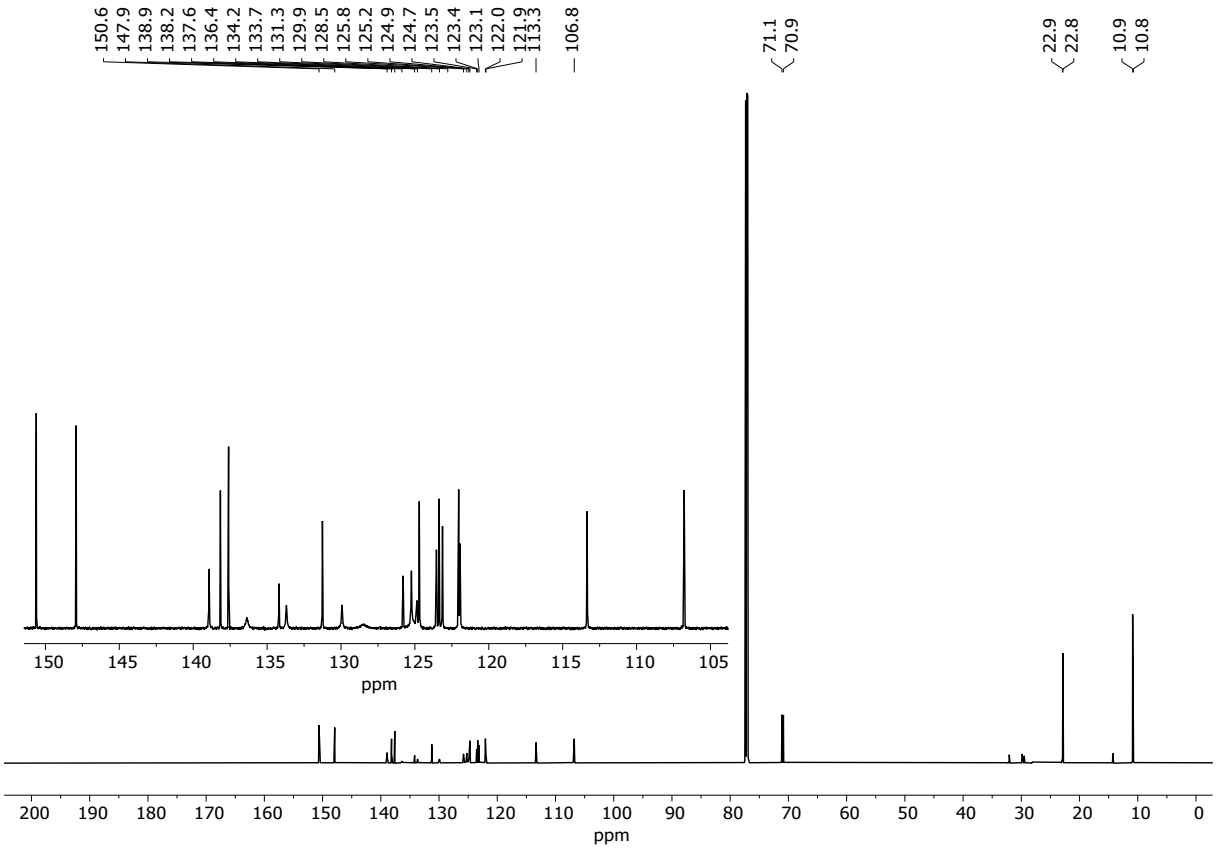

Figure S62. ^{13}C NMR spectrum of (*M*,*M*)-**DT** (176 MHz, $CDCl_3$).

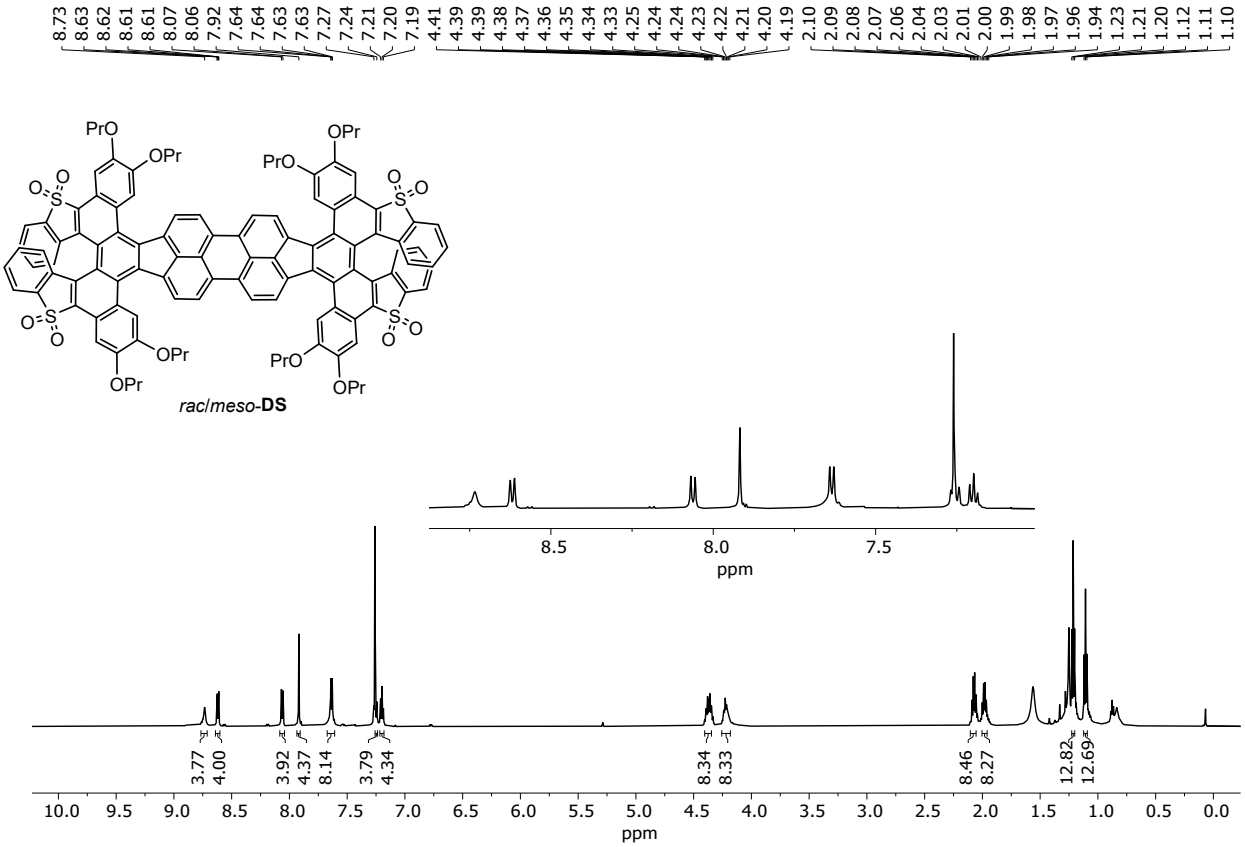

Figure S63. ^{1}H NMR spectrum of *rac*/*meso*-**DS** (600 MHz, $CDCl_3$).

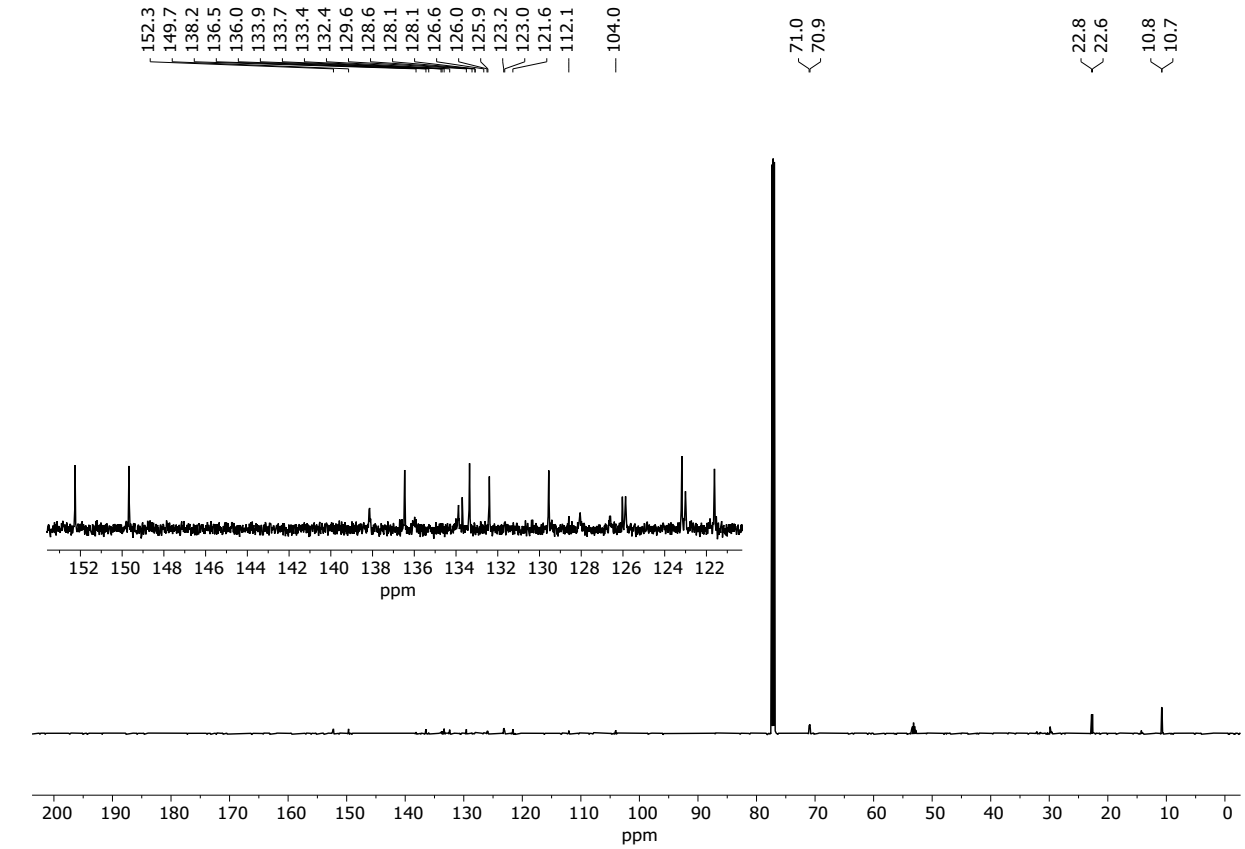

Figure S64. ^{13}C NMR spectrum of *rac*/*meso*-**DS** (151 MHz, $CDCl_3$).

13. References

1 G. R. Fulmer, A. J. M. Miller, N. H. Sherden, H. E. Gottlieb, A. Nudelman, B. M. Stoltz, J. E. Bercaw and K. I. Goldberg, NMR Chemical Shifts of Trace Impurities: Common Laboratory Solvents, Organics, and Gases in Deuterated Solvents Relevant to the Organometallic Chemist, *Organometallics*, 2010, **29**, 2176.

2 G. M. Sheldrick, A Short History of SHELX, *Acta Crystallogr., Sect. A: Found. Crystallogr.*, 2008, **64**, 112.

3 G. M. Sheldrick, Crystal Structure Refinement with SHELXL*, Acta Crystallogr., Sect. C: Cryst. Struct. Commun.*, 2015, **71**, 3.

4 C. F. Macrae, P. R. Edgington, P. McCabe, E. Pidcock, G. P. Shields, R. Taylor, M. Towler and J. van de Streek, Mercury: Visualization and Analysis of Crystal Structures, *J. Appl. Crystallogr.*, 2006, **39**, 453.

5 M. J. Frisch, G. W. Trucks, H. B. Schlegel, G. E. Scuseria, M. A. Robb, J. R. Cheeseman, G. Scalmani, V. Barone, G. A. Petersson, H. Nakatsuji, X. Li, M. Caricato, A. V. Marenich, J. Bloino, B. G. Janesko, R. Gomperts, B. Mennucci, H. P. Hratchian, J. V. Ortiz, A. F. Izmaylov, J. L. Sonnenberg, Williams, F. Ding, F. Lipparini, F. Egidi, J. Goings, B. Peng, A. Petrone, T. Henderson, D. Ranasinghe, V. G. Zakrzewski, J. Gao, N. Rega, G. Zheng, W. Liang, M. Hada, M. Ehara, K. Toyota, R. Fukuda, J. Hasegawa, M. Ishida, T. Nakajima, Y. Honda, O. Kitao, H. Nakai, T. Vreven, K. Throssell, J. A. Montgomery Jr., J. E. Peralta, F. Ogliaro, M. J. Bearpark, J. J. Heyd, E. N. Brothers, K. N. Kudin, V. N. Staroverov, T. A. Keith, R. Kobayashi, J. Normand, K. Raghavachari, A. P. Rendell, J. C. Burant, S. S. Iyengar, J. Tomasi, M. Cossi, J. M. Millam, M. Klene, C. Adamo, R. Cammi, J. W. Ochterski, R. L. Martin, K. Morokuma, O. Farkas, J. B. Foresman and D. J. Fox, *Gaussian 16 Rev. C.01*, Wallingford, CT, 2016.

6 P. J. Stephens, F. J. Devlin, C. F. Chabalowski and M. J. Frisch, *Ab Initio* Calculation of Vibrational Absorption and Circular Dichroism Spectra Using Density Functional Force Fields, *J. Phys. Chem.*, 1994, **98**, 11623.

7 A. D. Becke, Density-Functional Thermochemistry. III. The Role of Exact Exchange, *J. Chem. Phys.*, 1993, **98**, 5648.

8 C. Lee, W. Yang and R. G. Parr, Development of the Colle-Salvetti Correlation-Energy Formula into a Functional of the Electron Density, *Phys. Rev. B*, 1988, **37**, 785.

9 S. H. Vosko, L. Wilk and M. Nusair, Accurate Spin-Dependent Electron Liquid Correlation Energies for Local Spin Density Calculations: A Critical Analysis, *Can. J. Phys.*, 1980, **58**, 1200.

10 T. Clark, J. Chandrasekhar, G. W. Spitznagel and P. V. R. Schleyer, Efficient Diffuse Function-Augmented Basis Sets for Anion Calculations. III. The 3-21+G Basis Set for First-Row Elements, Li–F, *J. Comput. Chem.*, 1983, **4**, 294.

11 R. Krishnan, J. S. Binkley, R. Seeger and J. A. Pople, Self-Consistent Molecular Orbital Methods. XX. A Basis Set for Correlated Wave Functions, *J. Chem. Phys.*, 1980, **72**, 650.

12 S. Grimme, J. Antony, S. Ehrlich and H. Krieg, A Consistent and Accurate *ab initio* Parametrization of Density Functional Dispersion Correction (DFT-D) for the 94 Elements H-Pu, *J. Chem. Phys.*, 2010, **132**, 154104.
13 S. Grimme, S. Ehrlich and L. Goerigk, Effect of the Damping Function in Dispersion Corrected Density Functional Theory, *J. Comput. Chem.*, 2011, **32**, 1456.
14 T. Yanai, D. P. Tew and N. C. Handy, A New Hybrid Exchange–Correlation Functional Using the Coulomb-Attenuating Method (CAM-B3LYP), *Chem. Phys. Lett.*, 2004, **393**, 51.
15 M. Cossi, N. Rega, G. Scalmani and V. Barone, Energies, Structures, and Electronic Properties of Molecules in Solution with the C-PCM Solvation Model, *J. Comput. Chem.*, 2003, **24**, 669.
16 V. Barone and M. Cossi, Quantum Calculation of Molecular Energies and Energy Gradients in Solution by a Conductor Solvent Model, *J. Phys. Chem. A*, 1998, **102**, 1995.
17 Roy Dennington, Todd A. Keith and John M. Millam, *GaussView Version 6*, 2019.
18 J. R. Cheeseman, G. W. Trucks, T. A. Keith and M. J. Frisch, A Comparison of Models for Calculating Nuclear Magnetic Resonance Shielding Tensors, *J. Chem. Phys.*, 1996, **104**, 5497.
19 K. Wolinski, J. F. Hinton and P. Pulay, Efficient Implementation of the Gauge-Independent Atomic Orbital Method for NMR Chemical Shift Calculations, *J. Am. Chem. Soc.*, 1990, **112**, 8251.
20 R. Ditchfield, Self-Consistent Perturbation Theory of Diamagnetism, *Mol. Phys.*, 1974, **27**, 789.
21 R. McWeeny, Perturbation Theory for the Fock-Dirac Density Matrix, *Phys. Rev.*, 1962, **126**, 1028.
22 F. London, Théorie quantique des courants interatomiques dans les combinaisons aromatiques, *J. Phys. Radium*, 1937, **8**, 397.
23 T. A. Keith and R. Bader, Calculation of Magnetic Response Properties Using a Continuous Set of Gauge Transformations, *Chem. Phys. Lett.*, 1992, **194**, 1.
24 T. A. Keith and R. F. Bader, Calculation of Magnetic Response Properties Using a Continuous Set of Gauge Transformations, *Chem. Phys. Lett.*, 1993, **210**, 223.
25 A. Schäfer, C. Huber and R. Ahlrichs, Fully Optimized Contracted Gaussian Basis Sets of Triple Zeta Valence Quality for Atoms Li to Kr*, J. Chem. Phys.*, 1994, **100**, 5829.
26 F. Weigend and R. Ahlrichs, Balanced Basis Sets of Split Valence, Triple Zeta Valence and Quadruple Zeta Valence Quality for H to Rn: Design and Assessment of Accuracy, *Phys. Chem. Chem. Phys.*, 2005, **7**, 3297.
27 M. Garcia-Ratés and F. Neese, Effect of the Solute Cavity on the Solvation Energy and its Derivatives within the Framework of the Gaussian Charge Scheme, *J. Comput. Chem.*, 2020, **41**, 922.
28 Z. Wang, An Intuitive Graphical User Interface for Diverse Aromaticity Analyses, *Chemistry*, 2024, **6**, 1692.

29 D. Geuenich, K. Hess, F. Köhler and R. Herges, Anisotropy of the Induced Current Density (ACID), a General Method to Quantify and Visualize Electronic Delocalization, *Chem. Rev.*, 2005, **105**, 3758.
30 R. Herges and D. Geuenich, Delocalization of Electrons in Molecules, *J. Phys. Chem. A*, 2001, **105**, 3214.
31 F. Neese, Software update: The ORCA program system—Version 5.0, *Wiley Interdiscip. Rev.: Comput. Mol. Sci.*, 2022, **12**, e1606.
32 F. Neese, An Improvement of the Resolution of the Identity Approximation for the Formation of the Coulomb Matrix*, J. Comput. Chem.*, 2003, **24**, 1740.
33 F. Neese, F. Wennmohs, A. Hansen and U. Becker, Efficient, Approximate and Parallel Hartree-Fock and Hybrid DFT Calculations. A 'Chain-of-Spheres' Algorithm for the Hartree-Fock Exchange, *Chem. Phys.*, 2009, **356**, 98.
34 S. Grimme, A. Hansen, S. Ehlert and J.-M. Mewes, r^2SCAN-3c: A "Swiss Army Knife" Composite Electronic-Structure Method, *J. Chem. Phys.*, 2021, **154**, 64103.
35 K. Y. Cheung, X. Xu and Q. Miao, Aromatic Saddles Containing two Heptagons, *J. Am. Chem. Soc.*, 2015, **137**, 3910.
36 J. Bergner, C. Walla, F. Rominger, A. Dreuw and M. Kivala, Inducing Curvature to Pyracylene upon π-Expansion, *Chem. Eur. J.*, 2022, **28**, e202201554.
37 K. J. Laidler and M. C. King, Development of Transition-State Theory*, J. Phys. Chem.*, 1983, **87**, 2657.
38 H. Eyring, The Activated Complex in Chemical Reactions, *J. Chem. Phys.*, 1935, **3**, 107.